

Research Report

Fraunhofer Institute for
Nondestructive Testing IZFP

Title/Subject

**Development and test of a micromagnetic sensor
principle for the characterization of non-
ferromagnetic materials.**

Dirk Henn

QM/Ressourcenmanagement
Phone +49 681 9302-3856
Fax +49 681 9302-113856
Dirk.Henn@izfp.fraunhofer.de
www.izfp.fraunhofer.de

Customer
none

Report No: 150111-TW

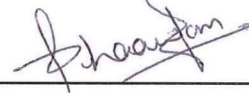
Date: 04.03.2015
Page No: Page 1 of 1

Author
Bhaawan Gupta


Department
Materials Char.

Phone
+4917686724050

Signature
Bhaawan Gupta



Release


Dr.-Ing. Jochen Kurz
(Head of department)

Keywords (max. 8)

Diamagnetism, paramagnetism, magnetic susceptibility, force measurement, non-destructive testing

Abstract

In ferromagnetic materials, magnetic domain walls interact with microstructure over similar mechanisms as dislocations do. This fundamental observation is the basis of micro-magnetic materials characterization. It is quite legitimate to assume that such a correlation exists between micro or electromagnetic and mechanical properties in para- and diamagnetic materials. The electrical conductivity of aluminium does reveal some information about material properties which can be assessed non-destructively using eddy current impedance measurements. There is much less known about the correlation between the mechanical properties and the magnetic susceptibility of non-ferromagnetic materials such as graphite, aluminium and plastics. There is no commercial non-destructive method which uses the concept of magnetic susceptibility for the characterization of dia- and paramagnetic materials. Some principles have been proposed in this work which use the magnetic susceptibility of the materials to determine the para- or diamagnetic properties and display their lateral distribution as an intensity map. Experiments also show that some of these principles are highly sensitive to even the smallest ferromagnetic impurity in non-ferrous materials.



Zertifiziertes Managementsystem
am Fraunhofer IZFP Saarbrücken

Distribution List 1x IZFP/Library

Without written agreement by Fraunhofer IZFP the report may not be reproduced or distributed or used for publication in extracts. Violation obligates damage compensation.

MASTER THESIS

Development and test of a micromagnetic sensor principle for the characterization of non-ferromagnetic materials

Computer and Communications Technology



Saarland University

Submitted by:

Bhaawan Gupta

Supervisors:

Prof. Dr. Andreas Schütze (Saarland University)

Dr.-Ing. Klaus Szielasko (Fraunhofer IZFP)

Reviewers:

Prof. Dr. Andreas Schütze (Saarland University)

Prof. Dr.-Ing. Hans-Georg Herrmann (Saarland University)

STATEMENT OF ORIGINAL WORK

I declare that all the material presented in this thesis is my own work and has not been written for me, in whole or in part, by any other person. I also declare that any data or information from the published or unpublished work of another person has been duly acknowledged in the work which I present in this thesis.

Date, Place

Bhaawan Gupta

ABSTRACT

Every material has characteristic magnetic properties which enable the materials characterization by using the concept of magnetic susceptibility.

In ferromagnetic materials, magnetic domain walls interact with microstructure over similar mechanisms as dislocations do. This fundamental observation is the basis of micro-magnetic materials characterization. There are commercial non-destructive testing devices for materials characterization of ferromagnetic materials. Therefore, a high number of non-destructive magnetic techniques have been developed and currently are used for the characterization of the ferromagnetic materials. Two important techniques for the non-destructive testing of ferromagnetic materials are magnetic flux leakage (MFL) and magnetic particle inspection.

It is quite legitimate to assume that a correlation exists between micro or electromagnetic and mechanical properties also in para- and diamagnetic materials. The electrical conductivity of aluminium does reveal some information about material properties which can be assessed non-destructively using eddy current impedance measurements. There is much less known about the correlation between the mechanical properties and the magnetic susceptibility of non-ferromagnetic materials such as graphite, aluminium and plastics. There is no commercial non-destructive method which uses the concept of magnetic susceptibility for the characterization of dia- and paramagnetic materials. However, using the low field sensing techniques at room temperature, the variation in the magnetic field because of the static magnetic susceptibility of a test object can be measured. It is assumed that this can provide information on all kinds of materials. Some principles are proposed in this thesis which use the magnetic susceptibility of the materials to determine the para- or diamagnetic properties and displays their lateral distribution as an intensity map. Experiments also show that some of these principles are highly sensitive to even the smallest ferromagnetic impurity in non-ferrous materials.

CONTENTS

| | |
|--|-------------|
| a) Acknowledgements | i |
| b) Acronyms | ii |
| Chapter | Page |
| 1. Introduction | 1 |
| 2. Fundamentals | |
| 2.1. Basics of magnetism | 4 |
| 2.1.1. Magnetic field and its generation | 4 |
| 2.1.2. Magnetic field pattern | 4 |
| 2.1.3. Material characterization based on magnetic properties | 6 |
| 2.1.4. Magnetic susceptibility | 6 |
| 2.1.5. Diamagnetism | 7 |
| 2.1.6. Paramagnetism | 7 |
| 2.1.7. Ferromagnetism | 8 |
| 2.1.8. Ferrimagnetism | 9 |
| 2.2. Magnetic field sensors | 10 |
| 2.2.1. SQUID | 10 |
| 2.2.2. Inductive method based sensors | 11 |
| 2.2.3. Magnetoresistive effect based sensors | 11 |
| 2.2.4. Hall effect | 12 |
| 2.2.5. Fluxgate sensors | 13 |
| 2.3. State of the art for NDT | 14 |
| 2.3.1. Some currently used methods in the field of non-destructive testing | 14 |
| 2.3.2. Methods for dia- and paramagnetic materials characterization | 16 |

| | | |
|---------------|------------------------|----|
| 2.4. | Measurement techniques | 21 |
| 2.4.1. | Strain gauge | 21 |
| 2.4.2. | Capacitive sensor | 22 |

3. Concept of novel NDT techniques

| | | |
|-----------------|---|----|
| 3.1. | Materials of interest | 24 |
| 3.2. | Different principles | 25 |
| 3.2.1. | Measurements using a fluxgate magnetometer | 25 |
| 3.2.2. | Force based measurements | 25 |
| 3.2.2.1. | Precision balance | 25 |
| 3.2.2.2. | Cantilever based methods (scanning system set-up) | 26 |
| 3.3. | Relation between susceptibility and force | 31 |
| 3.4. | Force over distance | 33 |
| 3.5. | Types of filters used | 34 |

4. Materials characterization and susceptibility imaging with fluxgate magnetometer

| | | |
|-------------|--|----|
| 4.1. | Single fluxgate magnetometer | 35 |
| 4.2. | Differential mode (Gradiometer set up) | 37 |
| 4.3. | Limitations | 39 |
| 4.4. | Conclusion | 40 |

5. Material characterization with a precision balance

| | | |
|-------------|-------------|----|
| 5.1. | Set-up | 41 |
| 5.2. | Evaluation | 42 |
| 5.3. | Limitations | 44 |

6. Material characterization and susceptibility imaging using a cantilever based approach

| | | |
|-------------|----------------------------------|----|
| 6.1. | Measurements with a strain gauge | 46 |
|-------------|----------------------------------|----|

| | | |
|---------|---|----|
| 6.1.1. | Using one strain gauge/quarter bridge | 46 |
| 6.1.2. | Half bridge circuit using two strain gauges | 47 |
| 6.1.3. | Results with FRP cantilever | 49 |
| 6.1.4. | Conclusion | 52 |
| 6.2. | Measurements using a capacitive sensor | 53 |
| 6.2.1. | Optimization of the set up | 53 |
| 6.2.2. | Defining a new filter and minimizing the noise | 57 |
| 6.2.3. | Set-up | 58 |
| 6.2.4. | Evaluation | 59 |
| 6.2.5. | Need of improvement | 67 |
| 6.2.6. | Evaluation with final sensor | 71 |
| 6.2.7. | Effect of thickness of the sample | 79 |
| 6.2.8. | Distance variation | 81 |
| 6.2.9. | Evaluation of plastics | 83 |
| 6.2.10. | Conclusion | 87 |
| 7. | Conclusion and applications | 88 |
| | References | 90 |
| | Appendix | 93 |

ACKNOWLEDGEMENTS

I have received support from several people in initiating and completing this research project. First and foremost, I would like to thank Prof. Andreas Schütze for being such a wonderful supervisor. His constant constructive feedback for my work always motivated me in the right direction. Regular discussions with him always led to a productive conclusion. I would like to thank Prof. Hans-Georg Herrmann, for accepting my request to be the second reviewer for this thesis work. I would also like to thank University of Saarland for giving me an opportunity to study in Germany and to understand the beautiful German culture.

I am indebted to all the members of 'Electromagnetic inspection methods' team at Fraunhofer IZFP who made work atmosphere really comfortable and enjoyable for me. Their constant interest in my work always has been encouraging for me throughout the whole course of my work.

I would also like to acknowledge the support that I have constantly received from my family.

For Dr. Klaus Szielasko: I might fall short of words for him. He has not just been a supervisor. I saw him in different roles and capacities, from an amazing mentor who has constantly encouraged me, to a wonderful friendly person who has contributed immensely in shaping and presenting my ideas. A conversation with him has always been full of inspiration and his approach of finding solutions to every problem successfully has made me learn a lot throughout the course of this thesis which I am sure of benefitting from it in my future.

ACRONYMS

- **NDT:** Non destructive testing
- **MFL:** Magnetic flux leakage
- **SQUID:** Superconducting Quantum Interference Device
- **AMR:** Anisotropic magnetoresistance
- **GMR:** Giant magnetoresistance
- **3MA:** Micromagnetic multi-parameter microstructure and stress analysis
- **IZFP:** Institut für Zerstörungsfreie Prüfverfahren
- **MFM:** Magnetic force microscopy
- **FRP:** Fibre re-inforced plastic
- **CFRP:** Carbon fibre reinforced plastic
- **PMMA:** Polymethyl methacrylate
- **PET:** Polyethylene terephthalate
- **PF:** Phenol formaldehydes
- **PC:** Polycarbonate
- **PVC-U:** Polyvinylchloride - unplasticised
- **ABS:** Acrylonitrile butadiene styrene
- **PS:** Polystyrene
- **PE-HD:** Polyethylene, high density
- **PE-LD:** Polyethylene, low density
- **PA:** Polyamide
- **PP:** Polypropylene
- **PUR:** Polyurethane
- **VMQ:** Vinyl methyl polysiloxane

Chapter 1: Introduction

Every material has characteristic magnetic properties. Objects cannot only be characterized by their size or by their composition but also by using their magnetic properties like magnetic susceptibility. The magnetic effect might be extremely weak but can be measured. Magnetic susceptibility is the physical quantity describing material properties in the external magnetic field. Magnetic susceptibility measures the magnetisability of any material [Dear]. This magnetic susceptibility of materials has been widely used to find minerals in soil, rocks etc., especially Fe-bearing minerals [Dear] enabling to classify different types of materials. Using the magnetic susceptibility of the materials, it is quite convenient to study all materials and additionally its application is safe, fast and non-destructive.

In ferromagnetic materials, magnetic domain walls interact with microstructure over similar mechanisms as dislocations do [Bozo, Cull, and Jile]. This fundamental observation is the basis of micro-magnetic materials characterization. The correlation between micro magnetic parameters and the mechanical hardness, strength and stress has been thoroughly studied to date, and there are commercial non-destructive testing devices for solving the inverse problem of measured quantity estimation using micro magnetic testing parameters as input.

Coupling between the stress and magnetic field is the main and important feature of the ferromagnetic materials consisting of various small magnetic domains in its microstructure [Pete]. Hence, it means that extent of magnetization might even result in the dimension variation of ferromagnetic materials and vice versa, i.e., the amount of stress also affects the magnetization of the ferromagnetic materials for which the magnetic NDT has always paid special attention to. The reason is that it lays down the physical basis for the evaluation of the stress status of ferromagnetic structures and components by magnetic based measuring methods.

As of now, the magnetic techniques which are one of the most important NDT technologies used characterize the mechanical features of ferromagnetic materials on the basis of the physical principle of magnetic-stress coupling mentioned above. Therefore, a high number of non-destructive magnetic techniques have been developed and currently are used for the characterization of the ferromagnetic materials.

The motivation behind this work is that it is quite legitimate to assume that a correlation exists between micro or electromagnetic and mechanical properties in para- and diamagnetic materials as well. The electrical conductivity of aluminium does reveal some information about material properties which can be assessed non-destructively using eddy current impedance measurements [Alle]. There is much less known about the correlation between the mechanical properties and magnetic susceptibility of non-ferromagnetic materials such as graphite, aluminium and plastics. There is no commercial non-destructive material characterization method which uses the concept of magnetic susceptibility. The state-of-the-art approach to susceptibility determination for these materials requires the use of Superconducting Quantum Interference Devices (SQUIDs), which require cryogenic cooling and cause high maintenance costs. In addition to this there are methods like Faraday's and Guoy's scale (discussed in the following chapters) which help in determining the magnetic susceptibility of materials but again they have some limitations regarding the size, shape, or the form of the test object.

Magnetic field sensors detect changes or disturbances in the magnetic field and based on this, information can be derived about the material properties. Using the low field sensing techniques at room temperature, the variation in the magnetic field because of the static magnetic susceptibility of the test object can be measured. It is expected that this can provide information on all kinds of materials. Some principles are proposed in this thesis which use the magnetic susceptibility property of the materials to determine to which extent the material is para- or diamagnetic. Experiments also show that few of these principles are highly sensitive to even the smallest ferromagnetic impurity in non-ferrous materials.

In this thesis, there are 7 chapters including introduction and conclusion. The second chapter discusses the fundamentals and the state of the art for the dia- and paramagnetic materials. The third chapter discusses the concept of novel NDT technique implemented in this work for the dia-and paramagnetic materials characterization. The fourth chapter introduces the first principle for the dia- and paramagnetic materials characterization using a fluxgate magnetometer and its limitations. The fifth chapter discusses the evaluation of samples using a precision balance. The sixth chapter discusses the

cantilever based approach utilizing the concept of force, with strain gauges and capacitive sensor. Finally the thesis is concluded with the comparison of all proposed sensors and the industrial application of the most efficient sensor principle in the last chapter.

Chapter 2: Fundamentals

In this chapter basic terminologies and basic phenomena and principles of magnetism, materials depending on their magnetic properties are discussed (ferromagnetic materials, dia- and paramagnetic, ferrimagnetic materials). In addition to this, state of the art for materials characterization in NDT, and basics of measurement techniques which have been used in this thesis, have been discussed.

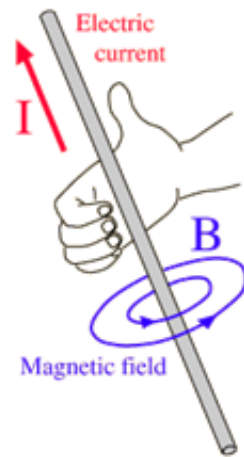
2.1. Basics of magnetism

2.1.1. Magnetic field and its generation

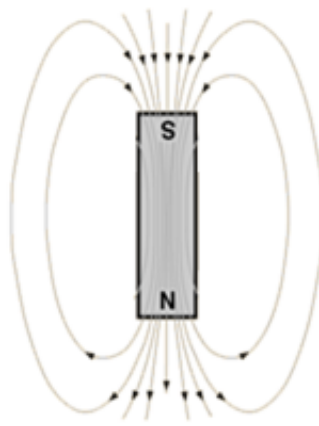
If we consider two parallel wires with electric current passing through both of them, the wires are attracted to each other if the direction of the current in both the parallel wires is same. The wires will repel if the direction of the current is opposite to each other [Nave]. The force which leads to attraction or repulsion is called magnetic force. The magnetic force acting on such moving charges is defined by the magnetic field. Magnetic field is the most basic and the fundamental part of magnetism. In permanent magnets, the magnetic behavior is due to the spins and the orbital motion of the electrons of the material leading to magnetization and the generation of the magnetic field [Bozo]. The pattern of the magnetic field is discussed and demonstrated in Figure 1 in the following section.

2.1.2. Magnetic field patterns

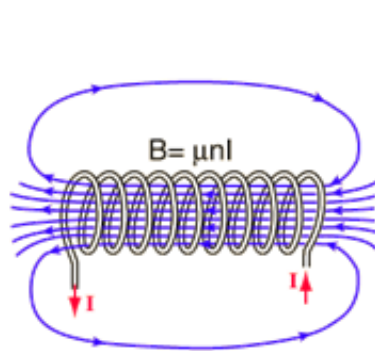
The field around a single current loop and a solenoid are similar to that of a bar magnet, where the field emerges from one end of the magnet (North pole) and passes through the air making a return path to the other end of the magnet (South pole) [Nave]. In figure 1 below, some of the magnetic field patterns generated by different sources are shown.



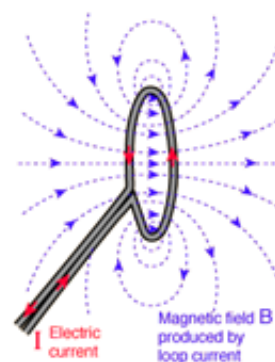
Current in a wire



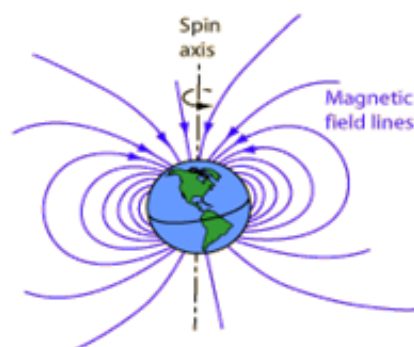
A bar magnet



A solenoid



A loop of wire



Earth

Figure 1: Magnetic field patterns [Nave]

2.1.3. Materials characterization based on magnetic properties

As per Faraday's law of magnetic induction, $\mathcal{E} = -\frac{d\Phi_B}{dt}$, i.e., the magnetic forces acting upon a material's electrons are affected whenever it is placed under the influence of an alternating magnetic field [Hayt]. Materials respond quite differently to the magnetic field which depends on factors like atomic and molecular structure of the materials or the overall magnetic field associated to atoms. The magnetic moment can be due to the change in motion of the electrons because of an external magnetic field or simply by motion of the electrons. Electrons exist in pairs in most of the atoms which spin in opposite directions as a result of which their magnetic fields get cancelled. However, materials with unpaired electrons tend to react to the external magnetic field since they have a net magnetic field. Based on this most materials can be classified as diamagnetic, paramagnetic and ferromagnetic materials.

2.1.4. Magnetic susceptibility

Magnetic susceptibility is the physical quantity describing the interaction of a material in the external magnetic field and measures the amount of magnetisability of a material [Dear]. In numerical terms, magnetic susceptibility is defined as the ratio between magnetization M of the material in the magnetic field and the field strength H [Yama]:

$$\chi = \frac{M}{H}, \text{ where } \chi \text{ is the susceptibility.}$$

Based on this magnetic property, the materials have been majorly classified as [Osta]:

- Diamagnetic materials : $-1 < \chi < 0$,
- Paramagnetic materials : $0 < \chi < 1$,
- Ferromagnetic materials : $\chi \gg 1$,
- Ferrimagnetic materials (explained in the following section).

The focus in this work will be entirely on diamagnetic and paramagnetic materials.

2.1.5. Diamagnetism

The first category is materials for which χ is small and negative and are known as diamagnetic materials. Their magnetic response opposes the applied magnetic field and thus is repulsive in nature to the applied field. There is no net magnetic moment per atom in such materials since all the electrons are paired, however, under the influence of external magnetic field, the realignment of the electron paths give rise to the diamagnetic properties of the materials [Yama]. Examples of diamagnets are copper, silver, bismuth, graphite. The strongest diamagnets are the superconductors with χ as -1 i.e., the magnetic field in the material is zero. The picture below, figure 2, demonstrates the diamagnetic effect where under the influence of an external magnetic field, pyrolytic graphite levitates over strong magnets due to repulsive force.

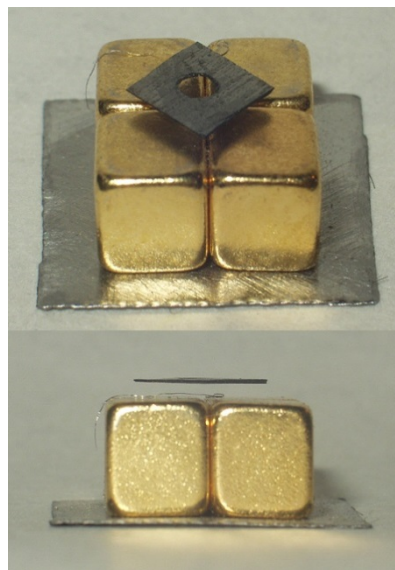


Figure 2: Diamagnetic behavior of pyrolytic graphite [Diam]

2.1.6. Paramagnetism

Materials for which χ is small and positive are known as paramagnetic materials. Their magnetic response supports the applied magnetic field and thus is attracted to the field [Jile]. The paramagnetic property of the materials is due to the presence of unpaired electrons in the atoms resulting in a net

magnetic moment. Due to thermal agitation the magnetic moments return to the randomly oriented state when the external field is removed as illustrated in the figure 3 below.

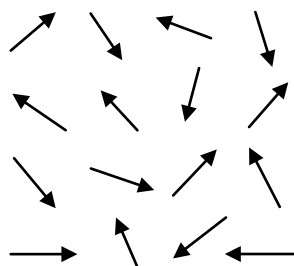


Figure 3: State of magnetic moments in paramagnetic materials without external field

2.1.7. Ferromagnetism

These materials show a very strong attraction to the applied external magnetic field and for them χ is positive and quite large comparatively. Like paramagnetic materials, these materials too have unpaired electrons which result in the net magnetic moment. But in addition to it, such materials possess magnetic domains where the atomic magnetic moments are aligned parallel resulting in a strong magnetization [Bozo]. When ferromagnetic materials are heated, the thermal agitation of the atoms results in a decrease in the degree of alignment of atomic magnetic moment. At a certain temperature, called Curie temperature, the thermal agitation becomes so high that the ferromagnetic material becomes paramagnetic [Spal]. The state of the magnetic moments inside a single domain of the ferromagnetic materials in the absence of a magnetic field is shown in figure 4 and in figure 5 the magnetic domains in a ferromagnetic material are illustrated.

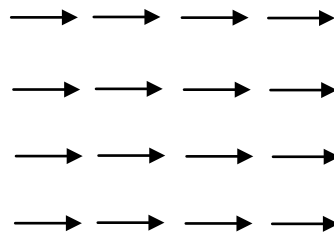


Figure 4: Magnetic moments inside a single domain in ferromagnetic materials

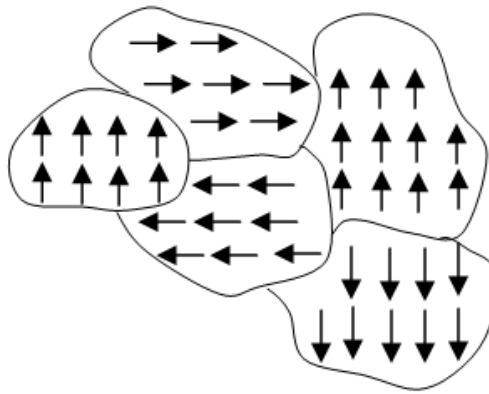


Figure 5: Magnetic domains in a ferromagnetic material

2.1.8. Ferrimagnetism

The magnetic moments in ferrimagnets are aligned oppositely and have different magnitudes so that a net magnetization exists in the domain. The ferrimagnets have quite a similar magnetic behavior as compared to ferromagnets but they have lower saturation magnetizations and their effect can only be seen in compounds [Spal]. The figure 6 below illustrates the magnetic moments in the ferrimagnets in the absence of a magnetic field.

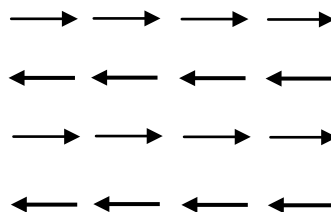


Figure 6: Magnetic moments in ferrimagnetic materials without external field

2.2. Magnetic field sensors

The biggest advantage of using the magnetic sensors or the magnetic based technology is that these sensors can indirectly measure many properties of the materials and hence are of huge significance in the field of non-destructive testing. In the following section the current prominent magnetic sensors and their working principles are discussed briefly.

2.2.1. SQUID

A Superconducting Quantum Interference Device (SQUID) is one of the most sensitive low field sensing devices. It consists of two parallel Josephson junctions which are used to measure extremely low current [Lenz]. The SQUID is capable of sensing the field in the range of fT up to 9 Tesla [Caru]. A SQUID is one of the most accurate devices that can be used to detect magnetic flux with very high sensitivity [Cull]. It is based on the magnetic field and electric current interactions when materials are cooled down to a temperature where materials lose resistance to the electricity flow and become superconductors. It consists of two parallel Josephson junctions as shown in figure 7 below. The current induced in the ring flows continuously in the absence of any obstruction and the magnitude of the induced current indicates the flux density [Lenz]. Since, for this principle to work, a superconducting state is necessary, which requires cryogenic cooling (e.g., 4.2K, liquid helium) [Osta] and high maintenance costs, the use of SQUID cannot be considered suitable for NDT under normal conditions.

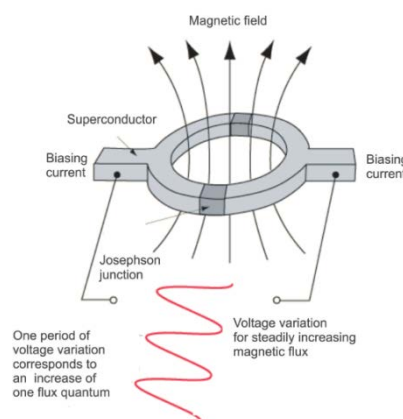


Figure 7: SQUID [Osta]

2.2.2. Inductive method based sensors

Induction method is based on the variation in the coil inductance as a result of the embedded specimen. A stable harmonic current generator is used which powers the unbalanced bridge of two identical coils. One coil has a reference yoke and in the other coil, the specimen is inserted [Osta].

2.2.3. Magnetoresistive effect based sensors

In the non-destructive testing field, magnetoresistive sensors are brought more into use nowadays compared to the traditional inductive sensors because of their capability of providing higher sensitivity, which is useful e.g., for the detection of small defects in structure of the materials. In addition to this, these sensors are much easier to use and are low cost sensors. The name of these sensors comes from the magnetoresistive property of the materials which change their resistance when exposed to a magnetic field.

2.2.3.1. Anisotropic magnetoresistance (AMR)

The anisotropic magnetoresistance effect occurs in ferromagnetic materials. The AMR effect can be defined by the difference in the scattering cross section of the atomic orbitals affected by the magnetic field [Schn]. When the direction of the magnetization is parallel to the direction of the current, the resistance produced by the scattering is maximum, and is minimum when the direction of current and magnetization are perpendicular to each other. The maximum sensitivity and the linearity can be achieved when the direction of the magnetization is 45° with respect to the current [Schn]. Figure 8 below, it demonstrates the disturbance in the electron orbitals on the application of magnetic field.

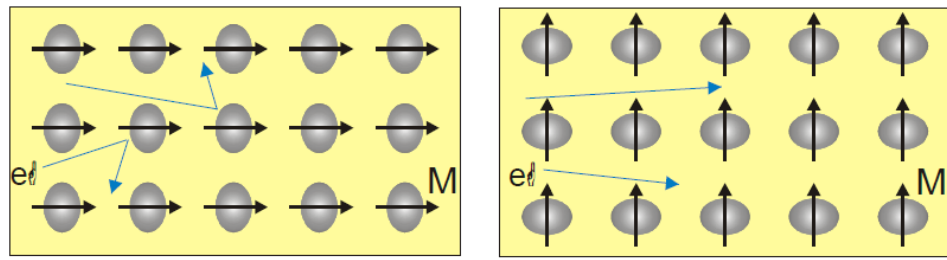


Figure 8: Electron orbital distortion and the scattering difference when the magnetic field M : (left) is parallel to the current denoted by e ; (right) is perpendicular to the current [Schn]

2.2.3.2. Giant magnetoresistance (GMR)

In a giant magnetoresistive sensor, a very thin non-magnetic metal spacer layer is sandwiched between two or more ferromagnetic metal layers [Schn]. GMR effect is obtained when the spacer layer is thin enough as compared to the average free path of the electrons such that the polarized electron spin in one of the layers can diffuse into the other layers well before their polarization is distorted by the scattering. The resistance of the ferromagnetic layers can be altered depending on whether the moments in both the ferromagnetic layers are parallel to each other or in the anti-parallel direction. If the moments of both the ferromagnetic layers are in the same direction, then there is less scattering at the interfaces, large mean free paths and lower resistance unlike when the moments are aligned in the anti-parallel direction as shown in the figure 9 below.

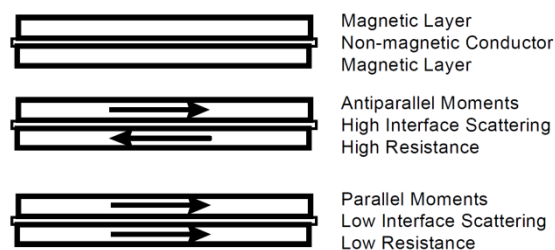


Figure 9: GMR principle illustration [Caru]

2.2.4. Hall effect

A constant current is passed through a thin sheet of a preferably semiconducting material. The output connections are perpendicular to the direction of the current [Hesa]. In the absence of the magnetic field, the

current distribution is uniform and there is no potential difference generated across the outputs as shown in figure 10. However, in the presence of the magnetic field perpendicular to the sheet surface, which deflects the current direction, a potential difference is generated across the output as shown in figure 11. The interaction (potential difference, 'V') is proportional to the vector cross product of the current 'I' and the magnetic field 'B' as shown in the equation, $V \propto I \times B$.

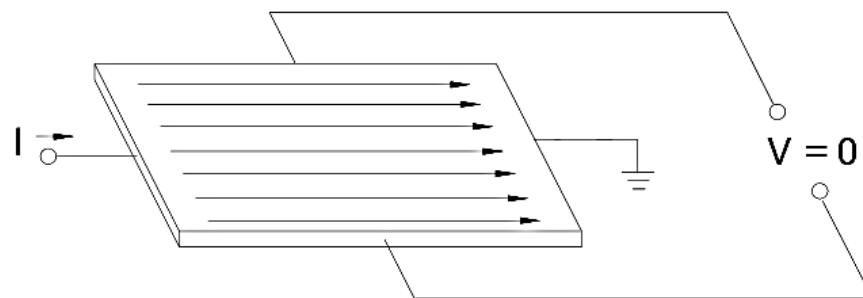


Figure 10: Hall effect with no magnetic field [Hesa]

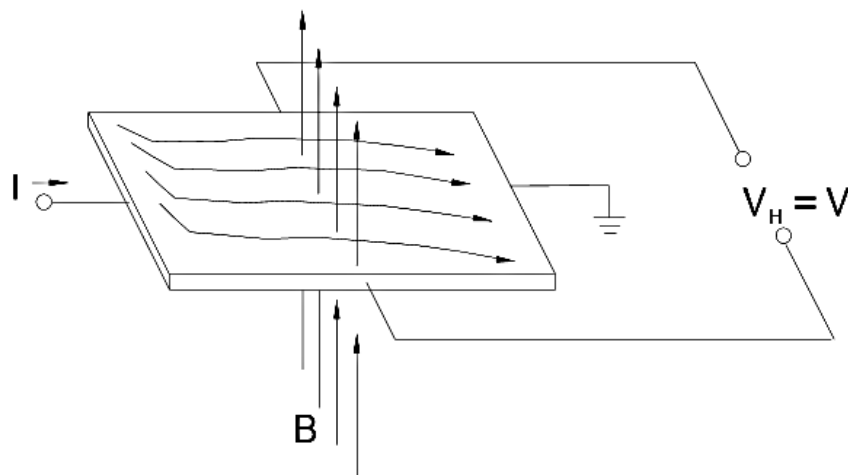


Figure11: Hall effect with magnetic field [Hesa]

2.2.5. Fluxgate sensors

Fluxgate magnetometers are based on the saturation of magnetic materials. A fluxgate magnetometer consists of a small, magnetically susceptible core wrapped by two coils of wire. An alternating electrical current is passed through one coil, driving the core through an alternating cycle of magnetic saturation. This constantly changing field induces an electrical current in the second coil, and this output current is measured by a detector. In a

magnetically neutral background, the input and output currents match [Evan]. The major application of fluxgate sensors has been in the detection of submarines, location of ferromagnetic bodies, missile navigation [Ripk].

2.3. State of the art for NDT

2.3.1. Some currently used methods in the field of non-destructive testing

2.3.1.1. Magnetic particle inspection

Magnetic particle inspection is a method which is used to locate surface discontinuities in ferromagnetic materials. The basic fundamental principle behind this method is that when a test object is magnetized, any discontinuity in the direction transverse to the direction of the magnetic field will lead to a field leakage. The presence of the leakage field due to the discontinuity can be detected by the application of finely distributed magnetic particles over the surface resulting in the gathering of particles due to the leakage field. These magnetic particles form an outline near the discontinuity and indicate its location, shape, size etc. [Asmh].

2.3.1.2. Magnetic Flux Leakage

This method is based on the same effect as described under 2.3.1.1. The field leakage or the flux leakage can be recorded by the use of magnetic field sensors like GMRs mentioned in section 2.2.3.2. The output signal of the sensors is pre-amplified, with an appropriate gain resulting in the detection of even very small defects [Izfp]. Figure 12 demonstrates the MFL in a ferromagnetic test object with a crack.

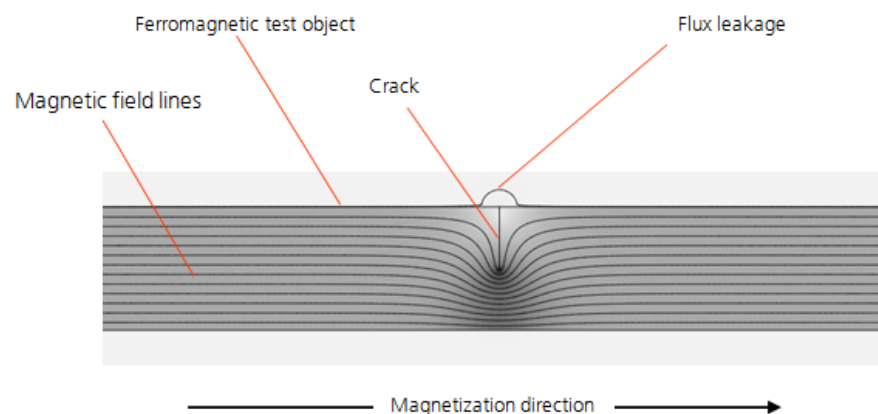


Figure 12: Flux leakage representation with a crack [Szie]

2.3.1.3. Micromagnetic multi-parameter microstructure and stress analysis (3MA)

3MA is a non-destructive electromagnetic testing method developed at Fraunhofer IZFP, whereby testing statistics are derived during magnetic hysteresis cycles. 3MA evaluates electrical and magnetic parameters which are influenced, for instance, by the microstructure, hardness, hardness depth, yield strength and residual stress. A 3MA probe consists of a magnetization unit (yoke core with magnetization coil) in order to magnetize the measuring sample with an alternating magnetic field, a Hall probe for measuring the time signal of the tangential magnetic field component, coil for detecting the magnetic Barkhausen noise, probe system for detecting the eddy current and the incremental permeability and a preamplifier [Izfp]. Figure 13 shows the principle set up of a 3MA probe.

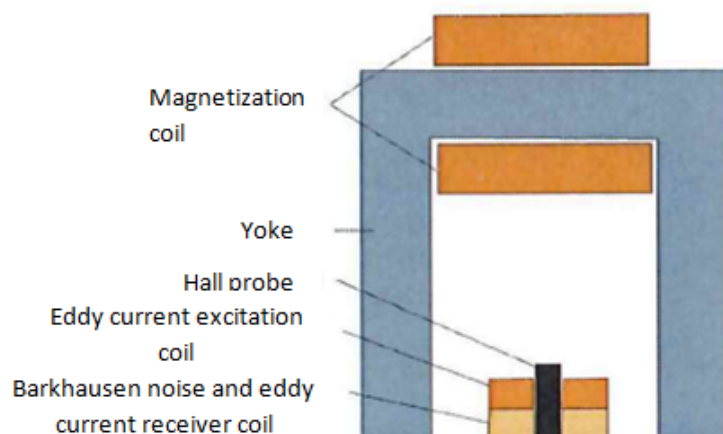


Figure 13: Principle set up of 3MA probe [Izfp]

Figure 14 below shows a standard 3MA probe with curved pole shoes to allow magnetization of flat surfaces as well as surfaces with a curve radius > 62 mm. In order to guarantee a good contact to the sample surface the Hall probe and Barkhausen noise measuring coil are spring mounted.

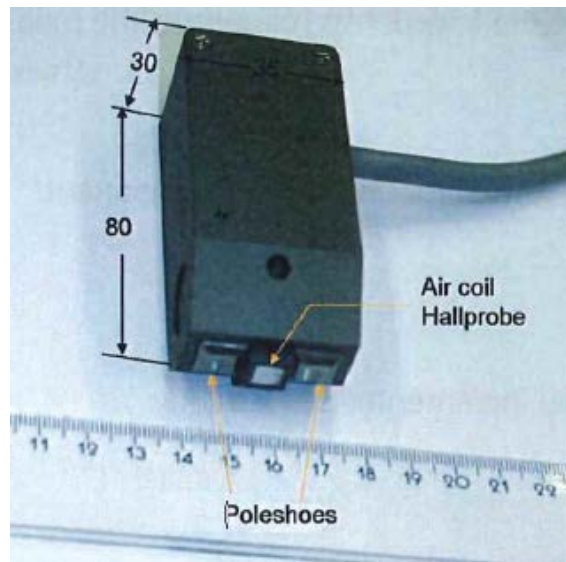


Figure 14: Standard 3MA probe with curved pole shoes and spring mounted sensor carrier [Izfp]

2.3.2. Methods for dia-and paramagnetic materials characterization

The work in this thesis is based on the magnetic susceptibility of the material and the force interaction between the non-ferromagnetic sample and the magnet. In the past, using the concept of magnetic susceptibility of materials and force interaction between sample and magnet, many principles have been developed for the characterization of non-ferromagnetic materials. However, none of these principles are used today in the industrial NDT. All existing solutions have their limitations regarding test object size or shape (some test objects can only be tested in the liquid form or in the form of a rod) of the test object. Hence, to date there has been no non-destructive method developed that could determine the quality or integrity of a non-ferromagnetic material based on magnetic field measurement without altering or testing the object non-destructively. Not much of the focus has been given to the characterization of non-ferromagnetic materials.

Additionally, not many developments have been made in the same area, despite of the many principles developed over the period of time. Some of such methods will be discussed briefly in this chapter.

There are few methods mentioned in the following section which could be used to study magnetic susceptibility of weakly magnetic materials (dia- and

para-). The basis of the principle lies in measuring the force acting on the test object when it is placed in a non-uniform magnetic field. A device used to perform such a measurement is called magnetic force balance or simply a magnetic balance [Cull, Jile].

2.3.2.1. Guoy's scale

Figure 15 below shows the principle set up of a Guoy's balance. The test object is held in a way such that the one end of it is suspended near the centre of the gap in between the parallel magnet pole pieces where the magnetic field is strong and uniform. The other end of the object lies in a region where there is a gradient in the field just near the gap between the edges of the pole pieces. This gradient in the field and the susceptibility of the object and displaced medium determines the force on the test object (whether the object will move up- or downwards). One major drawback of this method is that the test object has to be in the form of a rod and thereby not useful for practical non-destructive testing.

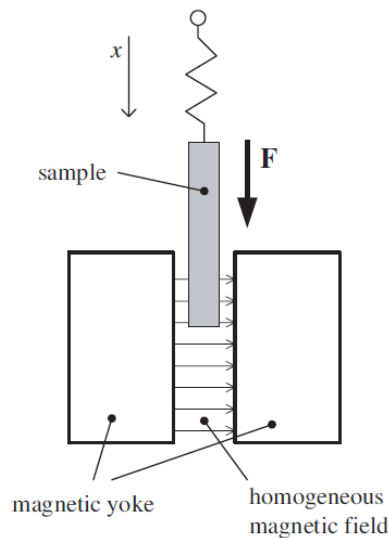


Figure 15: Guoy's method [Osta]

2.3.2.2. Curie method (Faraday method)

This method is also based on the principle of force measurement on the test object. In the physical set-up, the pole pieces of an electromagnet are placed and shaped in such a way that they produce a small region of linear magnetic field gradient in which a very small-sized test object is placed. Additionally, if

using an ordinary electromagnet, a set of small current carrying coils can be placed in the gap between the electromagnet to produce a local controllable field gradient [Cull]. The force is determined by placing the sample in a quartz capsule, suspended at the rod's end which is connected to the balance beam [Klaa]. This method is not that easy to be used as an absolute method since it is difficult to determine the field and its gradient exactly at the position where the sample has been placed. If the calibration is done properly by measurements on samples of known susceptibility, the device is capable of high precision and high sensitivity. The force acting on the sample in the magnetic field with gradient in a direction, for example, in x direction as shown in figure 16 is given by [Osta]:

$$F = \mu_0 \chi V H \frac{dH}{dx} \quad \text{eq. (1)}$$

Where, V is the volume of the sample,
H, is the field strength.

However this method cannot be used in the NDT world since the test samples that can be used must have a mass in the range of 1 to 20 mg [Morr]. A basic principle set up of a Faraday's balance is illustrated in the figure 16.

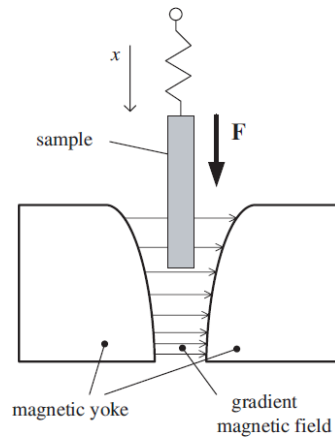


Figure 16: Faraday's balance / Curie method [Osta]

2.3.2.3. Alternative to magnetic balances

Spencer et al. proposed a substitute for Guoy and Faraday balances for measuring magnetic susceptibility of para- and diamagnetic materials. The basic theory behind is that the period of a pendulum changes when a

magnetic field is applied to the test object which is hung to the pendulum. The period of the pendulum is measured using a laser beam which is captured by a photodiode [Spen]. Figure 17 shows the principle set up for the proposed method. However, this also restricts the sample shape and size, thereby not so useful in NDT.

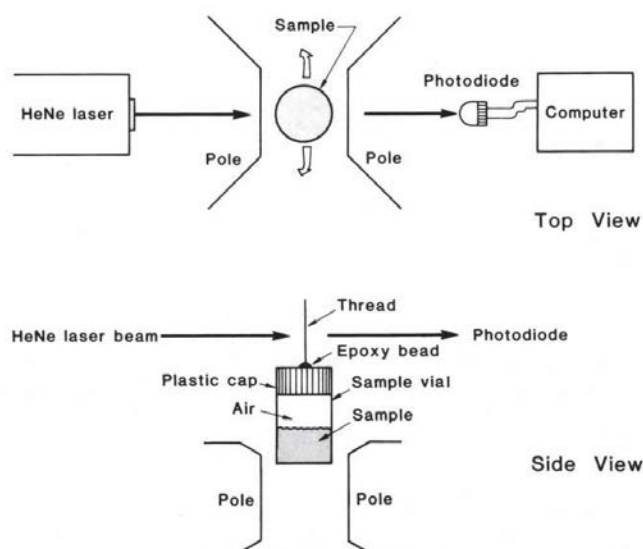


Figure 17: Alternative to Faraday's and Guoy's balance [Spen]

2.3.2.4. Quincke's method

Quincke's method is majorly used to determine the magnetic susceptibility of many liquefied materials and solutions. The solution under investigation is placed in a vertical U-tube with one wide bore at one end and the other with a narrow bore. The narrow end is placed in between the pole pieces of the electromagnet. It should be ensured that the surface of the liquid in the narrow end must align with the line of centres of the pole pieces when the field is off. When the current is switched on a strong field appears at the upper surface of the narrow column while the lower portion will be in a state of weaker field. As a result, a force will act upon the column and if the liquid is paramagnetic it will rise [Amri]. On the other hand, diamagnetic liquids will decrease their level, so that the level reading is proportional to the susceptibility. This method can only test samples in liquid form, hence it is not suitable for most NDT purposes. Figure 18 demonstrates a paramagnetic behaviour of the liquid with an increase in its level on the application of magnetic field.

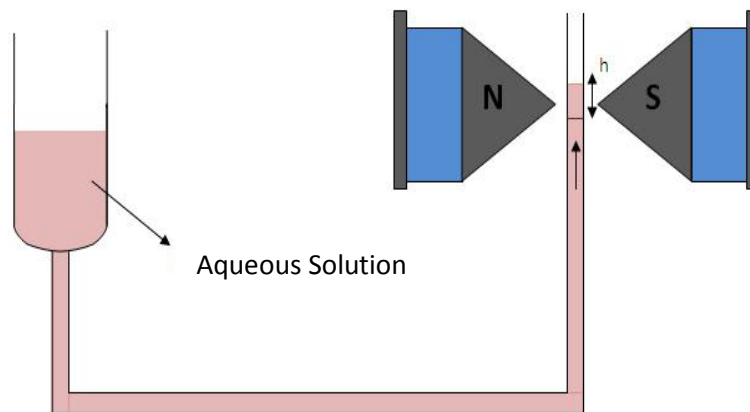


Figure18: Magnetic susceptibility measurement using Quincke's method [Amri]

2.3.2.5. Magnetic force microscopy (MFM)

Magnetic force microscopy is a special mode of operation of the atomic force microscope. Magnetic force microscopy is an imaging technique based on atomic force microscopy [Mart], in which magnetic forces or force gradients are measured to image the magnetic structure of a sample. A cantilever with a magnetic tip is used to measure the magnetic field of a sample via the force, given by the gradient of the magnetic energy. The strength of the local magnetostatic interaction determines the vertical motion of the tip as it scans across the sample. When the magnetic probe is brought near the surface of the sample approximately up to hundred nanometres, due to the mutual magnetic tip and sample interactions, there are considerable amount of changes in the cantilever stage which can be optically detected. These changes form a 2D image as the tip is scanned over the sample [Hend]. MFM reaches a high lateral resolution and allows to image, for instance, domain structure. However, the forces are too low to be applied to the characterization of dia- and paramagnetic materials. Figure 19, shows the MFM image of 100x100 micron scan of a transformer steel (FeS).

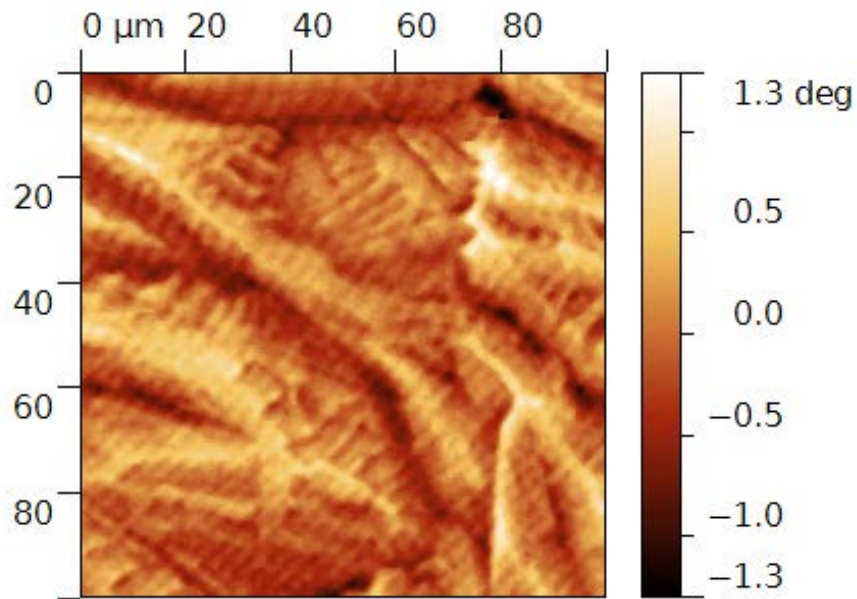


Figure 19: MFM image showing 100x100 micron scan of transformer steel [Amir]

2.4. Measurement Techniques

Two of the measurement techniques which have been used in this thesis to develop a sensor for the materials characterization of dia- and paramagnetic materials, have been briefly discussed below and how these techniques are implemented in developing a sensor has been explained in the next chapter.

2.4.1. Strain gauge

a) Strain

When a force is applied on a body, it leads to some deformation of the body, which is termed as strain. We can also express strain as a fractional change in length. Strain can be positive (tensile) or negative (compressive). Since it is defined as the ratio of change in length over original length, strain is dimensionless.

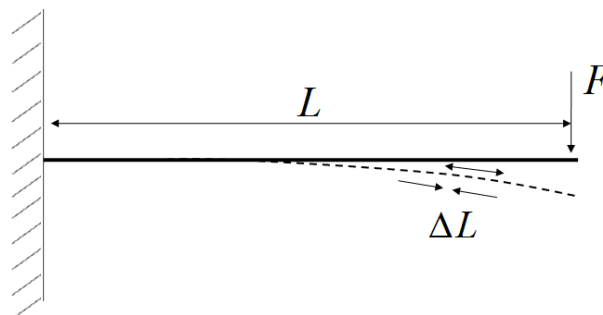


Figure 20: Strain depiction

According to the figure 20,

$$\text{Strain} = \varepsilon = \frac{\Delta L}{L} \quad \text{eq. (2)}$$

b) Principle of strain gauge

A strain gauge is made up of very thin and fine metallic wires arranged in the pattern of a grid as shown in the figure 21. Whenever a force is experienced by a strain gauge, the length of the wire (arranged in the grid pattern) increases, and its width and thickness decrease which affects its resistance. This change in resistance of the conductor can be measured easily and calibrated against the applied force. Thus strain gauges can be used to measure the effect of force exerted on a material. The input and output relationship of the strain gauges can be expressed by the term gauge factor or gauge gradient, which is defined as the change in resistance R for the given value of applied strain [Nati]. The technique how strain gauges have been used in the material characterization of dia- and paramagnetic materials has been explained in the next following chapter.

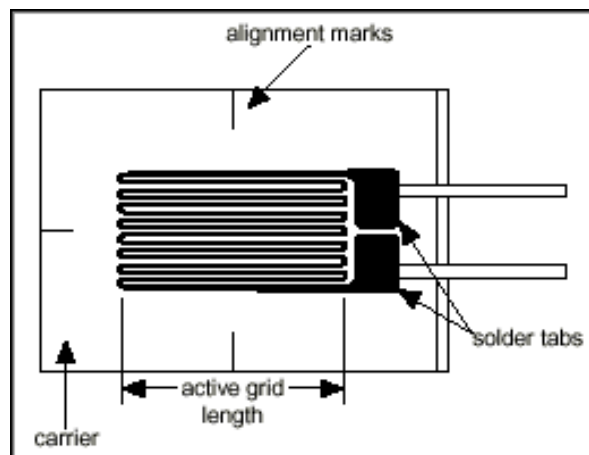


Figure 21: Strain gauge [Nati]

2.4.2. Capacitive sensor

The basic principle behind a capacitive sensor is based on the operation of an ideal parallel plate capacitor. The two electrodes are represented by the sensor and the opposite measuring object. The amplitude of the alternating

voltage on the sensor is proportional to the distance between the capacitor electrodes provided a constant alternating current flows through the sensor capacitor [Micr]. An ideal diagram of a capacitive sensor has been shown below in figure 22 and how this technique has been used to characterize dia- and paramagnetic materials has been explained in the next following chapter.

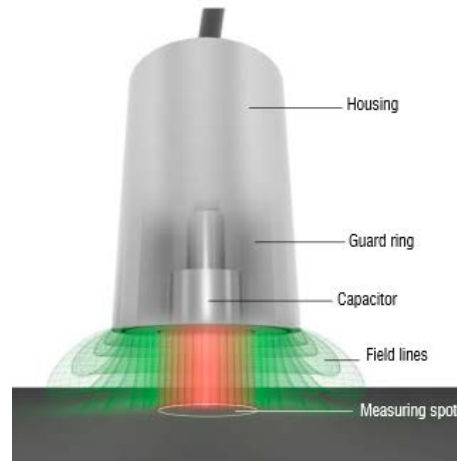


Figure 22: A capacitive sensor [Micr]

Chapter 3: Concept of novel NDT techniques

This chapter discusses the different concepts used in this thesis to characterize different materials as dia-or paramagnetic materials, the principles of which are described here.

3.1. Materials of interest

Since graphite is a well-known diamagnetic material and aluminium is paramagnetic in nature, hence, these samples are tested in the principles proposed below.

3.1.1. Graphite

Physical measurements of the graphite sample used shown in figure 23: 40 x 40x 10 mm.



Figure 23: Graphite sample used

3.1.2. Aluminium

Physical measurements of the aluminium sample used shown in figure 24: 40 x 40x 10 mm



Figure 24: Aluminium sample used

Other materials of interest which are studied in this work are different types of plastics, silicone glue, carbon fiber reinforced plastic (CFRP), pertinax (composite material from paper and a phenol formaldehyde synthetic resin), glass, brass etc. All these materials are non-ferromagnetic in nature.

3.2. Different principles

3.2.1. Measurements using a fluxgate magnetometer

The basic principle of a fluxgate magnetometer has been explained in chapter 2. This concept can be used to measure the response of the test samples to the applied external field as an output voltage when made to scan/move over the samples. The initial idea is to use one single magnetometer and to scan it over the samples and measure the output voltage. Since, the fluxgate magnetometers are highly sensitive and can easily be affected by near and far fields, in order to increase the effect size (signal to noise ratio), a differential set-up can be used. Further, the results could be improved by using an instrumentation differential amplifier, if the need be.

3.2.2. Force based measurements

The principle behind this approach is to check the interaction of forces between the magnet and the test sample. Since the magnet has its own magnetic field, which due to the magnetic susceptibility of the sample, will make the sample exhibit its magnetic properties and either attract (paramagnetic) the magnet or repel (diamagnetic) the magnet.

3.2.2.1. Precision balance

A precision balance can be used to measure the change in the weight when a test sample is brought near the magnet. Under the influence of the magnetic field of the permanent magnet which is placed on the balance, the sample when brought near to the magnet exhibits its magnetic susceptibility and displaying a positive or negative change in the reading. In case there is an attraction between the sample and the magnet, the magnet will tend to rise (attract the sample), which will impact its weight on the balance, and the reading will fall towards negative. In case, the sample repels the field of the magnet, the magnet will be pushed downwards by the sample, thereby increasing the weight reading to a positive value.

3.2.2.2. Cantilever based methods (Scanning system set-up)

The force based principle can be applied by using a simple cantilever which is free at one end and the other end is fixed. The magnet is attached to the free end of the cantilever on which the force is exerted by the sample when it is brought near to the sample as shown in figure 25.

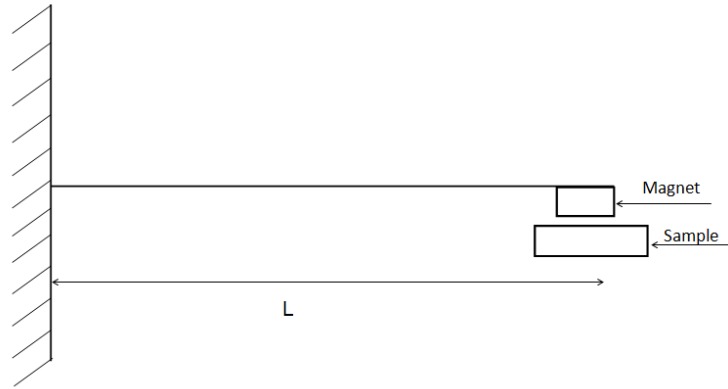


Figure 25: A schematic for cantilever based approach

3.2.2.2.1. Measurements using strain gauge

When the sample is exposed to the magnet fixed on the free end of the cantilever, it will lead to some deflection of the cantilever, calculating method of which is briefly presented in the following section. This deflection can be recorded as a strain experienced on the cantilever as a change of resistance by using a standard strain gauge on the cantilever.

To measure the strain, one needs highly accurate measurement of the small changes in the resistance. To measure such small changes in resistance, strain gauges are used in a Wheatstone bridge configuration with a voltage excitation source. A general Wheatstone bridge, as shown in figure 26 consists of four resistive arms with an excitation voltage, V_{in} , that is applied across the bridge. The output voltage of the bridge, V_{out} , is equal to [Nati]:

$$V_{out} = \left[\frac{R_3}{R_3 + R_4} - \frac{R_2}{R_1 + R_2} \right] V_{in} \quad \text{eq. (3)}$$

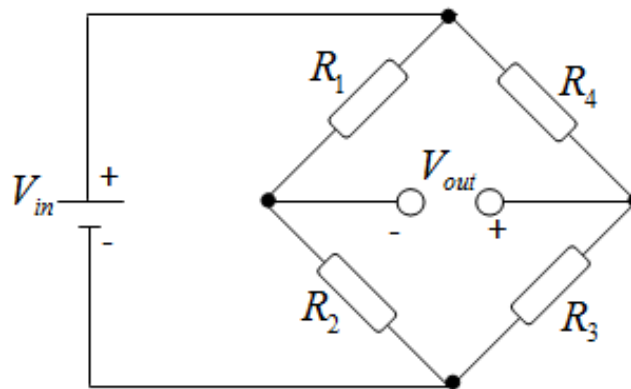


Figure 26: Wheatstone bridge

It is well known that the bridge is said to be balanced when the output voltage V_{out} is zero i.e., $\frac{R_1}{R_2} = \frac{R_4}{R_3}$. Any change in resistance in any arm of the bridge results in a non-zero output voltage and that's where the concept of measuring a strain using a strain gauge is applied.

3.2.2.2.2. Measurements using a capacitive sensor

The principle of capacitive distance measurement system is based on the concept of a standard parallel plate capacitor as explained in last chapter. For conductive targets, as used here, (though the cantilever's material is FRP, but a coat of copper is there to make it conductive) the sensor and the target (cantilever, in this case) opposite form the two plate electrodes. If a constant alternating current flows through the sensor capacitor, the amplitude of the voltage in the sensor depends on the distance between the two electrodes of the capacitor. Under the influence of magnet, the sample responds either by attracting the magnet or repelling the magnet which will lead to the deflection of the cantilever. As a result, the distance between the cantilever and the capacitive sensor (electrodes) will change. This deflection will lead to the change in the voltage. The voltage is demodulated, amplified and is measured as an analog signal at the output. These voltages are scaled by the measuring electronics in a way that they represent specific changes in distance. For a given amount of distance, the change in the voltage defines the sensitivity of the sensor. In this case, the sensing range is 1mm and the

maximum output is 10 volts which means that for every 0.1 mm change in distance, the output voltage changes by 1 Volt. Figure 27 below demonstrates the ideal schematic for the set up. However, a better set up and improvements have been shown in chapter 6.

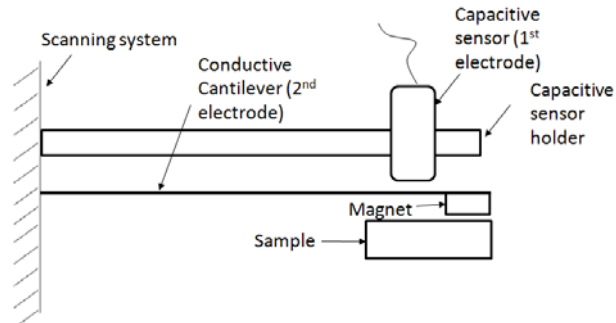


Figure 27: Ideal set up for using a capacitive sensor for measuring deflection

3.2.2.2.3. Types of cantilever used

Various types of cantilevers were used during the whole course of this thesis and based on the results the cantilever for the last method using a capacitive sensor was finalized.

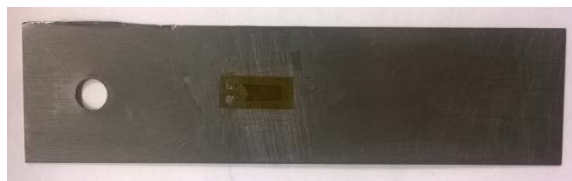
a) Pertinax

Dimensions: 115 x 25 x 0.5 mm



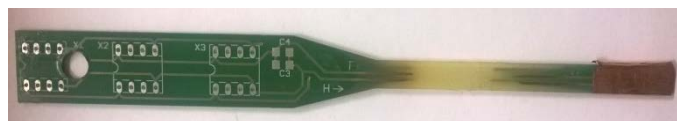
b) Soft steel

Dimensions: 100 x 25 x 0.5 mm



c) Fibre reinforced cantilever (FRP 1)

Dimensions: 135 x 15 x 0.5 mm



d) Fibre reinforced cantilever (FRP 2)

Dimensions: 160 x 15 x 1 mm



e) Fibre reinforced cantilever (FRP 3)

Same material as 'd' with different dimensions

Dimensions: 120 x 10 x 1 mm

3.2.2.2.4. Deflection calculation method

Based on the calculations of the deflection for the cantilever, suitable dimensions were determined. The need was to have an observable and detectable deflection but at the same time a cantilever with a material which does not get affected by temperature over the period of time. Hence, fibre-reinforced plastic is used as a final cantilever. Using the mathematical formulae for the deflection, the dimensions of the cantilever are finalized.

$$\delta = \frac{F \times L^3}{3 \times E \times I} \quad \text{eq. (4)}$$

Where, δ is the deflection,

L is the length of the sample,

F is the force applied,

E is the elasticity modulus,

I is the inertial moment.

$$I = \frac{b \times h^3}{12} \quad \text{eq. (5)}$$

Where, b is the width of the sample,

And h is the height of the sample.

For example, for the soft steel cantilever with dimensions.

L = 100 mm

b = 25 mm

h = 0.5 mm,

Using equation (5), Inertial moment is calculated.

And then putting the value of inertial moment in equation (4). The amount of deflection is calculated. For soft steel [E], $E = 200 \times 10^9 \text{ N/m}^2$,

Putting all the values determined in equation (4) results in a deflection of 64 microns on the application of 1 mN force.

3.2.2.2.5. Types of magnets used

A) Type of magnet: Cylindrical

Dimensions: 10 x 5 mm

Magnet material: Neodymium-Iron-Boron (NdFeB)



B) Type of magnet: Cylindrical

Dimensions: 10 x 10 mm

Magnet material: Neodymium-Iron-Boron (NdFeB)



3.2.2.2.6. Types of motion during scan

To determine the type of motion of the scanning system / sample, was also an important factor. Results have shown quite an effect of the motion. Following section covers the types of motions used during the scan of a sample.

a) Continuous motion

In this type of motion, the sensor (cantilever holding set up) / sample is made to move continuously in linear motion without any pause. This type of motion is useful in case high speed scans are required as it saves time. However, this type of motion may result in some loss of information which is demonstrated in the capacitive sensor section. Normally, the continuous scan speed used in the experiments in this thesis is 50 mm/s. Wherever a different scan speed is used, it has been mentioned along with the result. For an area scan of 160mm X 60mm in continuous motion, it takes about 1 hour 15 minutes in the scan speed of 50 mm/s.

b) Wait and move motion

The need of 'wait and move' motion was realized after the use of cantilever based approach since due to the continuous motion of the sensor, the cantilever never got enough time to return to its equilibrium position before it could take the next reading. The idea behind the wait and move motion is

that, the sensor moves a step, say for instance, 1 mm, then waits for enough time like around 1500 ms, and then records the reading. The wait concept is introduced so as the cantilever returns to its equilibrium position and then record the recording. After recording a measurement at one point, the sensor moves the next step. For an area scan of 160mm X 60mm in wait and move motion, it takes about 65 hours with a step size of 0.6 mm in Y direction and 1 mm in X direction. However, the step size doesn't matter since the resolution is defined by the size of the magnet only. But to get a better image with more pixels, the step has been varied in different experiments. In case of quick scans required, the step size can be increased to reduce the time of the scan.

c) Sensor motion vs. sample motion

After many experiments, it was concluded that since the cantilever can always be affected by the motion of the scanner, it is better to move the sample with wait and move motion so, that the cantilever is only minimally affected with the motion of the scanner.

3.3. Relation between susceptibility and force

Since the approaches discussed here are based on force measurements, it is important to note that there is a relation between the susceptibility of a material and the force between sample and the magnet. Equation (6), shows the relation between the two above mentioned parameters. Adapted from [Peym] and [Geim],

$$F_{mag} = \frac{\chi_p \cdot V_p}{\mu_0} B_x \cdot \frac{dB_x}{dx}, \quad \text{eq. (6)}$$

where B_x represents the magnetic field in one dimension, V_p represents the volume of a particle and $\mu_0 = 4\pi \cdot 10^{-7} \text{ Vs/Am}$, in air. If observed carefully, this equation is nearly the same as is equation (1) mentioned in chapter 2, under 'Curie method (Faraday's balance)' given by [Osta] to determine the susceptibility and force relation between the sample and the magnet.

It is assumed that under normal conditions, force acting on the whole test sample is sum of all the forces acting upon the single particles. Hence, for the simplification factor, force on a single particle is considered and susceptibility-

force relation of a single particle can be determined from the above mentioned formula.

Figure 28 shows the variation of the field strength, H , over a cylindrical permanent magnet with dimensions 10 x 10 mm, with increasing distance. The field strength has been measured using a Hall sensor and air as the medium. Depending on the location of any given particle with susceptibility χ from the sensor, H can be determined from the graph and then, using the formula (this case is without any sample and air as the medium);

$$B = \mu_0 H ; \quad \text{eq. (7)}$$

the magnetic field B in a specific particle's location can be calculated. As per formula (6), only B and its first order derivative need to be calculated to determine force interaction between the particle and the magnet.

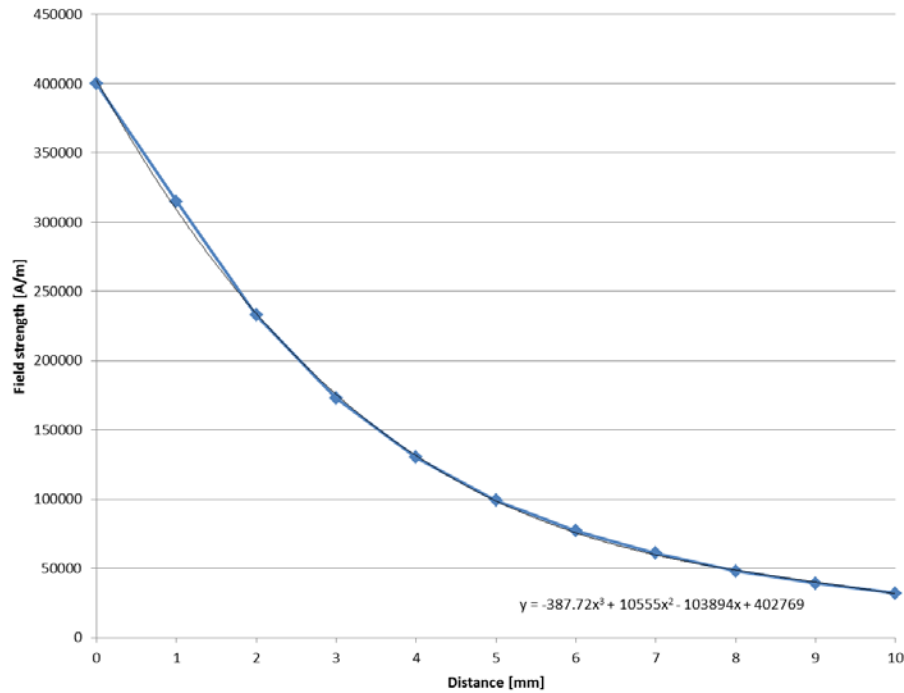


Figure 28: Field strength over distance using just a permanent magnet with air as the medium

As seen in the graph, a curve has been fit to match the field strength curve with equation shown in graph, where y is H and x is the point where H needs

to be determined. Multiplying H with μ_0 will give B . The equation shown in the graph can be differentiated in order to get $\frac{dB_x}{dx}$ parameter in the formula (6). It is interesting to note that susceptibility of a particle is directly proportional to the force exerted by the sample. It is very difficult to calculate susceptibility precisely, as it may vary with sample size and moreover the force exerted by every particle on the magnet is also not constant and may vary as per its location. However this method cannot exactly be used as it is for the cantilever based approach since, in the cantilever based approach, the force on the magnet varies the distance between the magnet and the sample. For normal situations, the force and susceptibility relation might be assumed as per equation (6). However, if a material is highly dia- or paramagnetic, it will deflect the cantilever to a larger extent. As a result, when the gap between the magnet and the sample increases, the force will decrease and vice versa. This formula can be used in cantilever based approach; however some errors might be expected from measurements. To precisely calculate the relation between the force and susceptibility in the cantilever based approach is quite complex and is beyond the scope of this thesis.

3.4. Force over distance

Figure 29 studies the relation of force over distance. It has to be noted that in this case using the equation (6), just the product $B \cdot \frac{dB_x}{dx}$ has to be determined for studying the force effect. However, for the calculation simplification, only $H \cdot \frac{dH_x}{dx}$, ($B = \mu_0 H$, where μ_0 is just a constant) has been plotted as a force factor. A red curve is a curve for an exponential equation which nearly fits the force factor curve. This implies that force over distance decays exponentially.

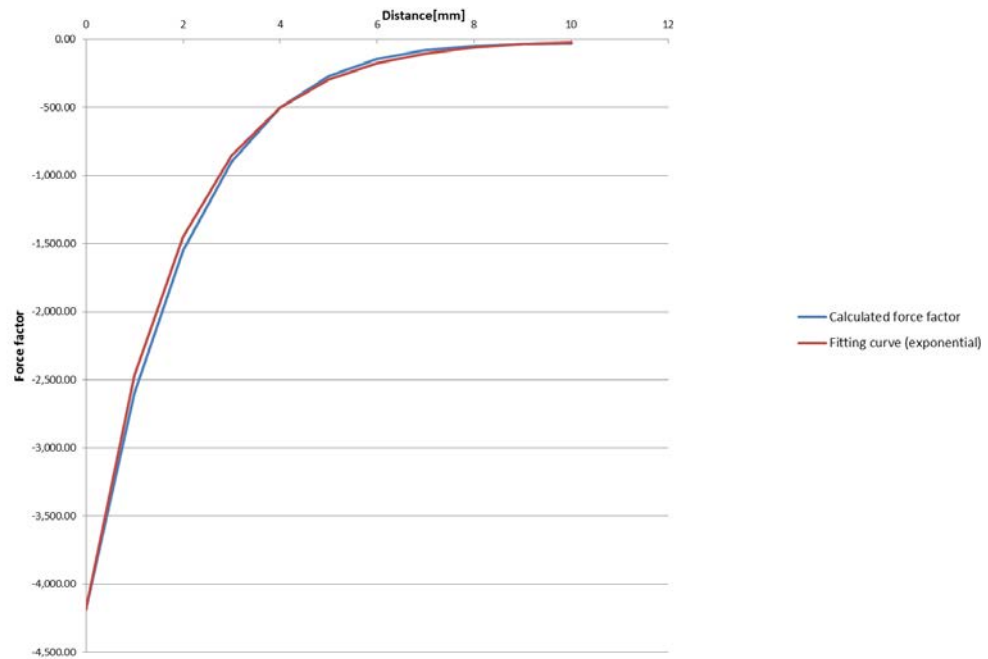


Figure 29: Graph showing the exponential decay of force over distance

3.5. Types of filters used

Following are the types of filters used for the signal and image processing of the results throughout the course of this thesis.

- a) **Subtract X-trace:** In this filter, a reference X-line is picked and its trace is subtracted from all the X-lines in the image.
- b) **Subtract Y-trace:** In this filter, a reference Y-line is picked and its trace is subtracted from all the Y-lines in the image.
- c) **Set reference – Subtract reference:** This filter enables to set all signals of one scanned level as a reference. These reference signals can then be used and subtracted from signals of another scanned level.

Chapter 4: Materials characterization and property imaging with fluxgate magnetometer

In the following experiments a fluxgate sensor from Stefan Mayer Instruments, FLC, has been used [Stef]. The magnetic field sensor FLC 100 is a fluxgate magnetometer with high resolution for the measurement of weak magnetic fields up to $100\ \mu\text{T}$. Application of this sensor can be where the sensitivity and stability of conventional magnetic field sensors (Hall or MR sensors) is too low, e. g. for the measurement of the earth's magnetic field (for navigation) or if ferrous objects should be detected at larger distances. The analog output voltage is proportional to the component of the magnetic field parallel to the detection coil. It has a single 5 V supply voltage and low current consumption of 2mA. The excitation frequencies are typically 17 kHz [Stef]. Figure 30 shows an image of the fluxgate used here.

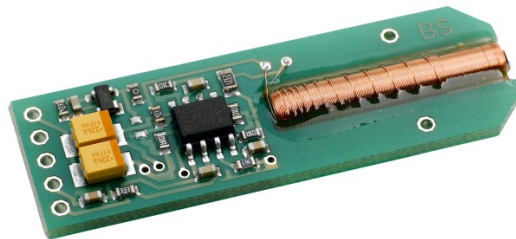


Figure 30: Fluxgate magnetometer used, FLC 100 [Stef]

4.1. Single fluxgate magnetometer

The single fluxgate magnetometer FLC100 is mounted mechanically on the scanning system which helps in determining the motion of the sensor. At a distance of approximately 25 cm, a rectangular permanent magnet of 30 x 30 x 5 mm is placed exactly under the sensor so as to provide external magnetic field in the whole set up. This distance can be varied, however it should not be too close to the sensor as it might saturate the sensor. The sample is held just below the sensor in case it is not conducting as this may induce eddy currents and might affect the sensor electronics. The set-up is fixed in a way that the magnet and the sensor always move simultaneously and the sample remains fixed at its position. Figure 31 demonstrates the idea of the physical set-up.

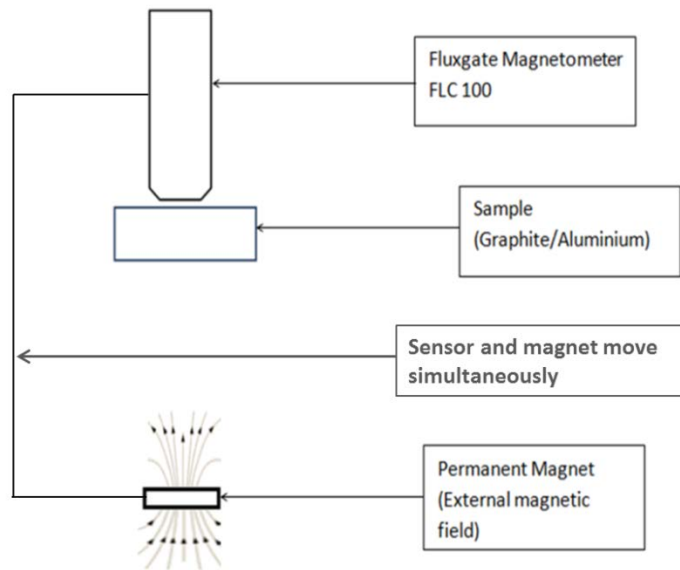


Figure 31: Ideal physical set up

A fluxgate sensor can sense any change caused by ferromagnetic materials in the surroundings and can easily be affected by near and far field influences. Thus, along with the measurement of the test object, many unwanted results could also be noticed. Figure 32 shows the scanned image of the graphite sample when tested with a single fluxgate magnetometer. The rectangular part highlighted in the image shows that graphite behaves diamagnetic and thus opposes the external magnetic field applied, therefore delivering a drop in the signal value which is demonstrated in Figure 33.

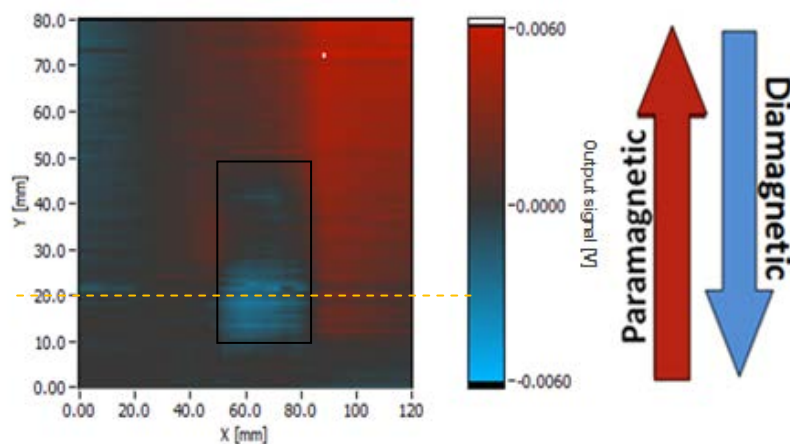


Figure 32: Generated image of graphite

Experiments with the single fluxgate magnetometer have shown that they are highly sensitive to near and far field influences. Hence, it is quite assumable that the fluxgate senses something ferromagnetic on the right side of the scan and thereby giving a paramagnetic effect. This noise could be removed by using a differential set up as shown in the next section. Figure 33 shows the graph of a line across x-axis direction.

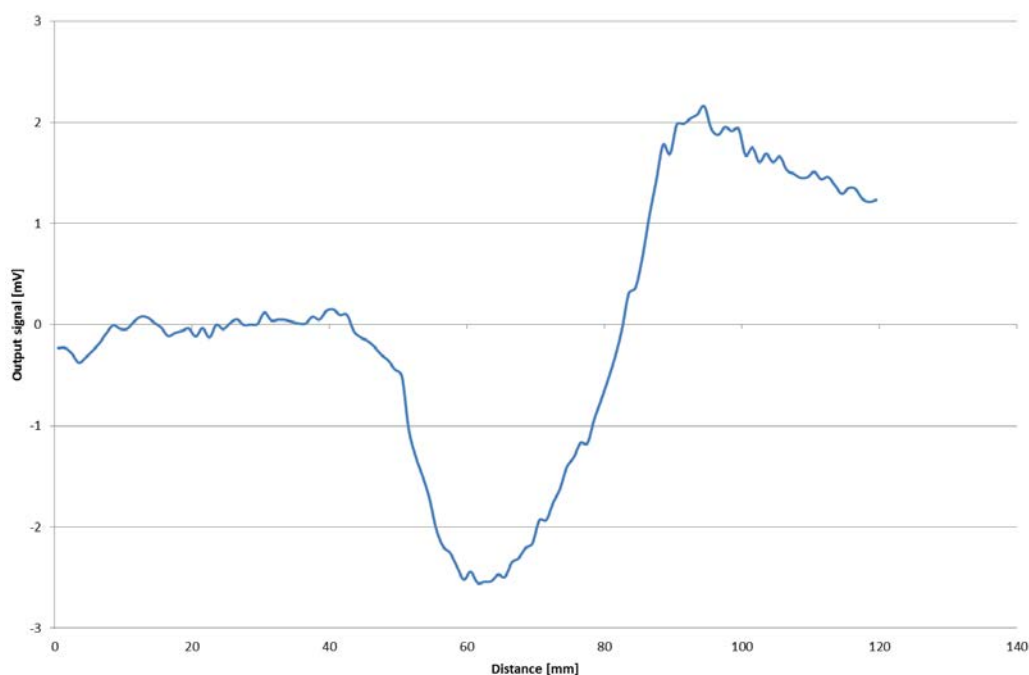


Figure 33: Signal graph for graphite along x-axis highlighted by a yellow dashed line in the scanned image

4.2. Differential mode (Gradiometer set-up)

It is quite evident in figure 33 that there is a gradient and noise in the signal. This could be due to the inhomogenous field around the surroundings at the end points of the scanned area. Using two similar fluxgates in the differential mode helps in eliminating the noise and increasing the effect size of the test object. In this set up the sensors are mounted on the X-axis of the scanning system. In the differential mode here, two FLC100 fluxgate magnetometers are used with one directly near the sample and the other one vertically above the first sensor so that it does not sense the sample but senses the same far field influences as by the first sensor. Then the output of these two sensors is the subtraction of the output of two sensors. In simpler terms, differential

mode can be applicable where there is a need to suppress noise from distant sources to focus on the anomalies from the shallow sources.

4.2.1. Graphite

Figure 35 clearly demonstrates the removal of gradient and noise upto a huge extent. The graph shows the plot along the x-axis of the scan. It is interesting to note that the SNR has improved tremendously. However, this image in figure 34 has also been filtered using a 'Subtract X-trace' filter. In this filter, a reference X-line is picked and its trace is subtracted from all the X-lines in the image. The gradient can be minimized if the whole physical set up of the experiment is placed at a place where there are minimum disturbances in the surroundings.

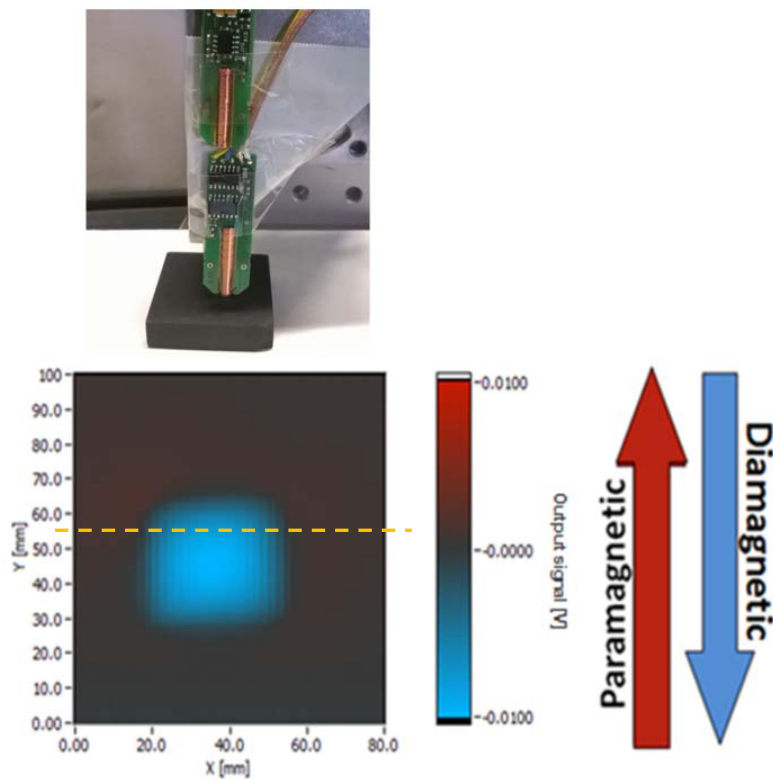


Figure 34: Physical set up (top), Generated image (bottom)

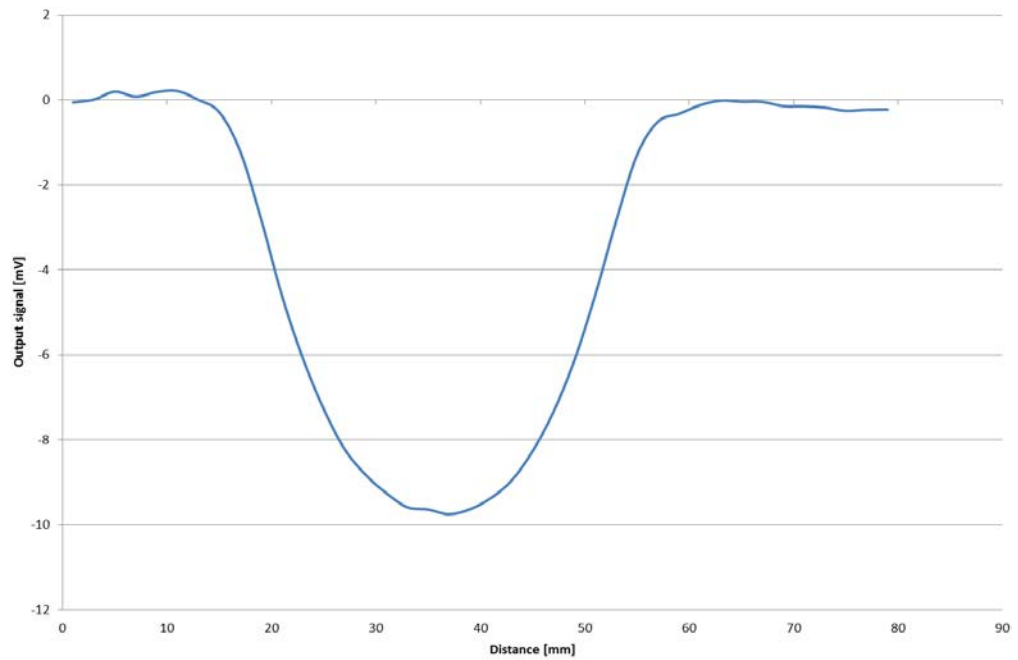


Figure 35: Signal for graphite in differential mode along x-axis direction as highlighted by a yellow dashed line in the scanned image

4.3. Limitations

The differential set up does eliminate noise and the gradient in the signal to a large extent. The signal expected from aluminum is just the opposite to graphite. However, when aluminium is scanned using a fluxgate, it generates a signal as demonstrated in figure 36, hence it is difficult to tell if it is the susceptibility of aluminum which responds to the magnetic field or the conductive nature of aluminum and the eddy current generation. The measuring effect might be superimposed by a damping induced error which makes it hard to tell the difference between conductivity and the susceptibility induced signal changes. In the signal it can be seen that the starting and the end position of the sample can be seen clearly.

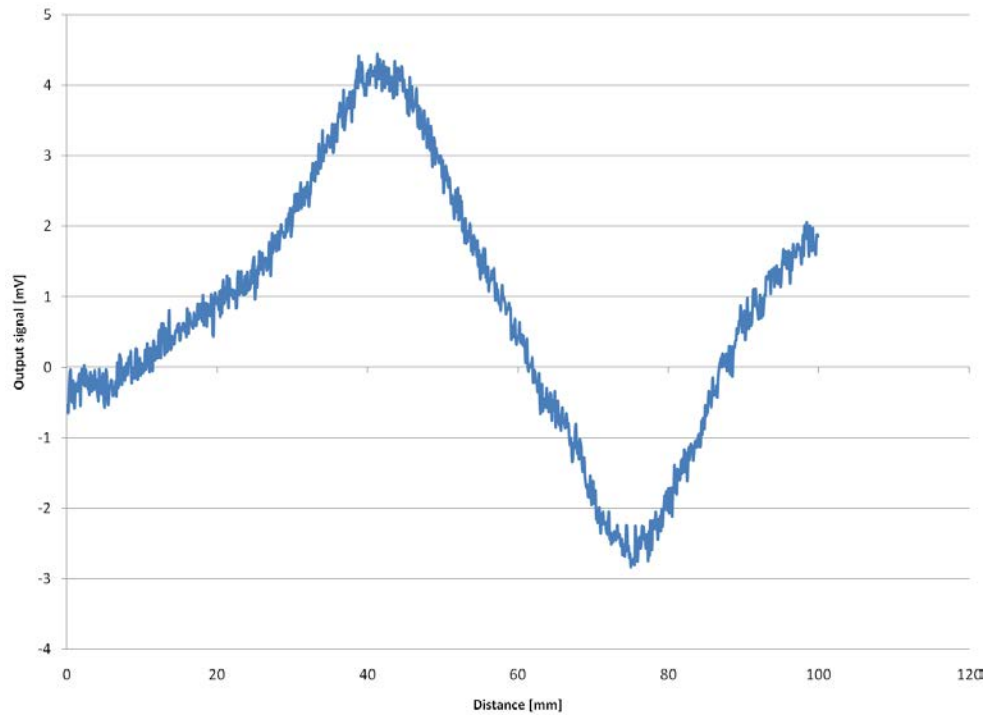


Figure 36: Signal for aluminium demonstrating more of its conductivity than susceptibility along x-axis

4.4. Conclusion

The fluxgate magnetometer can be useful in the non-destructive testing of non-conducting samples like graphite or few more (a result of some food samples is shown in the Appendix). As demonstrated above, the differential set up helps in improving the results for measuring the weak magnetic fields generated due to the interaction between the test sample and the magnetic field of the magnet used in the set up. However, when it comes to the testing of conducting materials, fluxgate magnetometers are ineffective because the measuring effect is superimposed by a damping induced error which makes it hard to tell the difference between conductivity and the susceptibility induced signal changes. Hence, there is a need to develop a method which could evaluate such small magnetic fields just on the basis of magnetic susceptibility. In the following chapters, principles based on the force based effects have been studied with different approaches.

Chapter 5: Material characterization with a precision balance

A regular precision balance has been used here to study the force effect caused by the test samples when brought near to a permanent magnet as shown in figure 37 below. The principle has been discussed in detail in the next section.

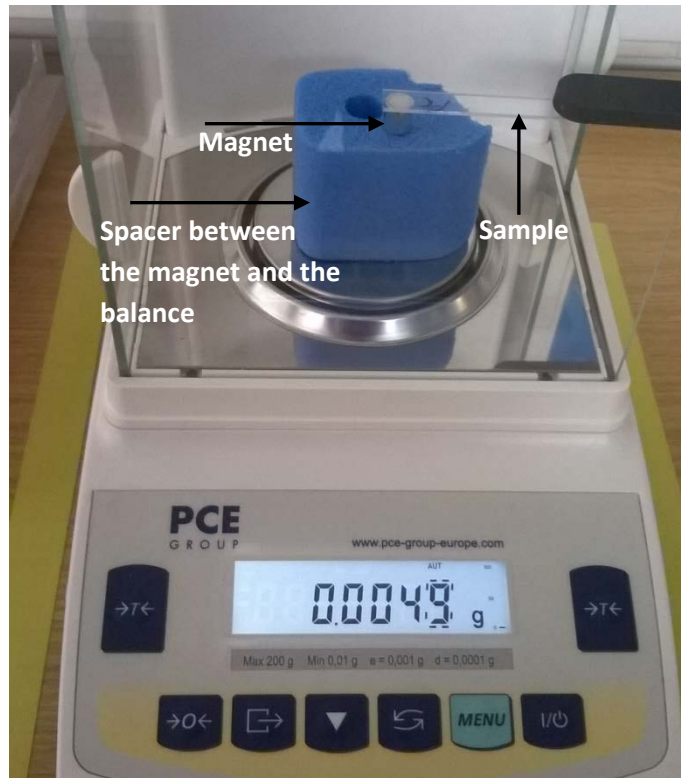


Figure 37: Precision balance used

5.1. Set-up

Based on the principle of Faraday's and Guoy's balance, in this approach, a high precision balance (load cell) is used. Due to high sensitivity, it is necessary that the balance is placed on a stable ground with no mechanical vibrations and airflows. A small magnet is placed at the centre of the pan over a spacer where the specimen is usually placed for its weight measurement. The principle behind this approach is to check the interaction of forces between the magnet and the test sample. Since the magnet has its own magnetic field, which, due to the magnetic susceptibility of the sample, will make the sample exhibit its magnetic properties and either attract (paramagnetic) the magnet or repel (diamagnetic) the magnet. Initially, when the magnet is put

on the precision balance, its weight is displayed. Then the reading is made to zero. The sample is brought near the magnet avoiding any physical contact. Under the influence of the magnetic field of the permanent magnet, the sample exhibits its magnetic susceptibility and changing the reading from zero to either positive or negative. In case there is an attraction between the sample and the magnet, the magnet will tend to rise (attract the sample), which will impact its weight on the balance, and the reading will fall towards negative. In case, the sample repels the field of the magnet, the magnet will be pushed downwards by the sample, thereby increasing the weight reading to a positive value. All the readings measured are in grams which are converted to mN with a factor:

$$\text{Since, } F = m \cdot g \quad \text{eq. (8)}$$

So for 1 gram-force = 9.80665 ~ 9.81 mN

Magnet used is 10 x 10 mm cylindrical magnet

5.2. Evaluation

In this experimental approach, graphite, aluminium and some different types of plastics are examined when brought near to the magnet with no contact. After placing the magnet on the measuring pan, the reading of balance is reset to zero so as to simplify the readings when specimen is brought near to it. The specimen is brought near the magnet approximately 1mm (since it is done manually, the exact distance of 1mm is difficult to maintain with different specimens). Aluminium as expected displays a paramagnetic behaviour since the reading displayed is negative, which in principle means the magnet is attracted towards the aluminium. However, in case of graphite, it repels the magnet and results in pushing the magnet towards the plate, thereby increasing the reading on the balance, as expected from its diamagnetic behaviour. Figure 38 shows the evaluation of different types of plastics. Figure 39 shows the graphite and aluminium effects over distance.

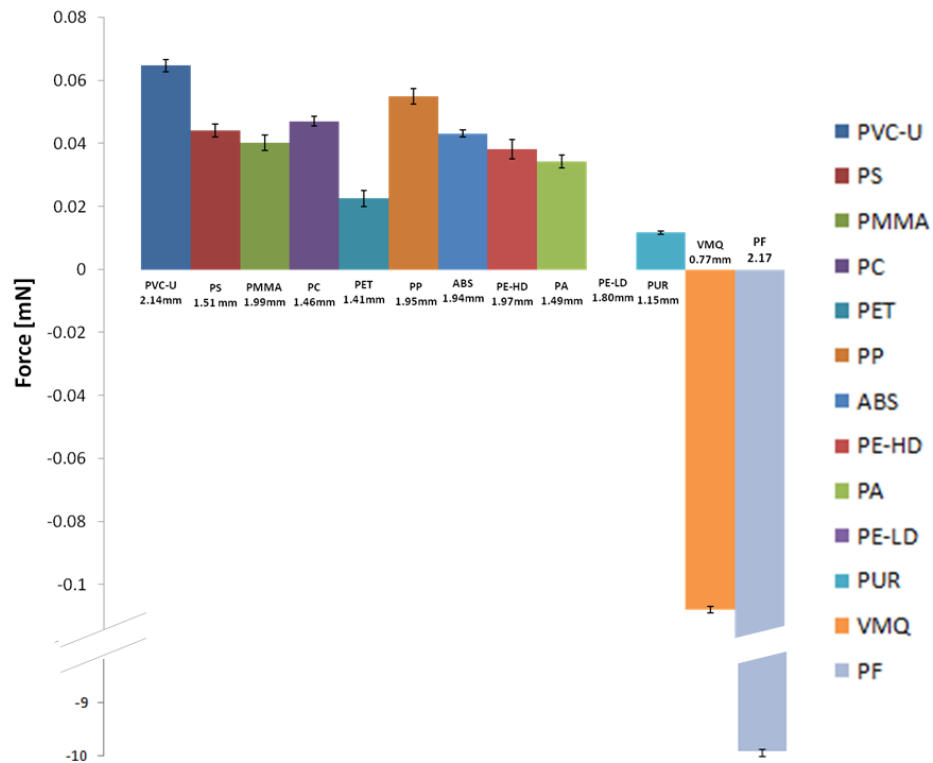


Figure 38: Evaluation of different plastics

In the figure above following are the plastic materials examined. The values in mm displayed near the bars indicate the thickness of the material. However, in case of PF it is expected that it is due to the ferromagnetic contamination in the sample. The error bars are computed taking standard deviation into consideration for each sample.

- PVC-U - Polyvinylchloride - unplasticised
- PS - Polystyrene
- PMMA - Polymethyl methacrylate
- PC - Polycarbonate
- PET - Polyethylene terephthalate
- PP - Polypropylene
- ABS - Acrylonitrile butadiene styrene
- PE-HD - Polyethylene, high density
- PA - Polyamide
- PE-LD - Polyethylene, low density
- PUR - Polyurethane
- VMQ – Vinyl methyl polysiloxane (Silicone rubber)
- PF - Phenol formaldehydes

Additionally, the distance dependency of forces between the specimen and the magnet over different distances has also been studied, results of which are as follows. This approach is quite useful but since all the things are done manually with hands and the distance between the sample and the magnet was also adjusted with hands without any scale, there is quite a scope of mis-measurement. However, an idea of the force decay can be interpreted.

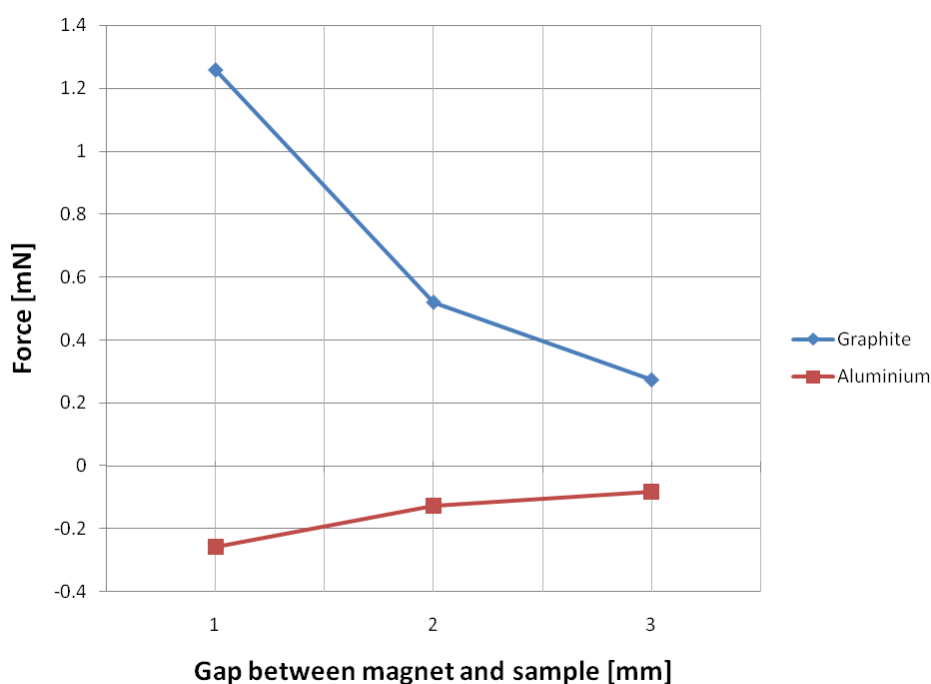


Figure 39: Distance dependency

5.3. Limitations

This approach is quite practical when the goal is just to determine the behaviour of the material, whether the material is paramagnetic or diamagnetic. The ferromagnetic materials will impact the reading on a very large scale. Since the experiments are done manually, it was difficult to maintain a gap of 1mm precisely between the sample and the magnet which might have affected the readings noted with different samples. If there is a need of exact and detailed results, this approach is not practical. However if somehow, the gap between the different samples and the magnet could be controlled perfectly and made constant throughout, this method could be used to generate the images of the sample by scanning the balance is made to communicate with the computer over serial communication and the required data could be recorded using data acquisition boards and the whole

method could be automated. The balance used in this approach was not sensitive enough to determine the impact of some plastic materials like PE-LD. However, this force based approach led to a new idea of sensing the materials using strain gauges which is described in the following chapter.

Chapter 6: Material characterization and susceptibility imaging using a cantilever based approach

The idea of utilizing the effect of force on the magnet by the test sample has proved to be quite informative regarding the determination of dia-and paramagnetic property of various materials. However this principle can be applied by using a simple cantilever which is free at one end and the other end is fixed. The magnet is attached to the free end of the cantilever on which the force is exerted by the sample when it is brought near to the sample.

6.1. Measurement with a strain gauge

In this approach, a cantilever is mounted on to the scanning system. The cantilever holds the magnet at its free tip. The strain gauge is attached on the surface of the cantilever which measures any kind of strain or force exerted on the magnet when it moves over the specimen. It is very important that the strain gauge is properly mounted with full contact onto the cantilever so that the strain is accurately transferred from the cantilever to the gauge. The sample is made stationary at one point and using the scanning system, the cantilever carrying the magnet moves over the sample. This approach is tested with three types of cantilevers made of soft steel, pertinax and an FRP (fibre reinforced plastic), the results of soft steel and FRP cantilever are demonstrated in the following sections. Pertinax was too flexible to be firm and used to bend over the period of time while the scanning system used to move and after some time made undesired contact with the sample.

6.1.1. Using one strain gauge/ Quarter bridge

If one of the resistors in the Wheatstone bridge in figure 26 explained in chapter 3, is replaced with an active strain gauge, any changes in the strain gauge resistance will unbalance the bridge and produce a non-zero output voltage. Figure 40 shows a quarter bridge circuit. This approach worked but however the results were very noisy and the signal to noise ratio was poor and the idea of using two strain gauges in a half bridge circuit had to be implemented, the result evaluation of which has been demonstrated in the next section.

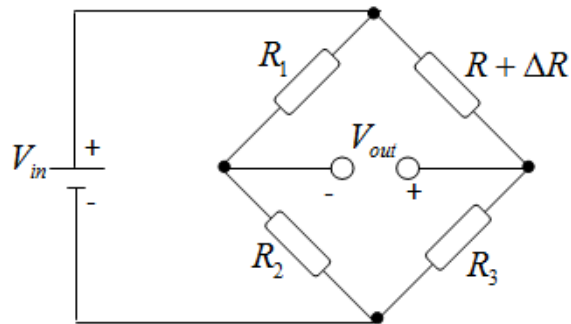


Figure 40: A quarter bridge

6.1.2. Half bridge circuit using two strain gauges

The sensitivity of the bridge to strain can be doubled by making two gauges active in a half-bridge configuration as shown in figure 41. One bridge is mounted in tension and the other is mounted in compression above and below the cantilever. Using a half bridge configuration yields an output voltage that is linear and approximately doubles the output of the quarter-bridge circuit in addition to the suppression of thermal influences which are quite prominent in the quarter bridge circuit.

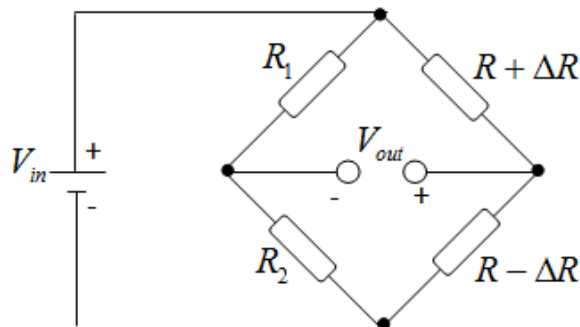


Figure 41: A half bridge circuit

6.1.2.1. Graphite using a soft steel cantilever

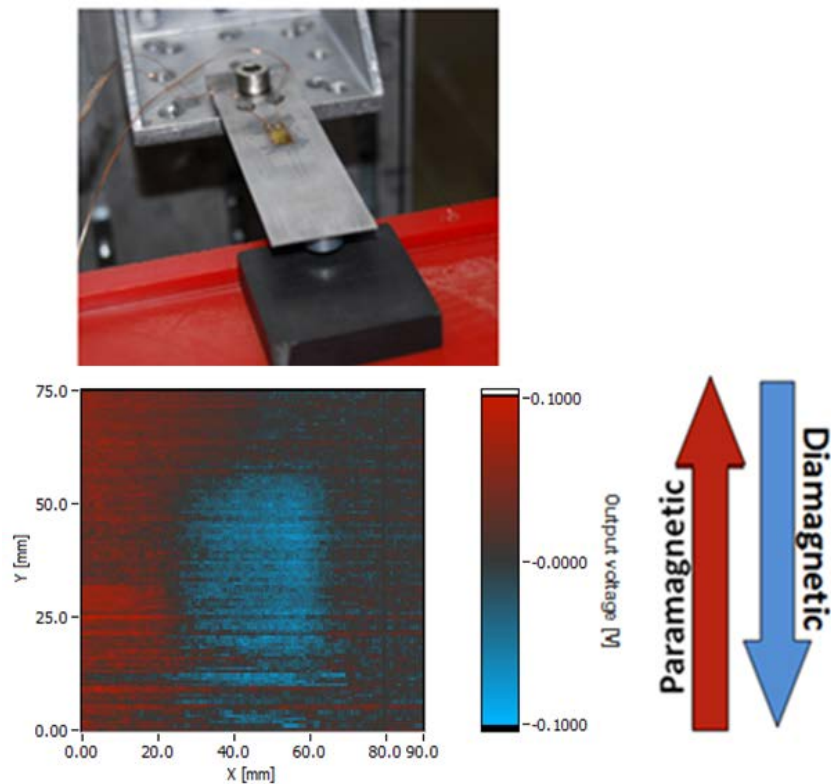


Figure 42: Set up (top), Generated image (bottom)

Configuration used for the scan

Sensor moves

| | |
|-------------------------|---|
| Magnet used: | Magnet A |
| Cantilever used: | Category B, soft steel |
| Sample: | Graphite |
| Motion: | Wait and move, scan along X-axis |
| Step size: | 0.5 mm step size along X-direction, 0.75 mm along Y |
| Filter used: | Subtract X-trace |

Graphite can easily be seen in the image above in figure 42; however the image is very noisy. To improve the noise, another cantilever (FRP 1) is used and the strain gauge in the lower side of the cantilever is shielded with an aluminium plate with an air gap as shown in figure 43 in next section so that it doesn't have any contact with the cantilever, so as to make sure that the

resistance of the lower strain gauge is constant and to avoid any direct exposure to the test sample and suppressing the thermal influence, if any. Now the resistance of the strain gauge could change only due to the force applied on the magnet by the sample.

6.1.3. Results with FRP cantilever

In this set up, not only the cantilever was changed, because of the length of the cantilever and the motion of the scanner, since, the motion is 'wait and move', the cantilever vibrates and takes time to be back at its zero position. So to lessen the vibrations and make the cantilever back to its zero position, aluminium is used at a little height above the magnet as shown in figure 43 which introduces eddy current damping effect and helps the cantilever to reach its equilibrium position.

6.1.3.1. Graphite using an FRP cantilever

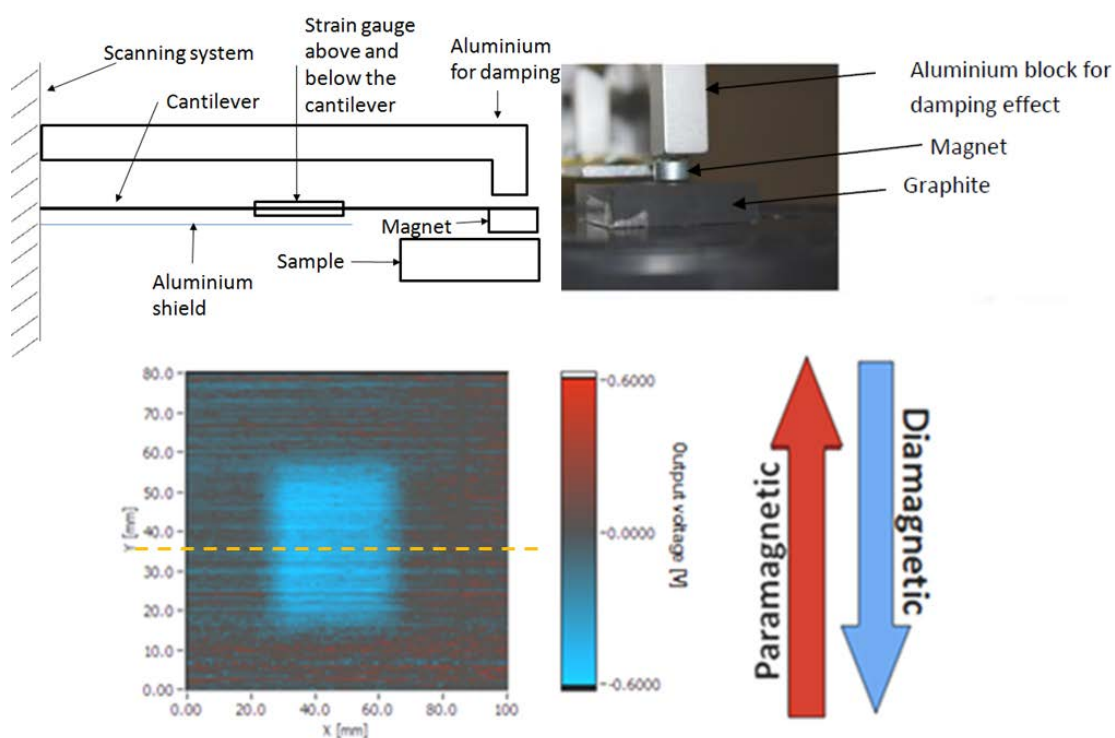


Figure 43: Set up (top), Generated image (bottom)

Configuration used for the scan

Sensor moves

| | |
|-------------------------|--|
| Magnet used: | Magnet A |
| Cantilever used: | Category C, FRP1 |
| Sample: | Graphite |
| Motion: | Wait and move, scan along X-axis |
| Step size: | 0.2 mm step size along X-direction, 0.8 mm along Y |
| Filter used: | Subtract X-trace |

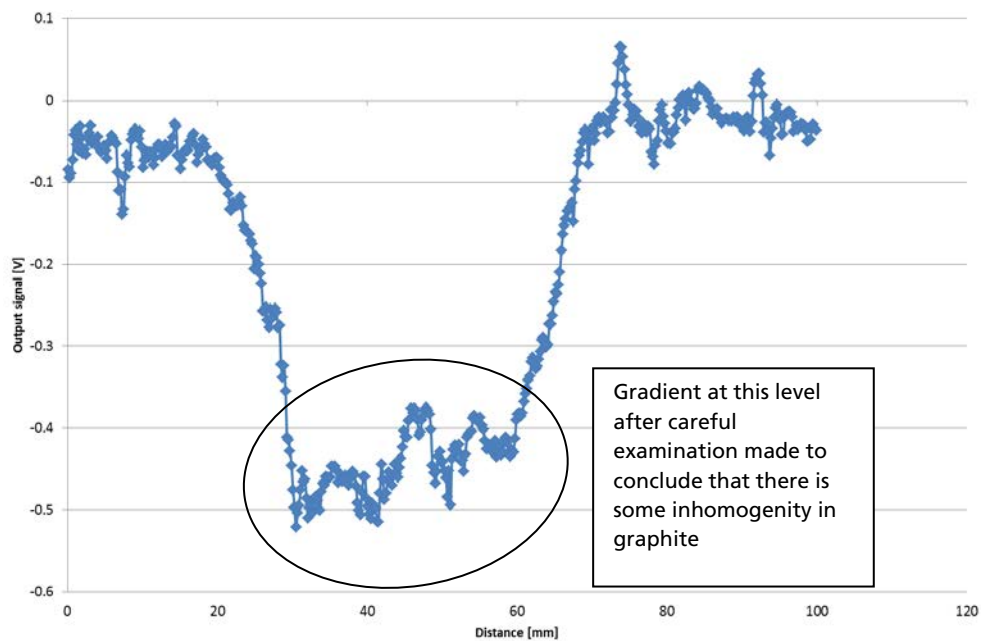


Figure 44: Signal for graphite along x-axis direction as highlighted by a yellow dashed line in the scanned image

The above result clearly shows the diamagnetic behaviour of the graphite as expected. However due to cantilever, it senses more vibrations due to the movement of the scanner and the SNR becomes poor.

6.1.3.2. Aluminium

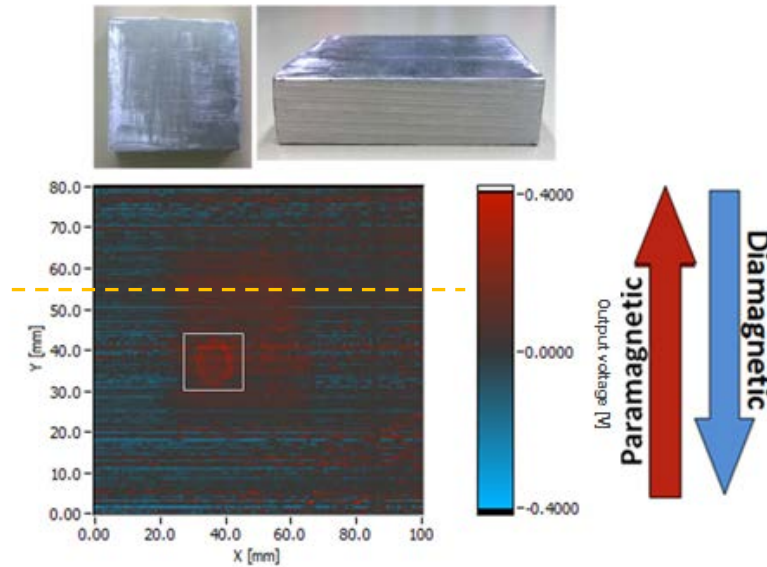


Figure 45: Set up (top), Generated image (bottom)

Configuration used for the scan

Sensor moves

| | |
|-------------------------|---|
| Magnet used: | Magnet A |
| Cantilever used: | Category C, FRP1 |
| Sample: | Aluminium |
| Motion: | Wait and move, scan along X-axis |
| Step size: | 0.1 mm step size along X-direction, 0.5 mm along Y. |
| Filter used: | Subtract X-trace |

The image in figure 45 above shows the image of an aluminium block. Aluminium shows exactly an expected signal from a paramagnetic material in comparison to a diamagnetic material. It is interesting to note the ring like structure in the highlighted part of the image. After careful examination and few experiments, it was concluded that there was some ferromagnetic impurity at the surface of the aluminium sample. The magnetic field gradient is stronger at the borders of a magnet, and hence it takes the shape of the outline of the magnet used for scanning the sample.

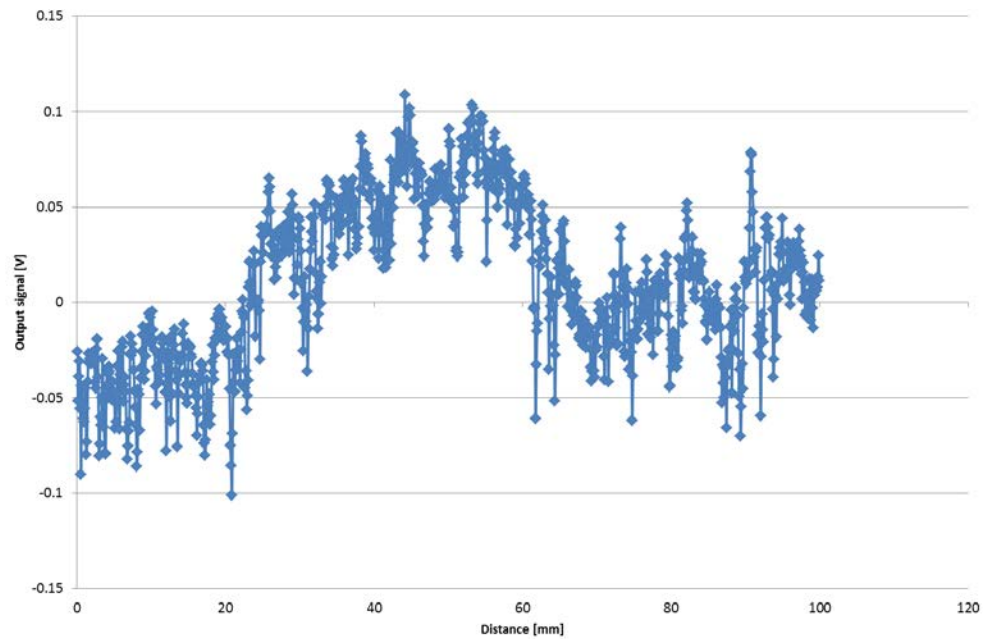


Figure 46: Signal analysis of aluminium block along x-axis as highlighted by a yellow dashed line in the scanned image

6.1.4. Conclusion

Though using an FRP cantilever and a half bridge circuit, it is quite evident that the results are promising but along comes the challenge of improving the signal to noise ratio. The full bridge would have improved the effect size even more, but along with that, it is expected that the noise level too will rise. This approach also revealed another application of this principle, to determine any ferromagnetic impurity in a non-ferrous material. A better and a modified approach is discussed in the next section using a capacitive sensor.

6.2. Measurements using a capacitive sensor

In the last section, the approach using a strain gauge did help in evaluating the nature of the samples but however, this approach was not successful in reducing the noise. In strain gauge approach, the basic phenomenon was to measure the strain caused in the cantilever due to the force on the magnet. However, it has to be noted that this force on the magnet causes a deflection which leads to the strain in the cantilever. In this chapter the idea of measuring the displacement of the cantilever is introduced and how this principle works more efficiently in comparison to the rest. To measure the deflection of the cantilever from its zero position on the application of the force, a capacitive sensor is used. The capacitive sensor measures the deflection/displacement from the zero position as a function of variation in the capacitance.

6.2.1. Optimization of the set up

6.2.1.1. Type of motion

It was important to finalize the type of motion to proceed for experiments and it was tested to check if in continuous motion, the principle works for conductive materials like aluminium. The motion was tested with various slower speeds and the graph below in figure 47 shows the results of the continuous motion at the rate of 3mm/s. It is quite evident that the signal over the graphite is normal as expected but in case of aluminium, still the eddy current effect is more prominent and the edges of aluminium are detected. Hence, it led to conclude that the motion has to be 'wait and move' for optimum results which are also shown in figure 48.

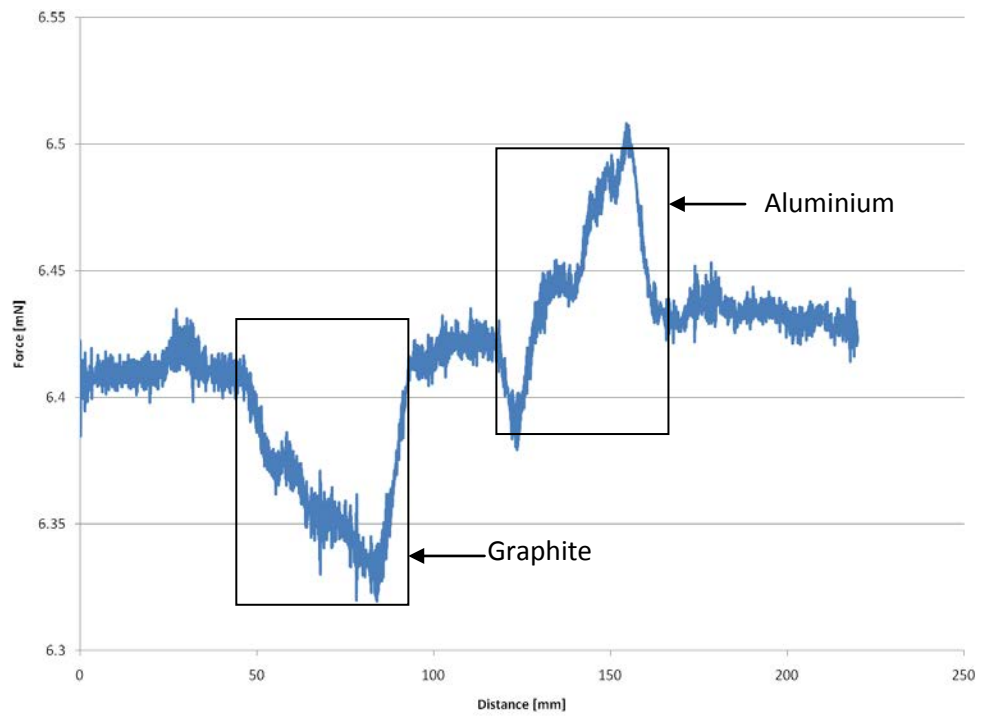


Figure 47: Scan of graphite and aluminium with a scan speed 3mm/s

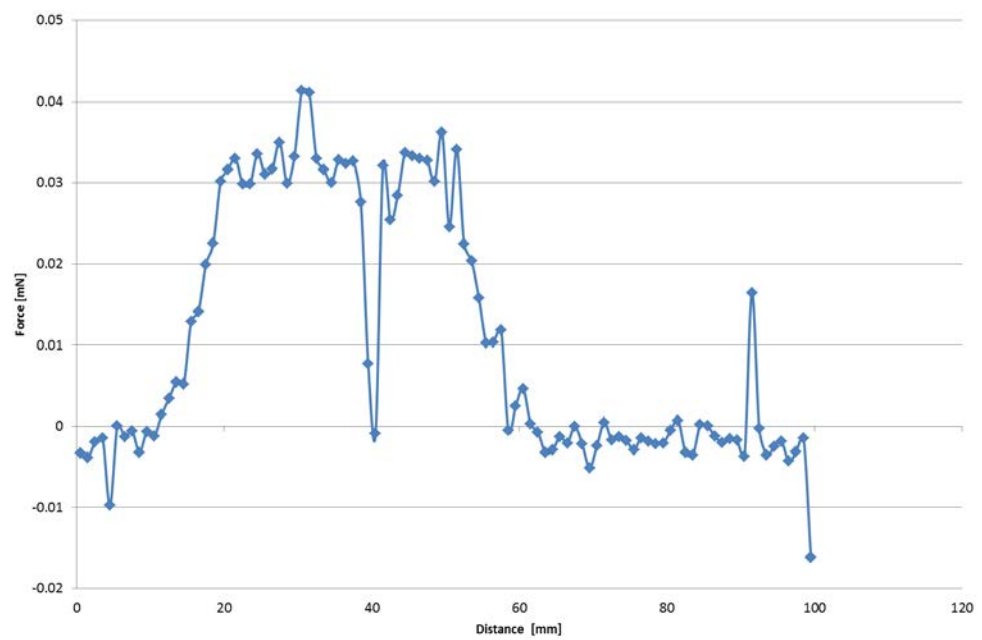


Figure 48: Scan of aluminium with wait and move motion

6.2.1.2. Choosing a magnet

Choosing a magnet of proper size and shape was also important. Higher the volume of the magnet, the farther the field lines stretch and thus affect the penetration depth in the sample. Effect of magnet size was examined using two same magnets but with different volumes, finalizing the magnet B as the magnet for performing the experiments. In figure 49, though the scan was just a linear scan and the set up was not so perfect, the signal is noisy but it does demonstrate the effect of magnets with different volumes. The two magnets used for evaluation are the same as presented in chapter 3.

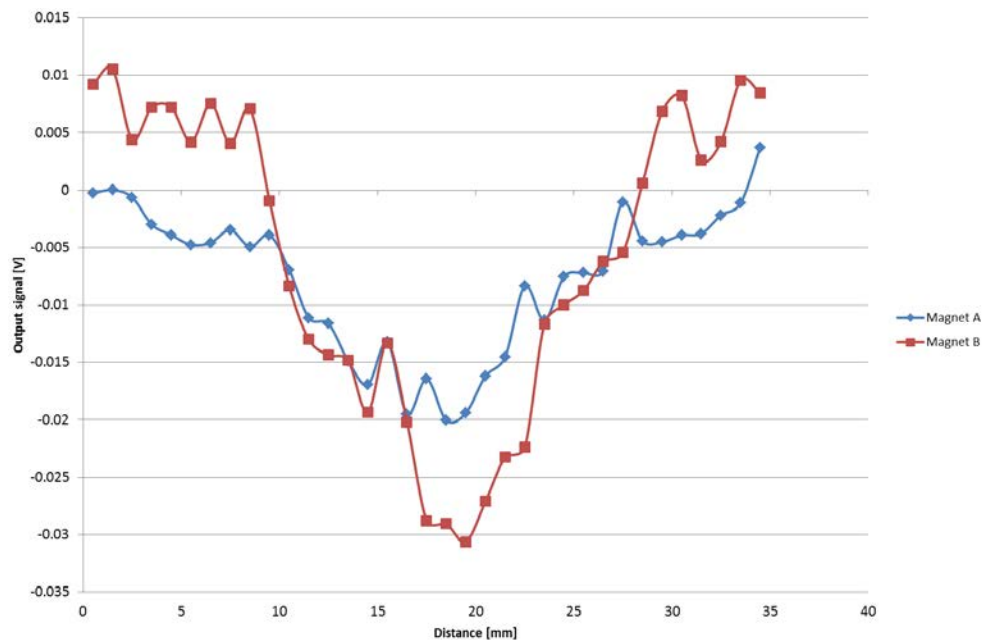


Figure 49: Effect size over a sample using two different magnets

6.2.1.3. Zero position adjustment

In the optimization of the sensor set up, when the magnet size was determined, it was noted that due to the weight of the magnet, the cantilever bends a bit downwards and it was difficult to get the cantilever back to its zero position since it was always bent. So in order to bring back the cantilever to its normal state, a little ferromagnetic ring (size determined after examining its effect size on the magnet) was placed on the top of aluminium as shown in figure 50 which would attract the magnet mounted

on the cantilever to a required level. Various damping techniques were tested, from using a viscous liquid and a screw as shown in figure 51 to using a secondary magnet on the upper side of the cantilever just at a distance of 1mm below the aluminium holder as shown in figure 50. This damping effect is explained in the following paragraph. After careful examination of results, it was finalized to use a secondary magnet on the upper side of the cantilever so as to get a better damping effect.

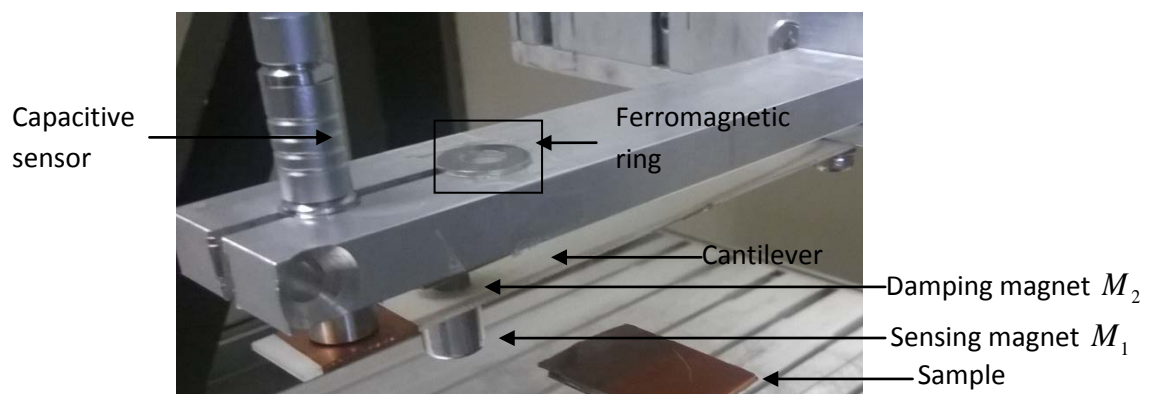


Figure 50: Sensor holder

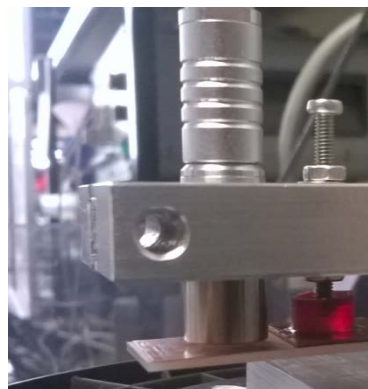


Figure 51: Damping using a viscous liquid and a screw

For damping, the principle of eddy current braking is used here where the eddy currents are induced in the conductor through electromagnetic induction due to the magnet nearby the conductive object. So, whenever there are vibrations due to the air flow or due to any mechanical reason or movement of scanner, this eddy current braking principle helps to damp the

magnet attached to the cantilever and thereby reducing the unnecessary oscillations.

6.2.2. Defining a new filter and minimizing the noise

Another idea introduced in this approach which is a part of optimization is a concept of scanning the sample at two Z-levels and then subtracting the two signals from each other. It is assumed that at a certain distance, the signals (interference) are sensed equally and if subtracted from each other, the interference can be removed to a large extent. A special filter was developed to perform this operation. This filter enables to set the signal of one level (where just interference is expected, in this case 7 mm level below the sensor) as a reference. This has been well demonstrated in figure 28 in chapter 3 explaining how the force decays over distance. This reference signal can then be subtracted from another Z-level of 1 mm below the sensor where the effect of the sample is expected to be seen. However, closer the sensor is to the sample, higher is the effect. But in this case, 1mm was chosen because samples were not perfectly flat and could have a contact with the sensor. The subtraction of these two signals then clearly shows that the noise is reduced and the drift is removed and the sample can be detected with a better signal to noise ratio. Results are shown in the 'evaluation' section.

Regarding the Z-offset, the sample is scanned nearly at 1 mm below the sensor and the other Z Level, being used is 7 mm below the sensor. With initial testing and experiments, it was noted that at nearly 7 mm distance from the sensor, the sample cannot be detected or has nearly zero effect (demonstrated in the results under 'distance variation'). If a smaller gap between two Z-levels is used, it might be the case that some information about the sample is lost on the subtraction of the signals of two levels. Therefore, after experiments, the gap difference of 6 mm was selected between the two Z-levels. Additionally, the software used has the option of setting the axis of the scanner at different Z-levels. The priority of movement of three axis chosen is: Initially it scans 1 mm below the sensor in the X-direction, and then scans the same line at 6+1 mm level from the sensor. After scanning the whole X-direction at two Z-levels at a fixed Y-point, it moves to scan the next Y-level, the same way. Similarly the whole sample is scanned at two Z-levels simultaneously. Hence, the scan generated through

this approach is reproducible. Had it been the case that the sample is scanned separately at the two Z-levels, it would have been difficult to reproduce the same results again and again since over a longer period of time, the interference might change.

6.2.3. Set up

Aluminium being a good conductor has been used as the material for the sensor holder so as to provide damping from the holder itself. It is important to understand how eddy current damping in aluminium helps in decreasing the amount of vibrations. In this set up as shown in figure 52 below, second magnet is just below the aluminium holder which being a good conductor with a conductivity of 3.50×10^7 S/m (20°C) [Serw] induces the eddy currents and damps the vibrations caused during the movement of the scanner and thereby reducing the unnecessary oscillations and bring back the cantilever to equilibrium.

The aluminum holder is made in such a way that the distance between the second magnet M_2 and the aluminium holder is just 1mm. This magnet is placed on the upper side of the cantilever as demonstrated in figure 50. The first magnet M_1 fixed below the cantilever, is used to move over the sample, depending on the interaction force between the magnet and the specimen, the cantilever attached to the magnet is deflected. The amount of deflection varies and depends on the material used for the cantilever. The magnet on the upper surface M_2 of the cantilever is used to have the damping effect as mentioned above. As described above, the principle of the capacitive sensor, works exactly as a parallel plate capacitor. The sensor acts as one electrode and the copper coated FRP cantilever acts as another. When the magnet M_1 moves over the specimen and due to the force interaction between the magnet and the specimen, depending on the specimen whether it is paramagnetic or diamagnetic, the cantilever moves either towards the specimen, thereby increasing the distance between the two electrodes or moves away from the specimen, decreasing the distance between two electrodes. In case if the specimen is diamagnetic, the magnet and the cantilever attached to it, will be repelled and hence there will be a decrease in the distance between the electrodes. The output voltage is calibrated in terms

of force. First a reference weight is taken and is put over the cantilever. The change in the output voltage is recorded. Then the weight of the reference sample is put in terms of mN. Then it is clear that this much of mN cause a change in the output voltage which becomes the conversion factor and is multiplied by the output voltage during the scan. This gives the output in terms of mN.

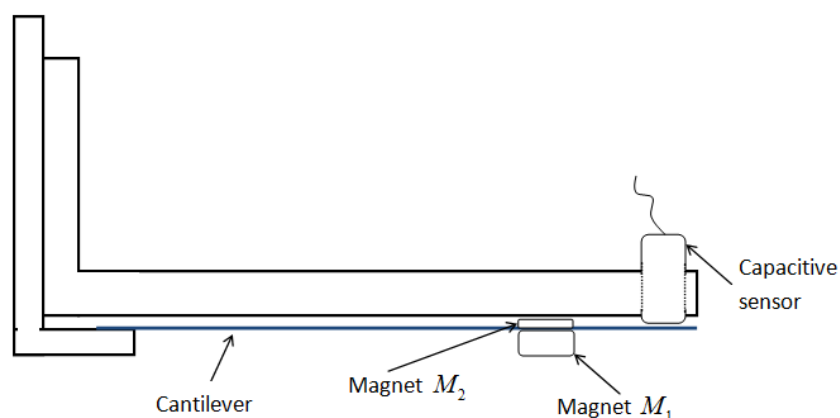


Figure 52: Sensor set up

Materials like wood, pertinax, glass, different types of plastics, cardboard, glue sandwiched between two glass sheets, plastics with pattern below its surface, cardboard with glue below its surface, carbon fiber reinforced plastics, super-paramagnetic particles, brass, have been examined using this principle.

6.2.4. Evaluation

6.2.4.1. Carbon fiber reinforced plastic with PVC object below

In this experiment a regular carbon fiber reinforced plastic (CFRP) sheet of dimensions 110 x 110 x 4 mm is examined under which a round shaped PVC made material is glued. The sample is scanned from the upper surface as shown in figure 54. The PVC behaves highly paramagnetic which is probably due to the color pigments used. PVC is a diamagnetic material which has been tested and examined in many scans during the practical course of this thesis. Some results are shown in the later part of this chapter. It is interesting

to note that this approach is highly sensitive and even images the centric hollow part (figure 53) of the PVC to some extent shown in the graph in figure 55 which also demonstrates the extent of improvement of the signal to noise ratio.



Figure 53: Hollow part of the PVC rubber used

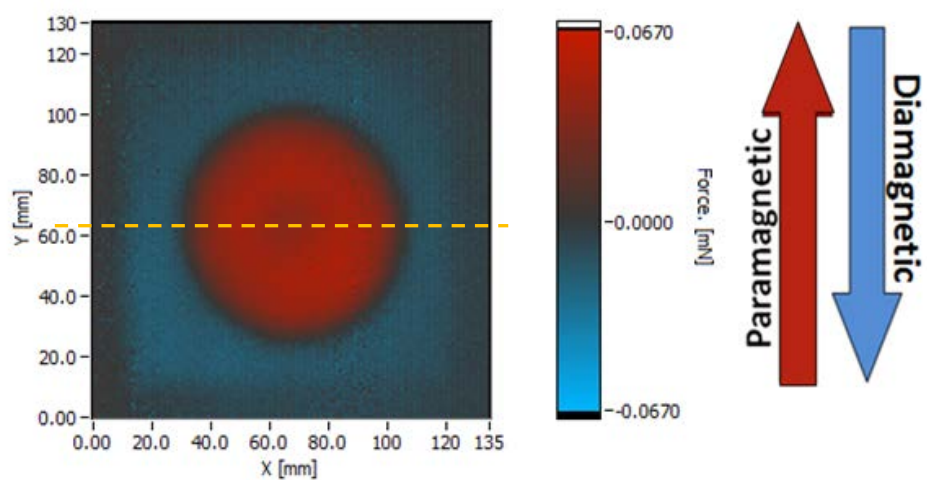
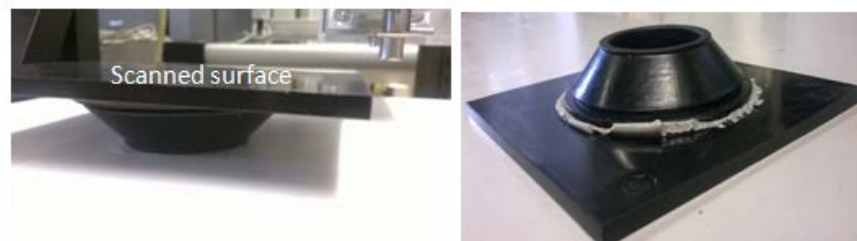


Figure 54: Sample (top), Generated image (below)

Configuration used for the scan

Two Z-level scan, Sensor moves

| | |
|-------------------------|--|
| Magnet used: | Magnet B |
| Cantilever used: | FRP 2 |
| Sample: | Round shaped PVC material below rectangular CFRP |
| Motion: | Wait and move, scan along Y-axis |
| Step size: | 1 mm step size along X-direction, 1 mm along Y |
| Filter used: | Set reference-Subtract reference |

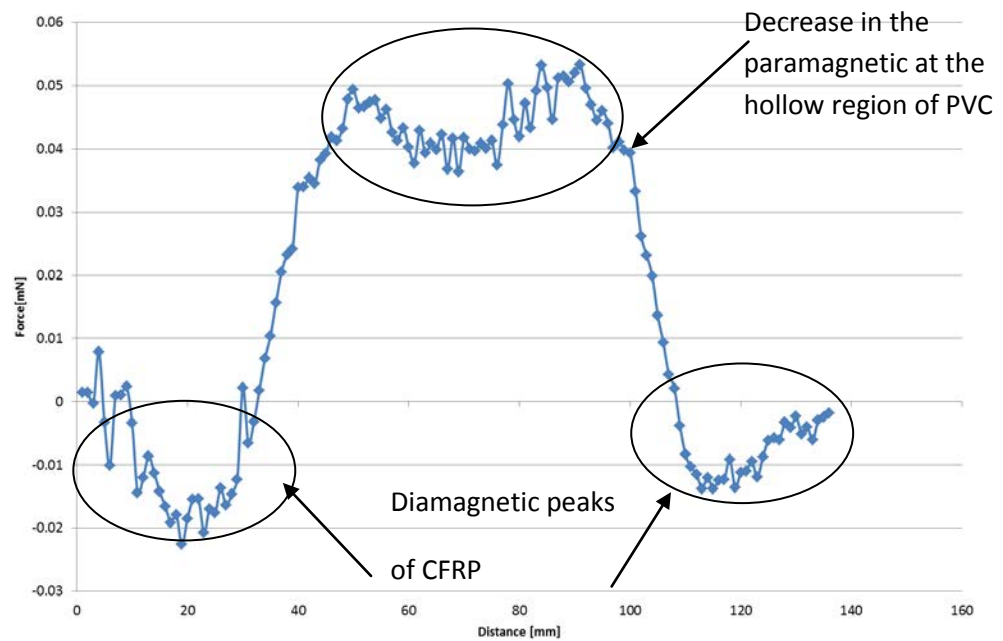


Figure 55: Graph showing the diamagnetic behavior of CFRP, paramagnetic behavior of PVC (color contamination), and a less paramagnetic behavior at the center where the PVC is hollow. The signal is along x-axis direction as highlighted by a yellow dashed line in the scanned image

6.2.4.2. Brass

A simple rectangular piece of brass with dimensions 45 x 30 x 10mm is examined which shows a highly paramagnetic behavior. The strength of the signal raised doubts regarding it being a ferromagnetic in behavior. However, when tested manually with the magnet, it showed no sensible response at all to the magnet. Figure 56 below shows the scanned image and the following graph in figure 57 shows its signal strength in mN depicting that it is strongly paramagnetic.

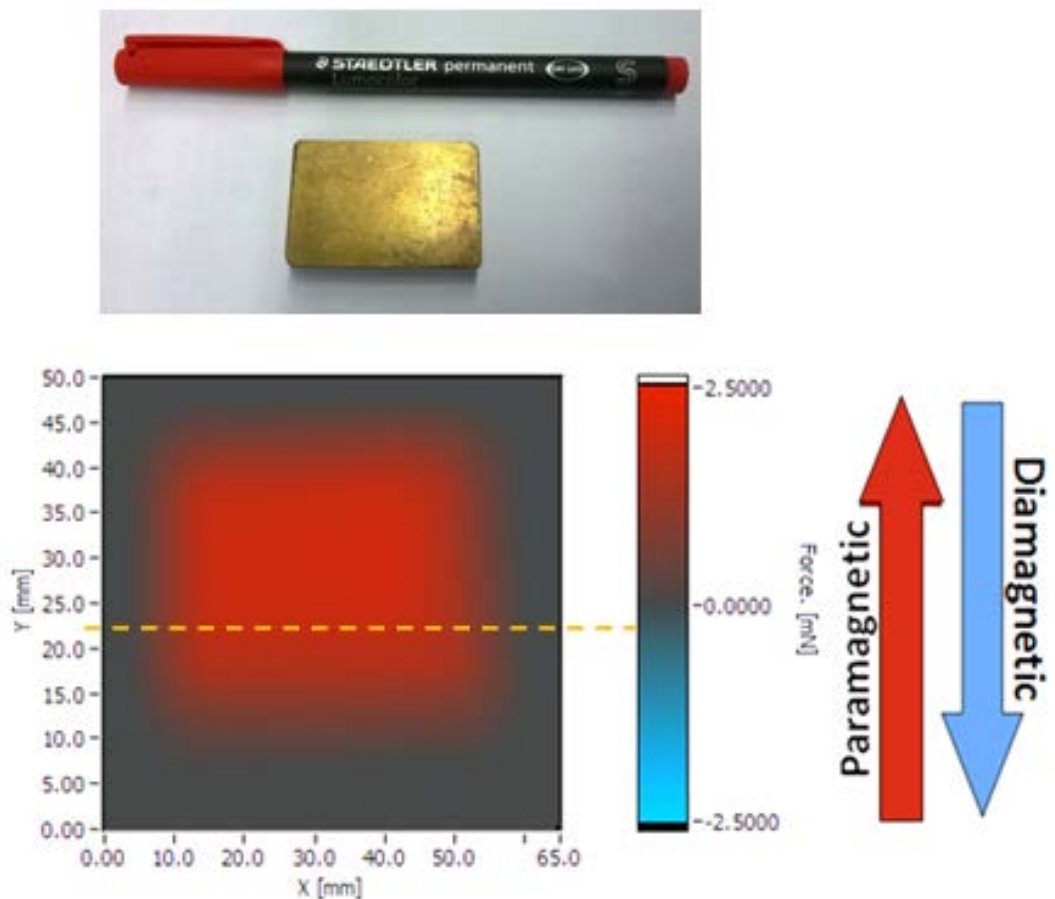


Figure 56: Sample (top), Generated image (below)

Configuration used for the scan

Two Z-level scan, Sensor moves

| | |
|-------------------------|--|
| Magnet used: | Magnet B |
| Cantilever used: | FRP 2 |
| Sample: | Brass |
| Motion: | Wait and move, scan along Y-axis |
| Step size: | 0.5 mm step size along X-direction, 0.5 mm along Y |
| Filter used: | Set reference-Subtract reference |

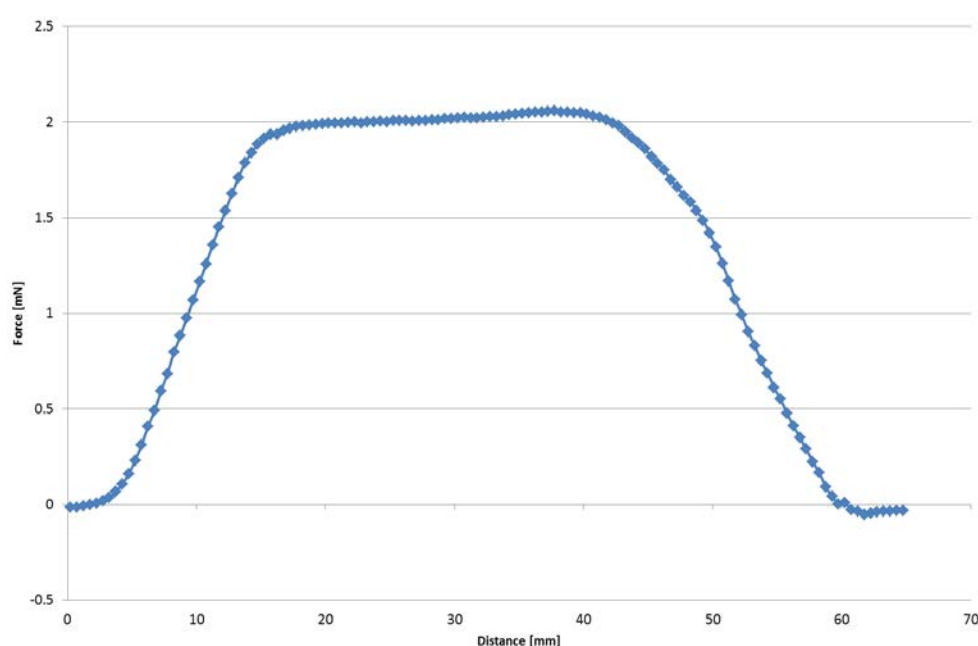


Figure 57: Signal for brass showing its paramagnetic behavior. The signal is along the x-axis direction as highlighted by a yellow dashed line in the scanned image

6.2.4.3. Glue, glass slides and pertinax

In this scan two glass slides are joined together which are mounted on the pertinax at the edges as shown in figure 58 below. These glass slides are 1 mm thick each and on the lower side of the glass slides, marks with different types of glue are made. However due to the varied thickness of the glue marks, it was difficult to distinguish between the different glue types but, air, glue, pertinax and glass slides can very well be distinguished. At the joint of

two glass slides, in the scanned image, a ring like structure is visible. This is due to a ferromagnetic impurity (possibly due to the tape that was used to join two glass slides) to the detection of which this principle is highly sensitive. This effect was discussed in 'strain gauge' section.

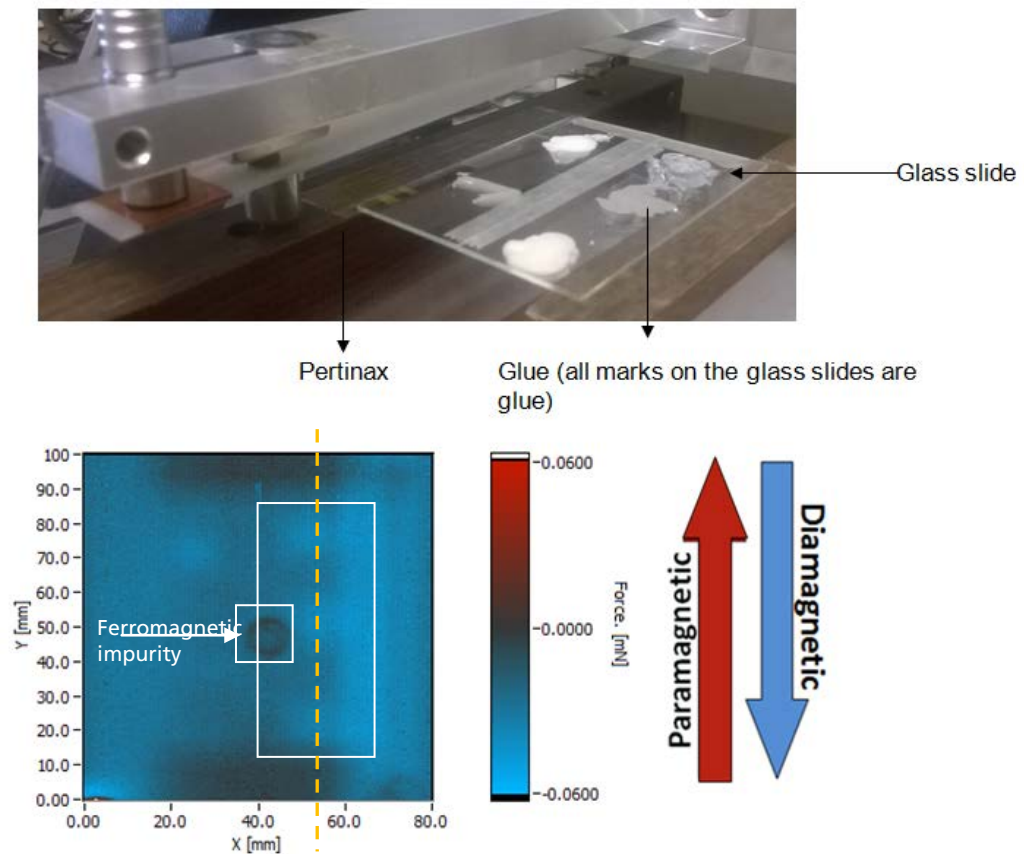


Figure 58: Sample (top), Generated image (below)

Configuration used for the scan

Two Z-level scan, Sensor moves

| | |
|-------------------------|--|
| Magnet used: | Magnet B |
| Cantilever used: | FRP 2 |
| Sample: | Glue, glass slides and pertinax |
| Motion: | Wait and move, scan along Y-axis |
| Step size: | 0.5 mm step size along X-direction, 0.5 mm along Y |
| Filter used: | Set reference-Subtract reference |

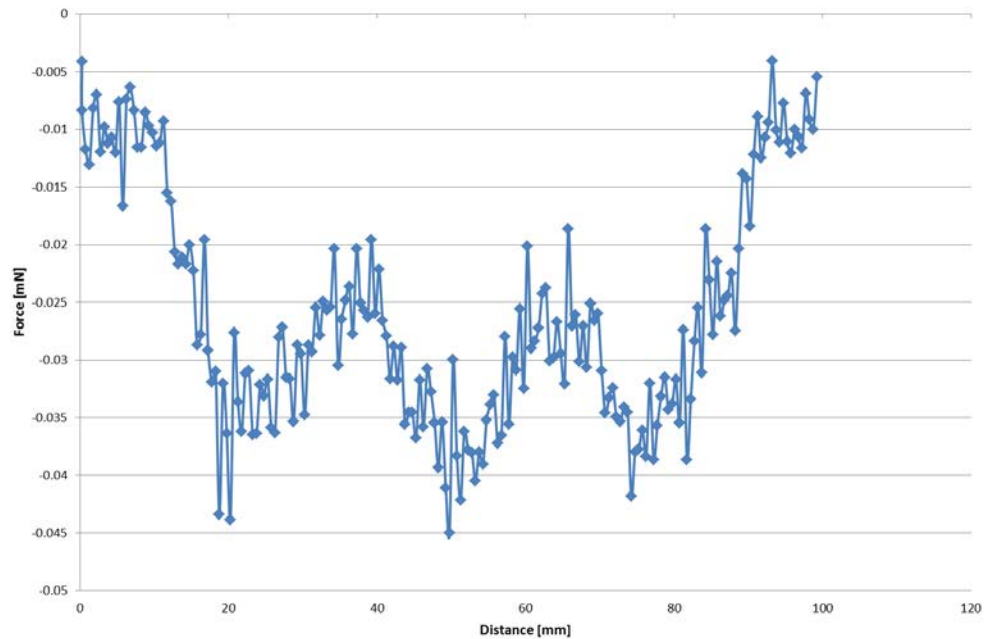


Figure 59: This particular graph shows the signal over the three glue marks in the highlighted part of the scan in figure 58, depicting the diamagnetic peaks. The signal is along the y axis direction as highlighted by a yellow dashed line in the scanned image

6.2.4.4. Aluminium block

This is the scan of the aluminium block which was also used for the fluxgate experiments, strain gauge measurements and for precision balance set up too. However, some artifacts were encountered due to air inflows or when there is some major disturbance near the experimental area during the scan in the Y direction. Artifacts are highlighted in figure 60 and hence, an improvement was required to avoid such effects, which is explained in the next section.

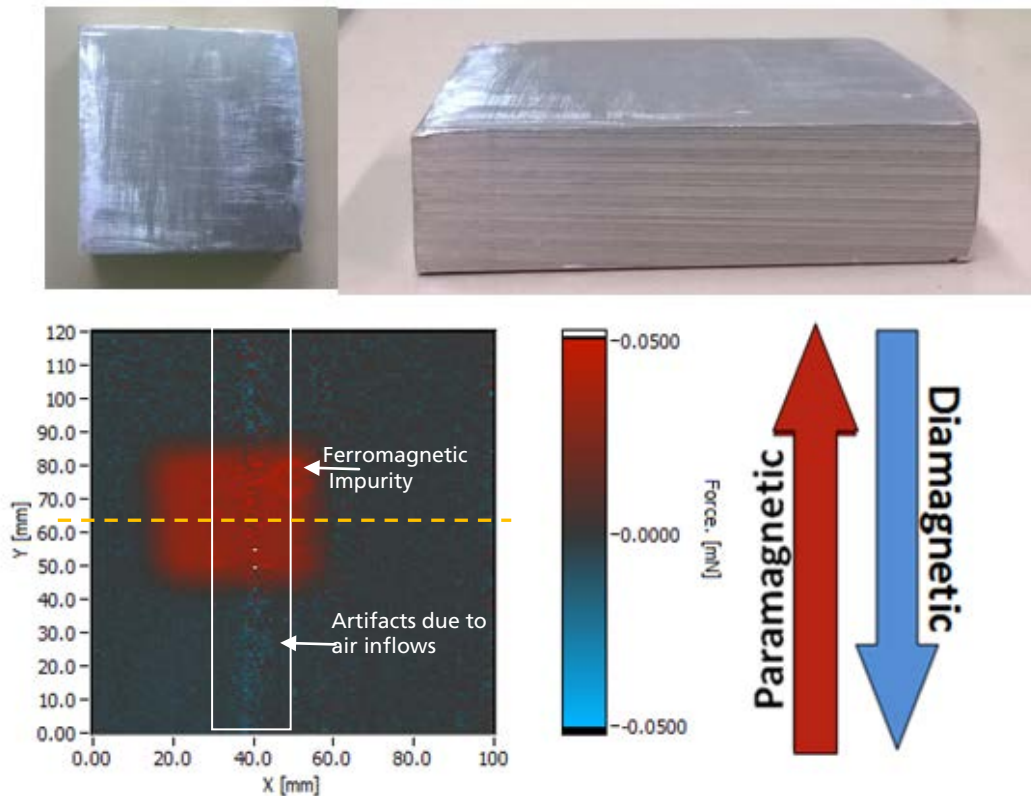


Figure 60: Sample(top), Generated image (below)

Configuration used for the scan

Two Z-level scan, Sensor moves

| | |
|-------------------------|---|
| Magnet used: | Magnet B |
| Cantilever used: | FRP 2 |
| Sample: | Aluminium block |
| Motion: | Wait and move, scan along Y-axis |
| Step size: | 1 mm step size along X-direction, 0.75 mm along Y |
| Filter used: | Set reference-Subtract reference |

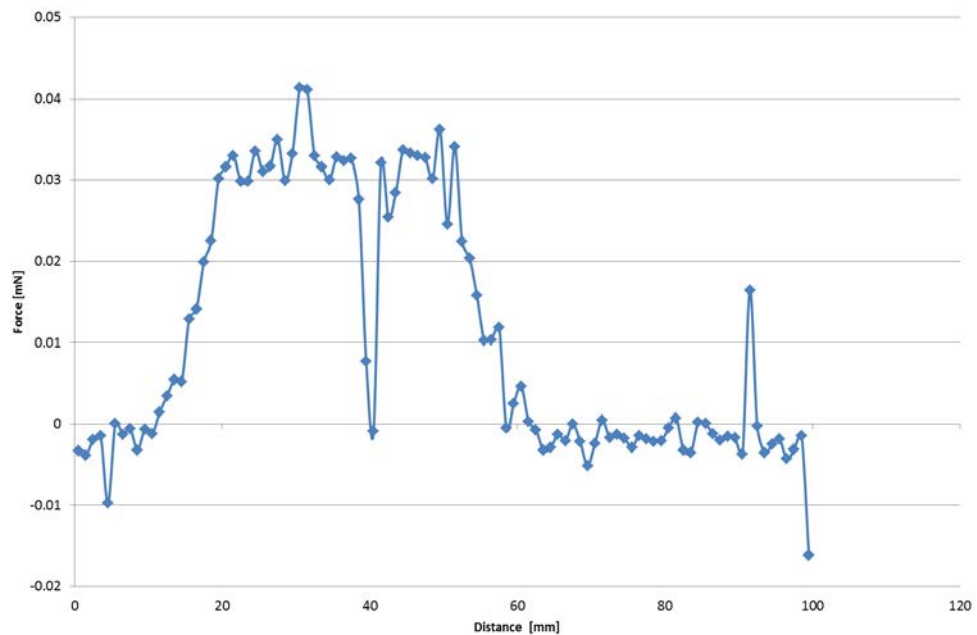


Figure 61 : The graph demonstrates the paramagnetic behavior of aluminium, the falling peak shows the artifacts due to air inflows and the major physical disturbance near the experimental area. The signal is along the x axis direction as highlighted by a yellow dashed line in the scanned image

6.2.5. Need of improvement

This set up was nearly perfect for the sample testing, however a shortcoming of this sensor was that it could be affected by the air inflows very easily since it was not enclosed, the effects of which can be seen, e.g. highlighted in figure 60. So an all new final set up was designed for controlling the air inflows to some extent. This set up was majorly made out of copper and to decrease the weight on the cantilever due to the second magnet, the new final holder has been designed in a way that there is only one magnet and this magnet also helps in creating damping effect. Also the length of the cantilever is decreased from 160 mm to 120 mm so as to avoid vibrations. Since, longer the cantilever more will be the deflection and more it is likely to bend over the period of time. Like in the previous set up, a ferromagnetic ring was placed over the aluminium holder, in this sensor holder, a small magnet is placed so as to bring back the cantilever to an equilibrium state in case there is any bending over the period of time. The idea of the sensor holder is

presented in the figure 62 below. Additionally, the inside view of the set-up is also shown in the pictures following. Another important difference in this approach was to make the sensor static to avoid any unnecessary vibrations due to mechanical movement and the sample was moved instead.

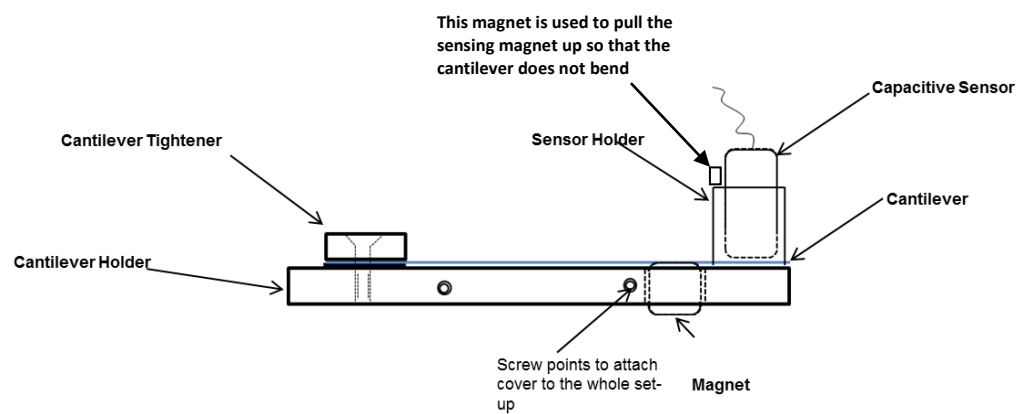


Figure 62: Diagram demonstrating the idea of final sensor (not scaled)

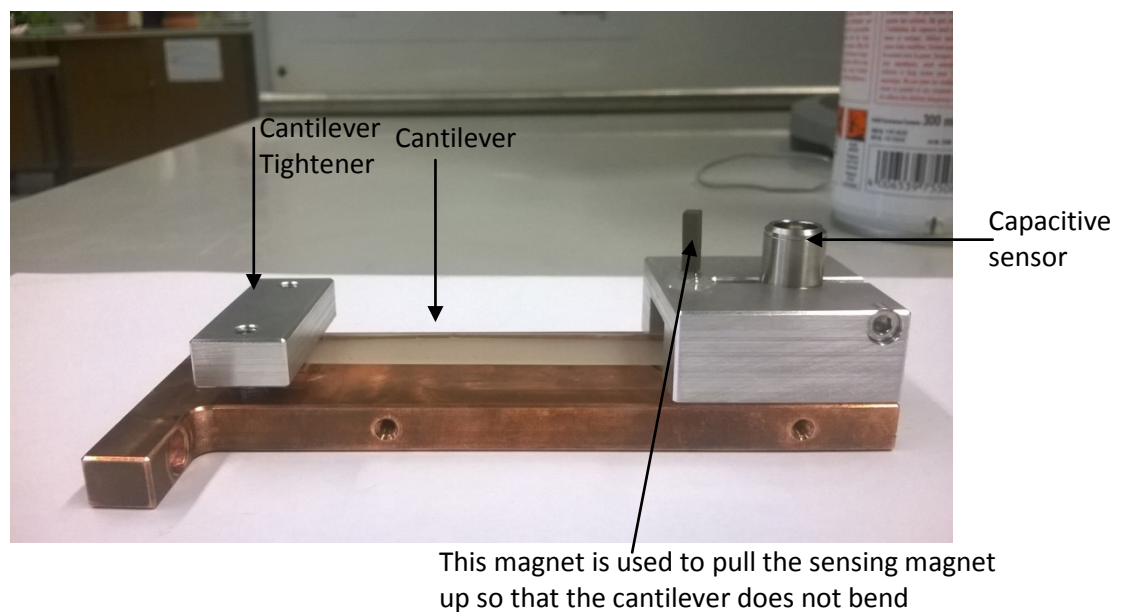


Figure 63: Internal side view of sensor

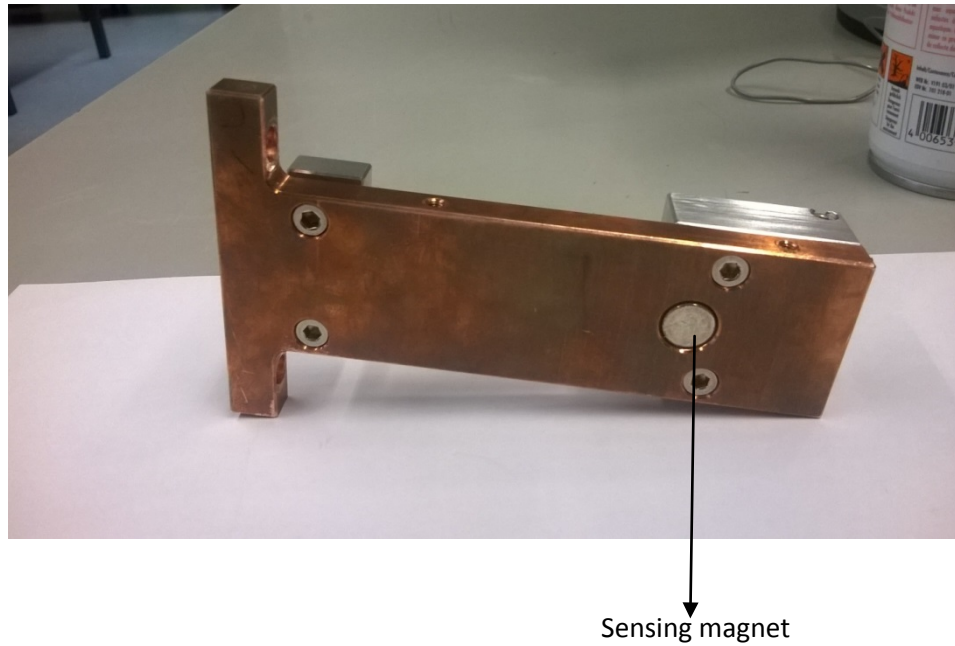


Figure 64: Bottom view of sensor

Regarding the usage of copper for damping, in the new set up, the cylindrical sensing magnet is surrounded by copper all around it. In the earlier set up, the area of exposure between the magnet and the aluminum was lesser as compared to the new set up. Since conductivity of copper 5.96×10^7 S/m [Gian] is higher than aluminum, in the new set-up, the damping is improved, firstly by increasing the exposure area between the magnet and the conductor and secondly by using copper as a conductor. The image of the final sensor has been shown in figure 65.

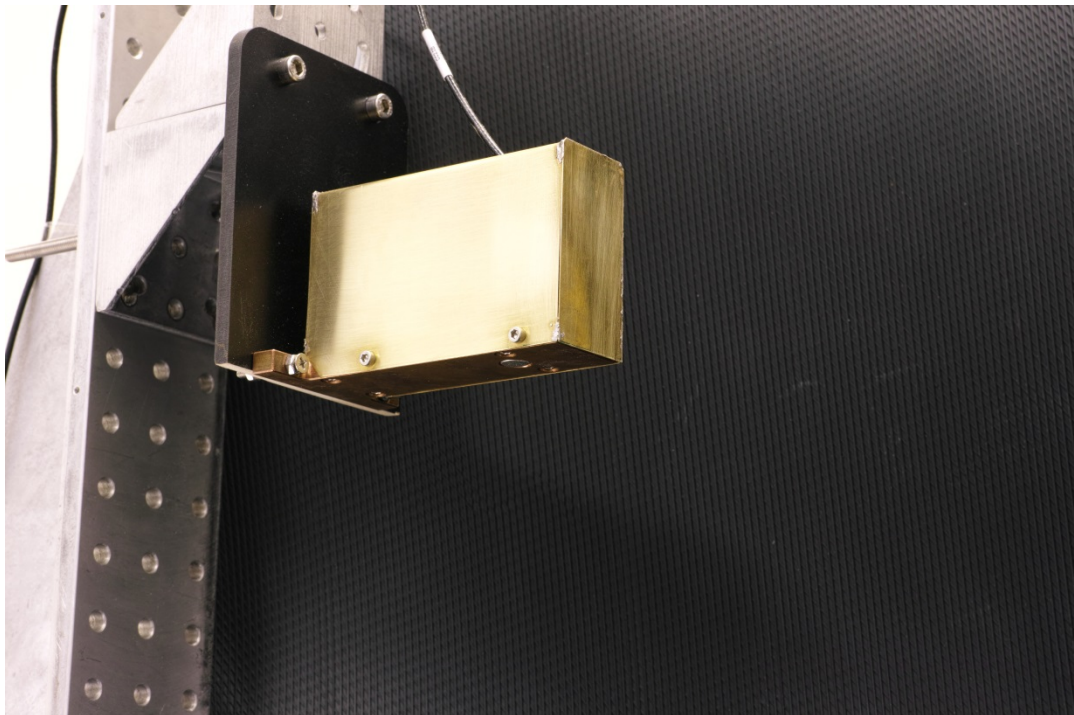
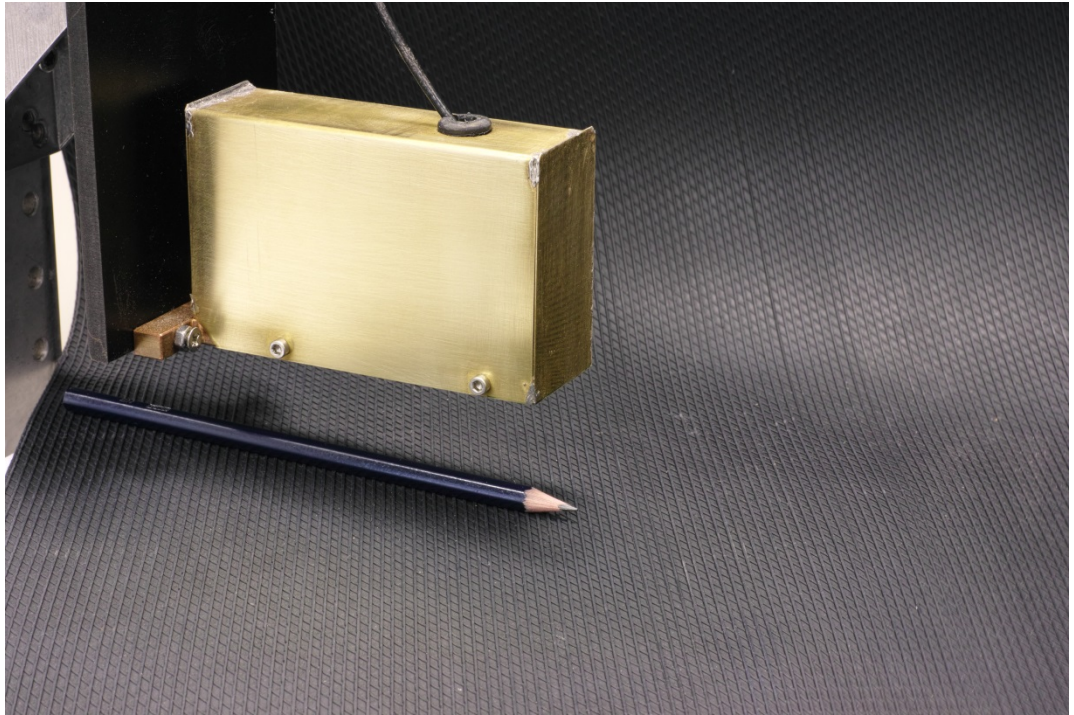


Figure 65: Final sensor

6.2.6. Evaluation with final sensor

6.2.6.1. Glue sandwiched between aluminium

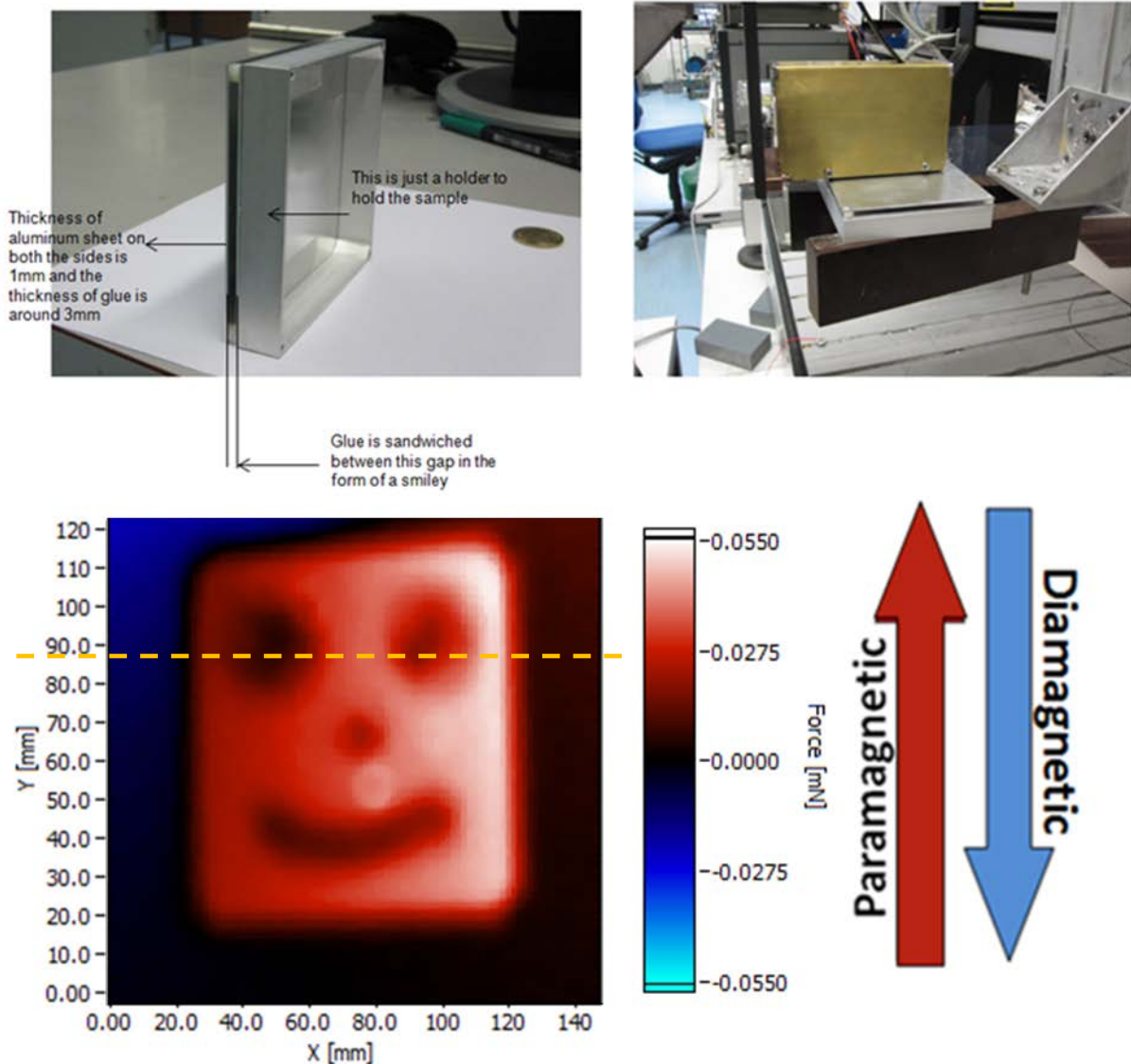


Figure 66: Sample (top), Generated image (below)

In this experiment normal silicone glue is sandwiched in the form of a smiley with a thickness of 3 mm in between two aluminium sheets of thickness 1mm each as shown in figure 66. The sample was not quite parallel to the sensor hence little gradient can be noticed in the image. As determined in the last section, the glue demonstrates a diamagnetic behavior whereas aluminium shows its expected paramagnetic behavior. The new filter was totally a major breakthrough since without subtracting the two signals, the image what is achieved is as shown below in figure 67. It is clear that the

sample cannot be detected at all if the two signals are not subtracted from each other because of high interference as compared to the effect size of sample.

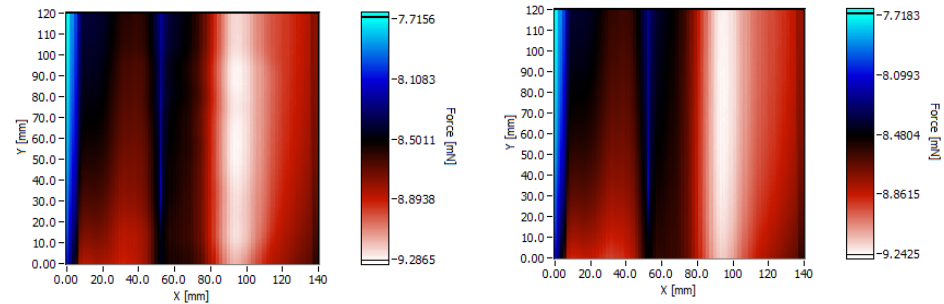


Figure 67: Scanned image without filter: 1 mm from sensor (left), 7 mm from sensor (right)

Configuration used for the scan

Two Z-level scan, Sensor static- sample moves

Magnet used: Magnet B
Cantilever used: FRP 3
Sample: Glue sandwiched between two aluminium sheets
Motion: Wait and move, scan along Y-axis
Step size: 1 mm step size along X-direction, 0.6 mm along Y
Filter used: Set reference-Subtract reference

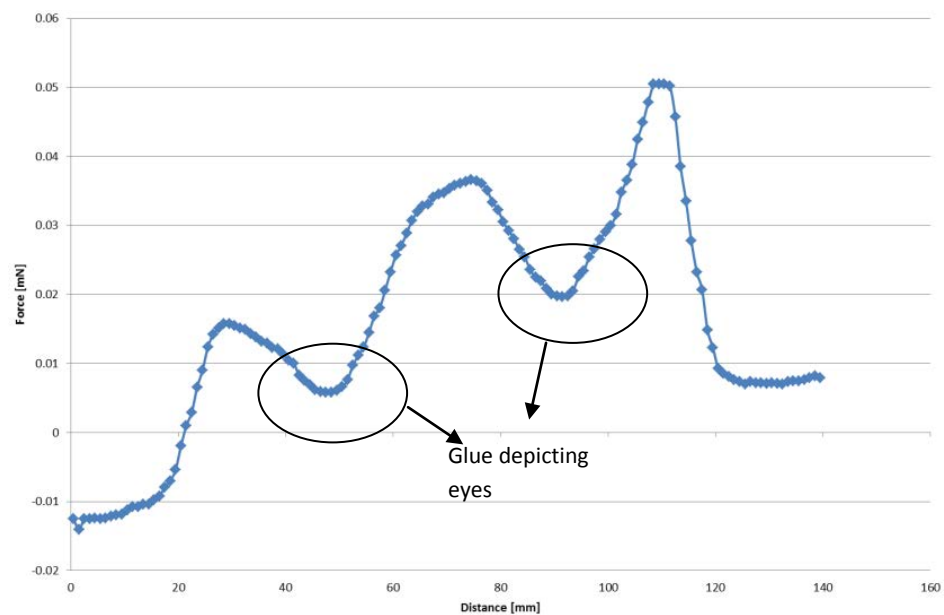


Figure 68: Graph demonstrating the diamagnetic behaviour of glue over the eyes of the smiley. The signal is along the x axis as highlighted by a yellow dashed line in the scanned image

6.2.6.2. IZFP inscribed on PVC

A PVC sample has been inscribed with 'IZFP' with varied depths as shown in figure 69. It was difficult to maintain a constant distance between the sample and the sensor since the sample was already bent. The sensor was in a closer proximity on the right side and there was quite a gap of around 3 mm to 0.5 mm from left to right (from 'I' to 'P'). Hence, a gradient can be seen in the signal as shown in figure 71. Figure 70 shows the set up for the experiment and the scanned image.

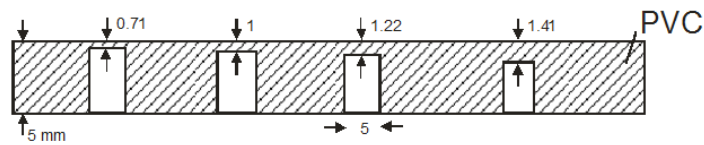


Figure 69: Depth of IZFP inscribed on PVC

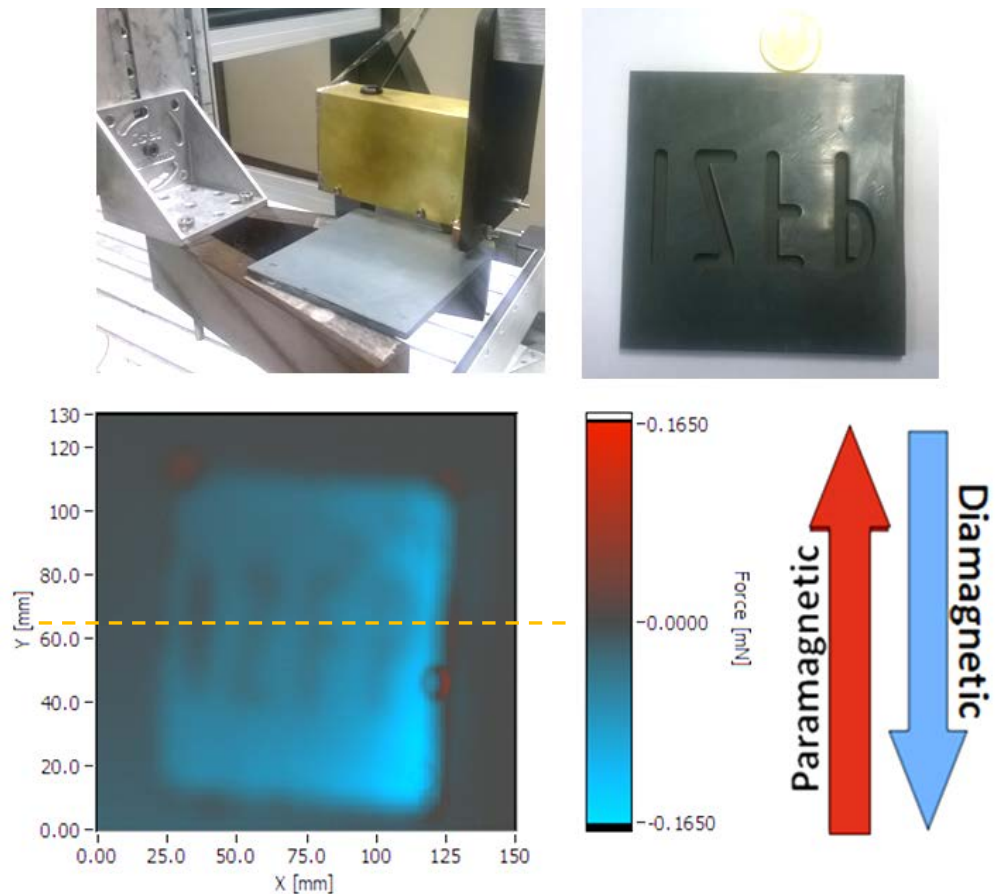


Figure 70: Sample (top), Generated image (below)

Configuration used for the scan

Two Z-level scan, Sensor static- sample moves

| | |
|-------------------------|--|
| Magnet used: | Magnet B |
| Cantilever used: | FRP 3 |
| Sample: | IZFP inscribed on PVC sample |
| Motion: | Wait and move, scan along Y-axis |
| Step size: | 1 mm step size along X-direction, 0.7 mm along Y |
| Filter used: | Set reference-Subtract reference |

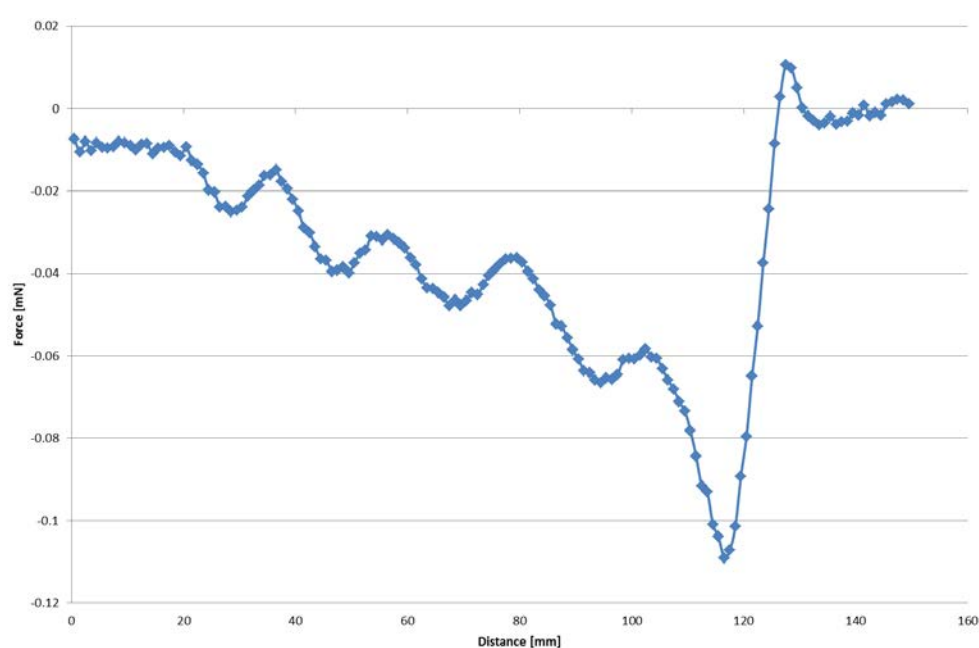


Figure 71: Signal analysis, demonstrating diamagnetic behavior of the sample, for the scanned image shown in figure 70. The signal is along the x axis as highlighted by a yellow dashed line in the scanned image

In this case also, since the sample was also not flat as discussed above and moreover due to the physical mounting limitations, a gradient can be seen in the signal.

6.2.6.3. IZFP inscribed on PVC with continuous motion

As discussed in previous sections, because of the enclosed set up of the sensor, it was assumed that to speed up the scan speed, the same sample examined in 6.2.6.2., is examined under continuous motion in this case with a scan speed of 50mm/s. However it is quite evident that a lot of information is lost with continuous mode. The image also shows that the signal to noise ratio has also been worsened. The major reason behind this could be because the cantilever does not have enough time to return back to its equilibrium position before it could take the next reading. As a result, some information is compromised as shown in figure 72, when the scan is made in a continuous motion increasing the speed of the scan.

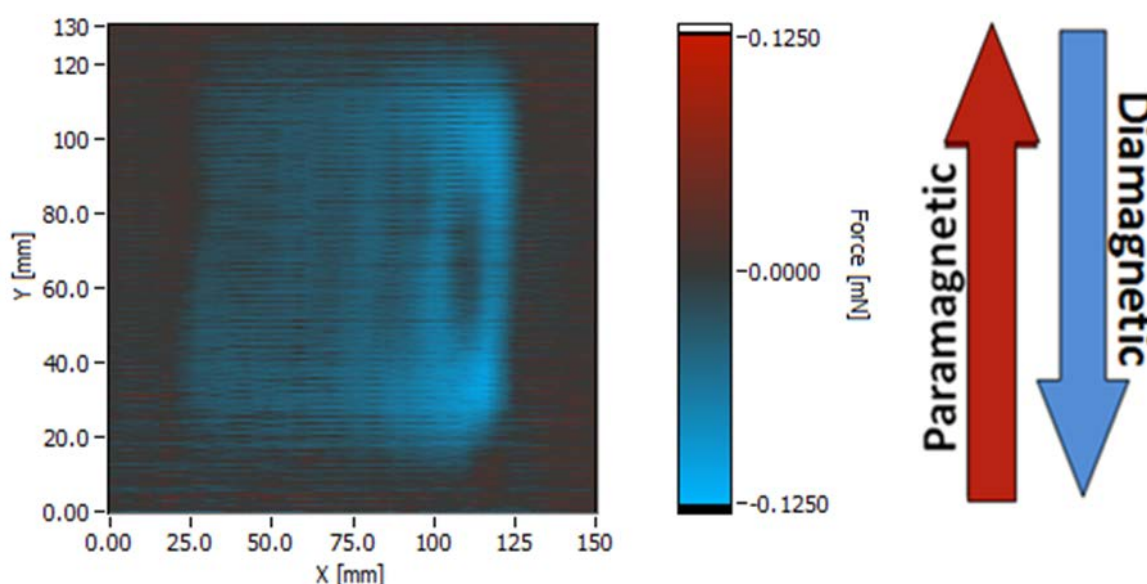


Figure 72: IZFP inscribed sample scanned image, using a continuous motion with moving average

Configuration used for the scan

Two Z-level scan, Sensor static- sample moves

| | |
|-------------------------|--|
| Magnet used: | Magnet B |
| Cantilever used: | FRP 3 |
| Sample: | IZFP inscribed on PVC sample |
| Motion: | Continuous motion with moving average, 50mm/s scan speed |
| Filter used: | Set reference-Subtract reference |

6.2.6.4. Graphite

In this experiment, the regular graphite sample is examined with the new sensor being static and the graphite moving as shown in figure 73. Being highly diamagnetic, this sensor also helps conclude the improved signal to noise ratio. However, in figure 74, as demonstrated in strain gauge section, the inhomogeneity of graphite can also be seen in this case with this sensor.

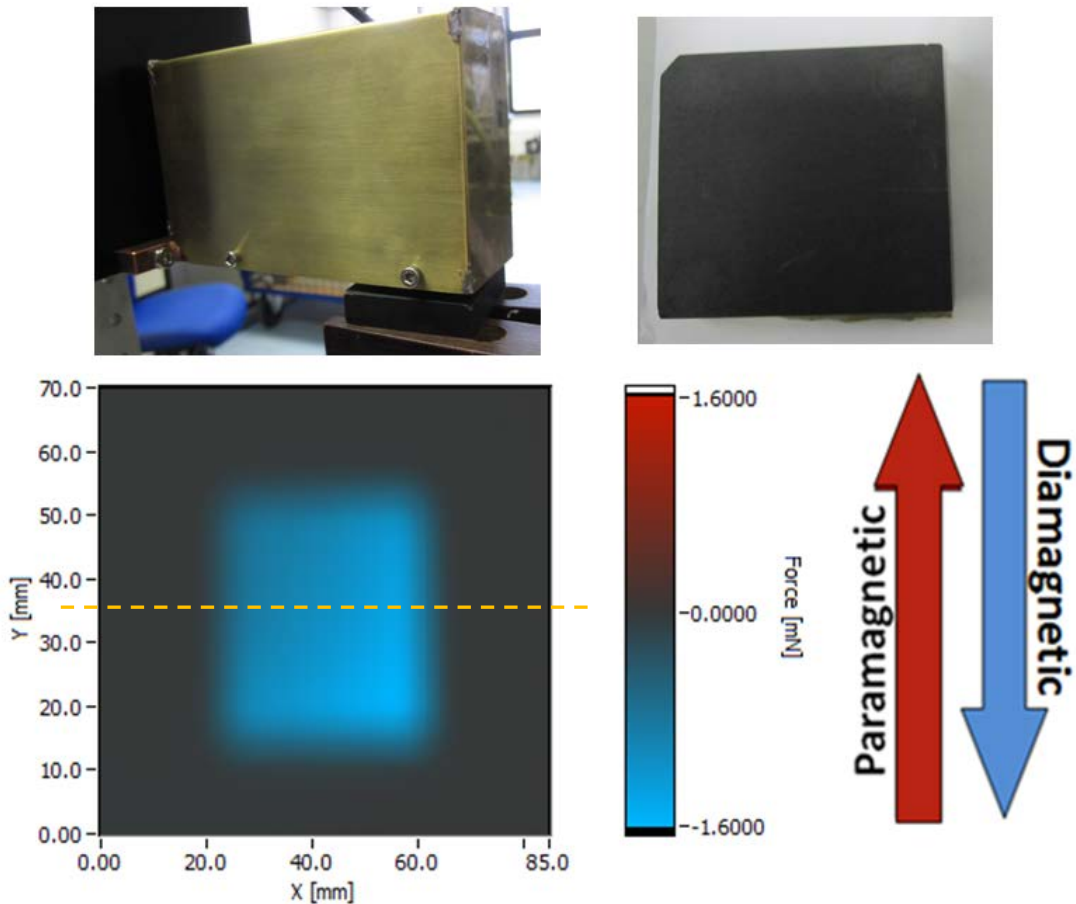


Figure 73: Set up (top), Generated image (bottom)

Configuration used for the scan

Two Z-level scan, Sensor static- sample moves

| | |
|-------------------------|---|
| Magnet used: | Magnet B |
| Cantilever used: | FRP 3 |
| Sample: | Graphite |
| Motion: | Wait and move, scan along Y-axis |
| Step size: | 0.65 mm step size along X-direction, 0.3 mm along Y |
| Filter used: | Set reference-Subtract reference |

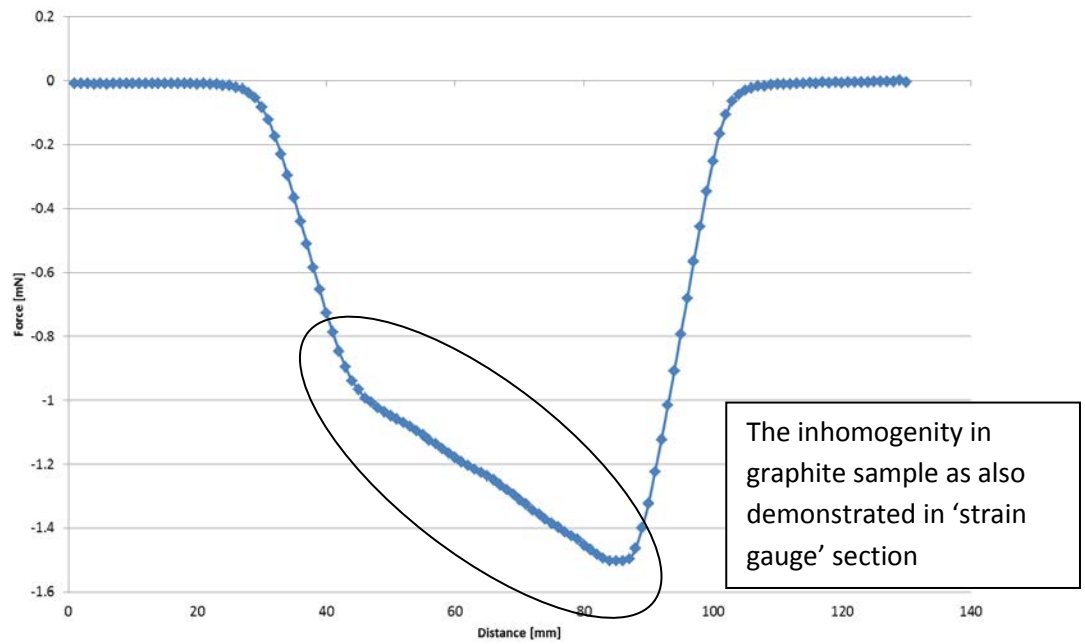


Figure 74: Diamagnetic behaviour of graphite. The signal is along the x axis as highlighted by a yellow dashed line in the scanned image

6.2.6.5. Aluminium

In this experiment as shown in figure 75, the same aluminium has been scanned which was used in last set up. It can be clearly seen that this set up has improved the signal to noise ratio as well as the eliminated the effect of air which was noticeable in the last set-up. The aluminium behaves paramagnetic as expected.

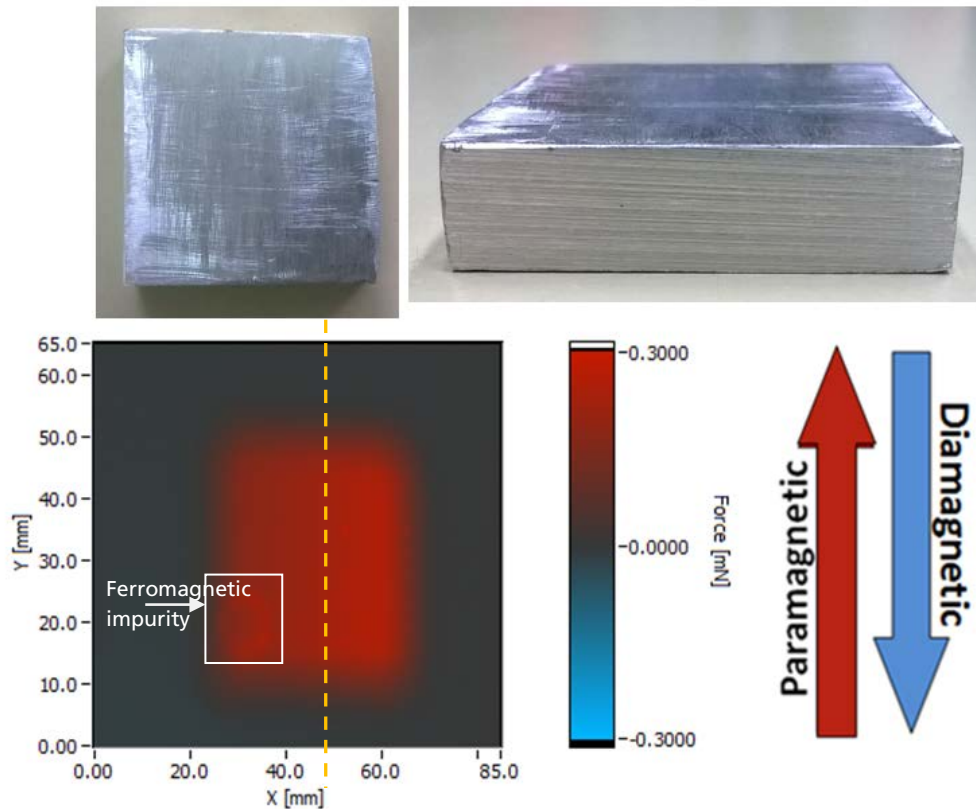


Figure 75: Sample (top), Generated image (bottom)

Configuration used for the scan

Two Z-level scan, Sensor static- sample moves

| | |
|-------------------------|---|
| Magnet used: | Magnet B |
| Cantilever used: | FRP 3 |
| Sample: | Aluminium |
| Motion: | Wait and move, scan along Y-axis |
| Step size: | 0.65 mm step size along X-direction, 0.3 mm along Y |
| Filter used: | Set reference-Subtract reference |

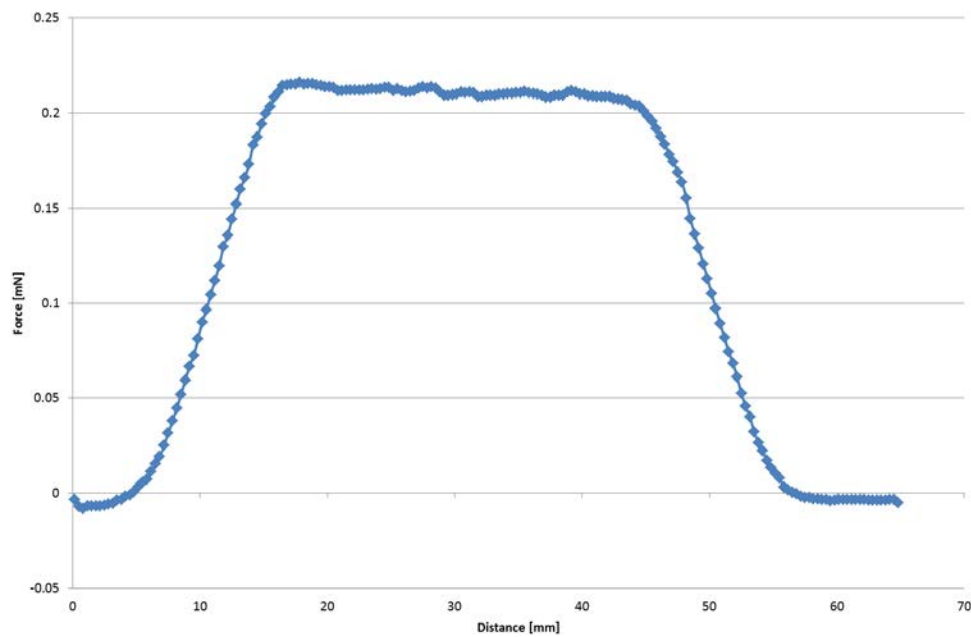


Figure 76: Signal analysis of aluminium block depicting a strong paramagnetic behaviour. The signal is along the y axis as highlighted by a yellow dashed line in the scanned image

6.2.7. Effect of thickness of the sample

In this experiment, a regular glass slide of 1 mm is taken into consideration and its effect on the sensing magnet has been studied. To make sure the thickness is increased in a fixed amount, a stack of glass slides is made over one another as shown in figure 77. It has to be noted that this scan was performed in the continuous motion hence some noise could be noticed. However, to reduce the noise and the signal quality a 'moving average filter' was used to smoothen the signal while the sample moved, after taking the average values but still in some part of the image noise could be seen. It is well evident that with this approach it is possible to derive information about a sample well between 2-3 mm below the sample surface as shown in figure 78. The tilt in the signal is because the sample was not perfectly parallel to the sensor.

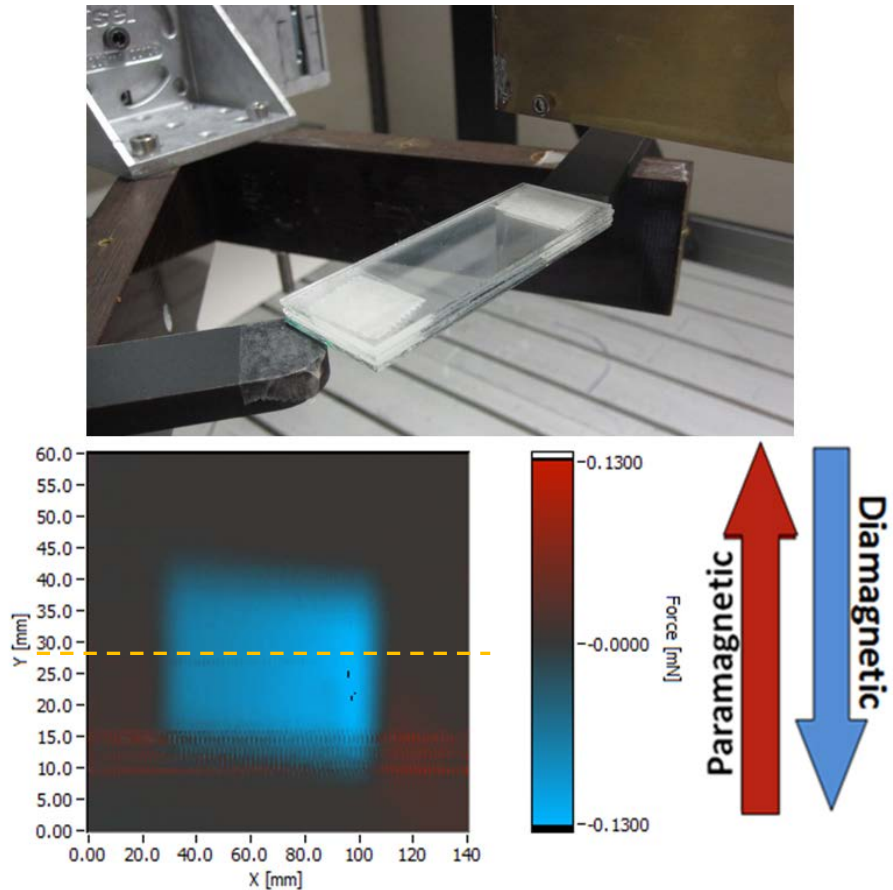


Figure 77: Sample (top), Generated image (bottom)

Configuration used for the scan

Two Z-level scan, Sensor static- sample moves

| | |
|-------------------------|--|
| Magnet used: | Magnet B |
| Cantilever used: | FRP 3 |
| Sample: | Glass slides |
| Motion: | Continuous motion with moving average filter, with a scan speed of 50 mm/s |
| Filter used: | Set reference-Subtract reference |

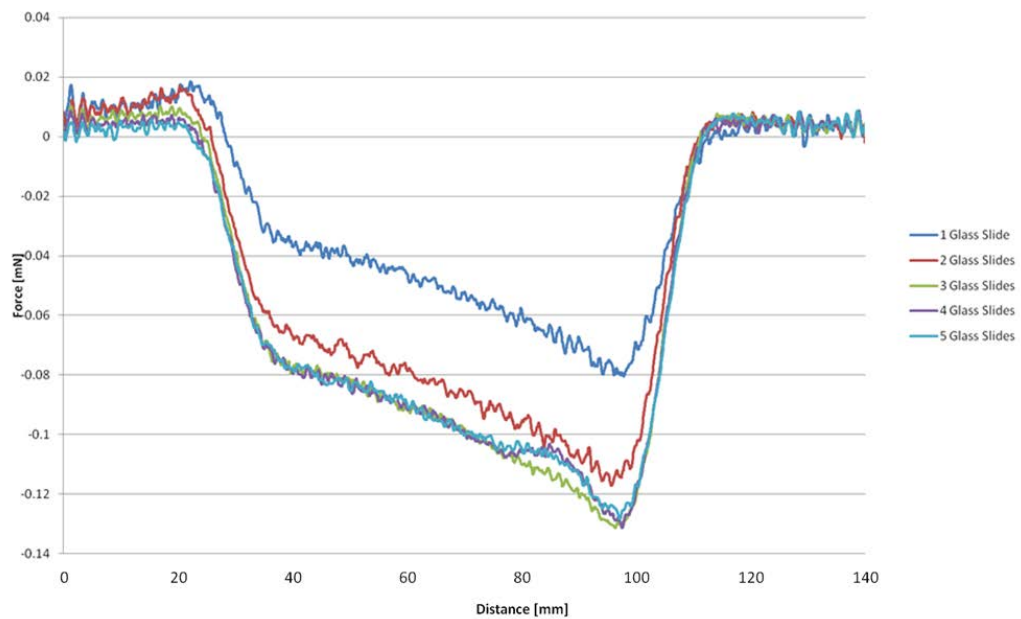


Figure 78: Thickness variation sample and its effect, the reason for the gradient is because of the non-constant gap between the sensor and the sample. The signals are along the x axis direction as highlighted by a yellow dashed line in the scanned image

6.2.8. Distance variation

In this experiment the same set up is used like in the last section but with only 5 slides (5 mm thickness) and the effect is studied over the distance varying from 1 mm to 7 mm. It can be seen in figure 79 that the sample cannot be detected at all nearly at 6 mm - 7 mm from the sensor.

Configuration used for the scan

Two Z-level scan, Sensor static- sample moves

| | |
|-------------------------|--|
| Magnet used: | Magnet B |
| Cantilever used: | FRP 3 |
| Sample: | Glass slides |
| Motion: | Continuous motion with moving average filter, with a scan speed of 50 mm/s |
| Filter used: | Set reference-Subtract reference |

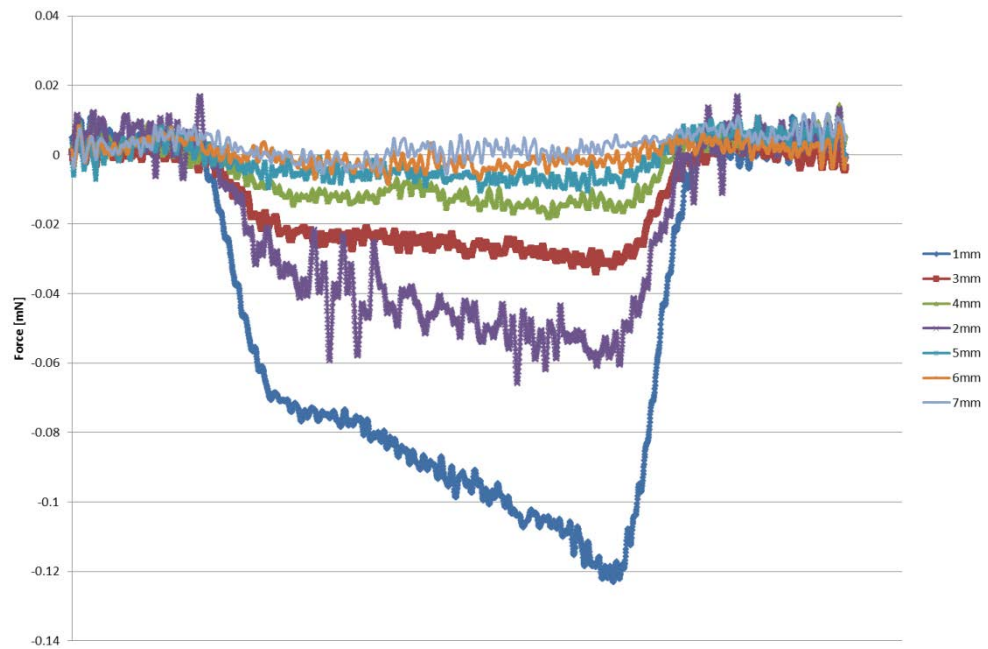


Figure 79: Effect studied with distance variation ranging between 1 mm - 7 mm. These signals are scanned along the x axis direction

The following graph in figure 80 also verifies the exponential decay of force over distance which was demonstrated in figure 29 in chapter 3. The blue dots are the measured data over distance and the red line is the exponential fitting curve.

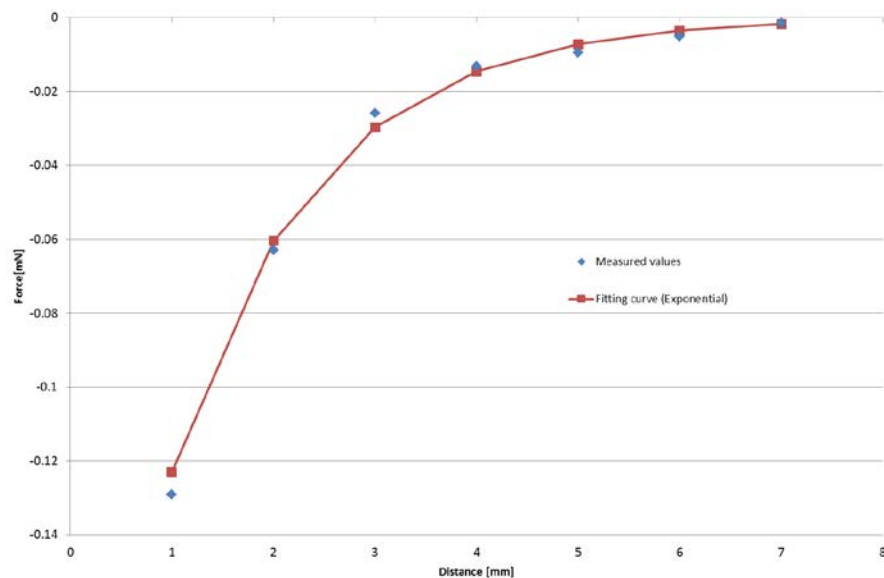


Figure 80: Graph verifying the exponential decay of force as presented in chapter 3 with the measured data

6.2.9. Evaluation of plastics

In this section following plastic materials are examined. The idea was to examine all the plastics in one scan, however, the physical set up had put some limitations. However, 7 kinds of plastics could be scanned all together at one time glued with a normal packing tape. It was difficult to maintain the constant distance between the samples as all were of different thickness and moreover the physical mounting of the sensor also was not perfect to maintain a constant gap between samples and the sensor.

- PA –Polyamide
- PS –Polystyrene
- PC - Polycarbonate
- PET - Polyethylene terephthalate
- PE-HD - Polyethylene, high density
- PMMA - Poly methyl methacrylate
- PP - Polypropylene
- ABS - Acrylonitrile butadiene styrene
- PVC-U - Polyvinyl chloride - Unplasticised
- PUR – Polyurethane
- PE-LD - Polyethylene, low density
- PF - Phenol formaldehydes

In the initial images, two-two samples are stuck on a glass plate of 10 mm as a base and then examined. As discussed in 'effect of thickness variation' section, the effect of the sample can be studied up to nearly a depth of 2-3 mm, hence, samples being mostly less than 2 mm in thickness, the result are expected to be the cumulative effect of the plastic samples and the glass plate which acts as a base for the plastics. Not all the images of the samples are presented here. One image is presented in figure 81 and the rest images are attached in the Appendix. However, in figure 82, the signals of all the plastic samples have been put up together for reference.

6.2.9.1. PA, PS

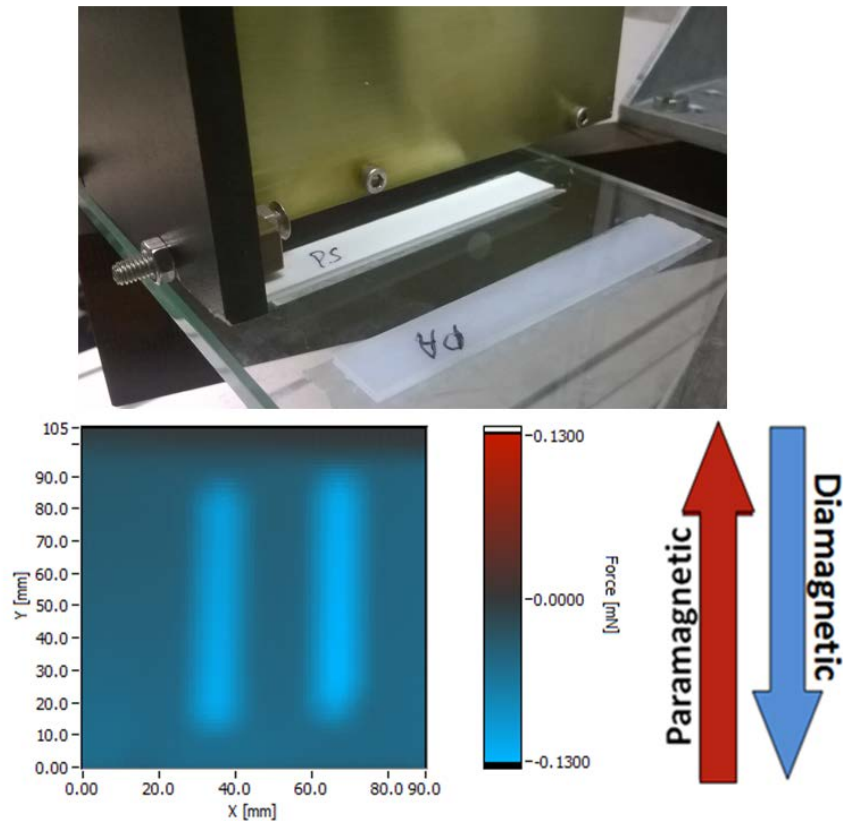


Figure 81: Set up (top), Scanned image of the plastics PA and PS (bottom)

6.2.9.2. Evaluation of plastics with glass as a base

Scanned images of all the plastic samples have been shown in the Appendix. The following signals depict the dia-and paramagnetic behaviour of plastic samples with glass as a base of 10 mm thickness. The bars in negative show that these samples are repelled by the magnet and are diamagnetic. The VMQ tested in chapter 5 could not be tested here because it was difficult to mount the sample since it was a tube like sample. However, it is interesting to note that PE-LD when tested with precision balance didn't show any response, but with the capacitive sensor the effect of PE-LD is quite noticeable. The error bars in this graph are computed by taking standard deviation into consideration for each sample.

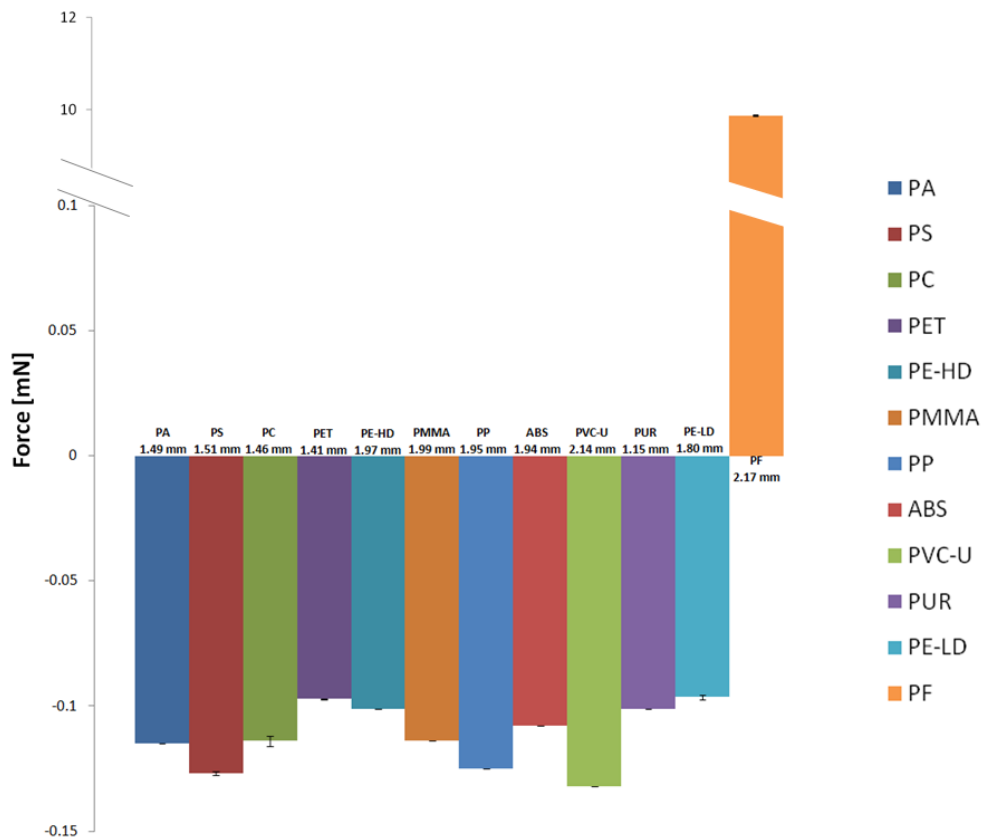


Figure 82: Evaluation of plastics with glass as a base

6.2.9.3. Six plastics mounted on a packaging tape (~30-35 microns)

In this experiment, 6 plastics samples are pasted in to a packaging tape whose thickness is normally around 30-35 microns, as shown in figure 83. The red layer in the scan is the tape which shows a paramagnetic behaviour, however it is assumed because of the colour. The blue marks depict the diamagnetic behaviour of plastics. However in the intersectional area of tape and plastics, this area is paramagnetic, since, plastics are less diamagnetic as compared to the paramagnetism of tape. Hence, the net effect in the intersectional area is paramagnetic. This also shows that how highly sensitive this sensor is, that it can sense materials with such a low thickness too. However, the effect size of different plastics in this case cannot be compared since the distance between the samples and the sensor was not constant.

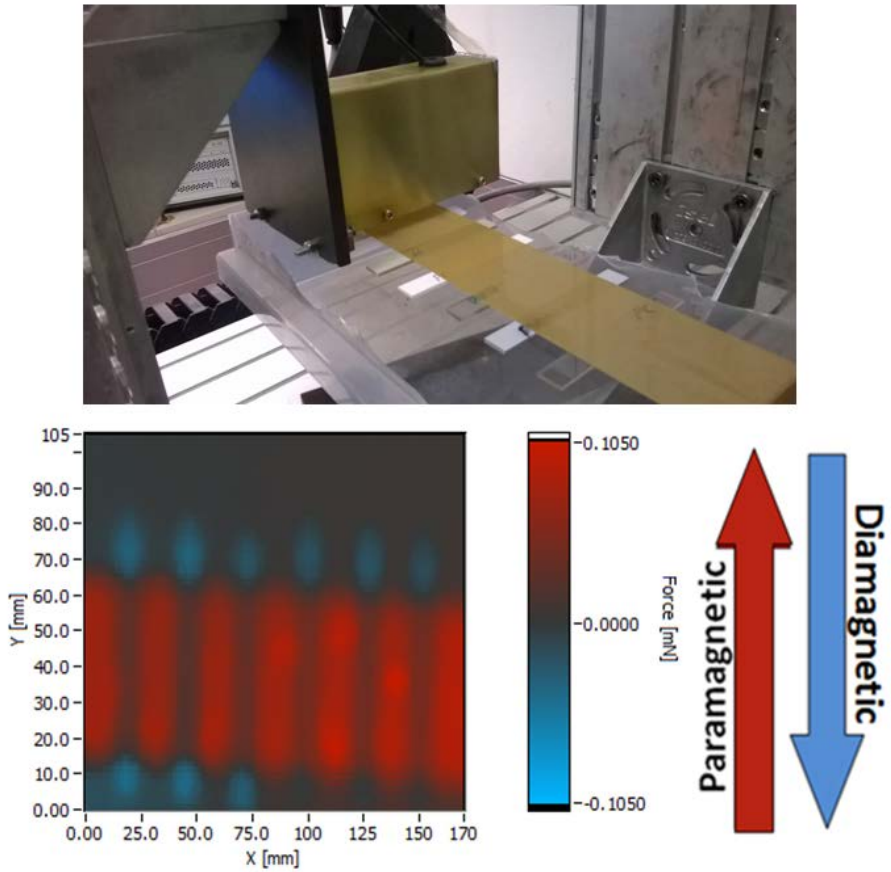


Figure 83: Set up (top), Scanned image (bottom)

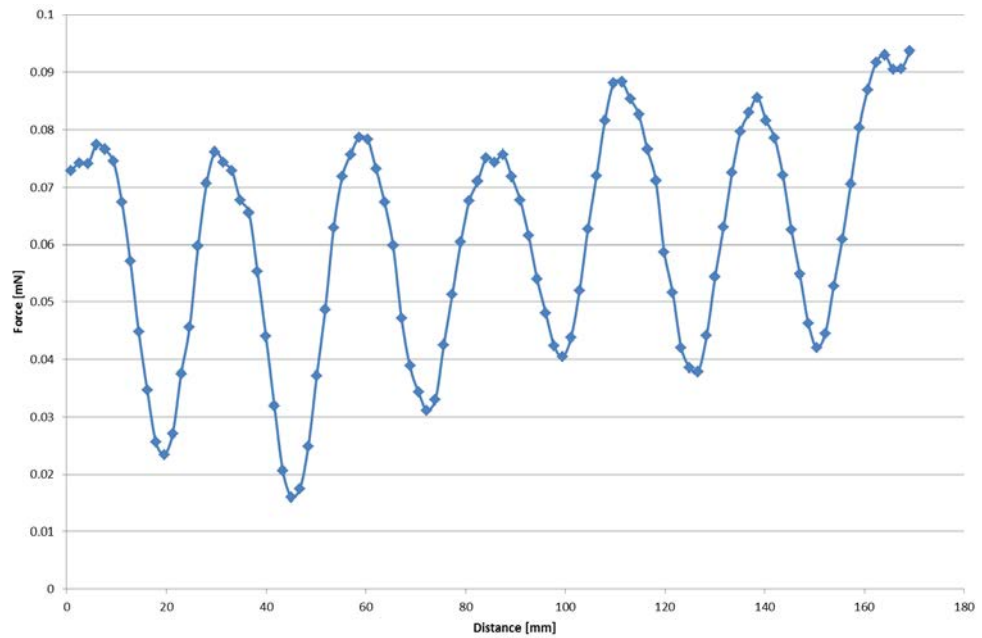


Figure 84: Graph showing the signal variation with different plastics when glued to a packing tape

6.2.10. Conclusion

This capacitive sensor based method has proved to be beneficial in all terms from signal to noise ratio to the qualitative characterization of the materials. However, this sensor can further be improved by designing the set up in a way that there is always a closed loop control that can maintain a constant gap between the sensor and the sample. To get a better resolution and sensitivity, a conical soft-magnetic material may be used over the magnet as shown below in figure 85 which would concentrate the flux at a particular specific point. This increases the flux density B and its gradient ∇B , thus increasing the force interacting with each particle according to equation (6) explained in chapter 3. However, this will also limit the volume affected by the field and thus the number of particles that contribute to the force. Therefore, a trade-off has to be found between increasing resolution and gradient on the one hand, and the associated loss of interaction volume and force on the other hand. Additionally, the closer the sample is to the sensor, the higher is the effect.

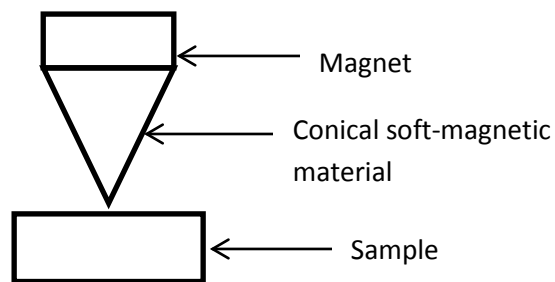


Figure 85: Proposed magnet solution for increased sensitivity and resolution

Chapter 7: Conclusion and applications

Some approaches towards non-destructive testing of dia-and paramagnetic materials have been discussed in this thesis work. Fluxgate magnetometers with single and differential set up have been used to determine graphite and aluminium. Differential configuration for the fluxgate magnetometers is sufficient for the detection of non-conducting materials but due to the eddy current generation in conducting materials such as aluminium, the measuring effect was superimposed by a damping induced error which made it hard to tell the difference between conductivity and susceptibility induced signal changes.

Initial test experiments using the force-based principle with a precision balance, led to another concept of using a strain gauge on a cantilever holding a magnet. This approach measures the strain caused by the force exerted by the test sample on the magnet causing a deflection of cantilever. This approach was improved using a half bridge circuit but still the signal to noise ratio was found to be too low for practical use, although in highly diamagnetic materials, effects were detected.

Finally, using the concept of displacement from the zero position and measuring that displacement because of the force on the magnet from the test sample, using a capacitive sensor and a cantilever set-up, this method has proved to be the best in terms of sensitivity, signal to noise ratio, effect size caused by the sample. However, the major breakthrough is the approach of scanning the test sample at two Z-levels and then subtracts the signals from each other. Along with a closed box around the sensor, the sample moves and the sensor remains static to avoid any unnecessary vibrations of the cantilever which may affect the reading. The enclosed sensor is capable of high speed scan in a continuous motion but however, this may lead to some loss of information because of the inertial state of the cantilever which does not give ample time to take the next reading. Hence, for better scanned images and the signal, 'wait and move' type of motion is recommended which also has a drawback slow speed of the scan. This approach is also capable of studying the effect well below the surface up to 3 mm as shown in the last chapter. Additionally, a scan of super paramagnetic particles, in Appendix, shows that this sensor is highly sensitive to detect these particles

which could not be seen using regular GMR sensors. Other than determining dia-and paramagnetic materials, though unintended, but experiments showed that this set up is highly sensitive to even the minutest of the ferromagnetic particles in the test samples and hence, this principle can also be used to determine the purity of the objects which are meant to be completely non-ferromagnetic. Because of the high sensitivity to ferromagnetic particles, this principle may also be used to image the ferromagnetic bars or objects in the floors or pillars made of concrete.

This final sensor can still be improved if the sensor is designed in a way that a constant gap could be maintained in between the sensor and the sample. In many of the results shown, in this work, variable distance was also one major reason for the gradient in the signal levels. Also, this sensor designed here was limited to the size of the sample because of some limitations with the mounting part of the entire sensor to the scanning system. Bulging out of screws below the base of the physical sensor set up, limited the size of the sample if it was intended to be scanned just below 1 mm of the sensor. Additionally, qualitatively, the resolution and sensitivity could be improved if the magnet size is small radially, or even pointed as proposed in the previous chapter demonstrated in figure 85, but however the volume affected by the field and thus the number of particles that contribute to the force will also decrease. Figure 86 below shows the important parameters of the approached used in this thesis.

| Sensor → Parameter ↓ | Fluxgate magnetometer | Strain gauge | Capacitive sensor set-up |
|-------------------------|--------------------------|--------------|-----------------------------|
| Cost | -- | - | --- |
| Vibrations | + | +++ | ++ |
| SNR | ++ | + | +++ |
| Ease of use | + | ++ | +++ |

Figure 86: Summary of approaches used in this work

'+++': Maximum, '++': Average, '+': Minimum;

'---': Most expensive, '--' : Normal cost, '-': Cheap

References

- [Amir]** Amiri M.S., Ph.D. thesis (submitted 2015); Development of a novel method for local residual stress measurement using micromagnetic microscopy.Saarland University.
- [Amri]** Amrita Vlab.
URL:<http://amrita.vlab.co.in/?sub=1&brch=192&sim=854&cnt=1>, as of December 2014.
- [Asmh]** Allen W.; Mahroter R.G.: Investigation into the electrical conductivity and mechanical properties of aluminum alloys subjected to elevated temperature exposure. US Naval report no. NAEC-AIVIL-2083, Aeronautical Materials Laboratory, November 1964.
- [Bozo]** Bozorth R.M.; Ferromagnetism. Van Nordstrand, Princeton. 1951.
- [Caru]** Caruso M.J., Smith C.H., Bratland T., Schneider R.; A new perspective on magnetic field sensing.
URL:http://www51.honeywell.com/aero/common/documents/myaerospacecatalog-documents/Defense_Brochures-documents/Magnetic_Literature_Technical_Article-documents/A_New_Perspective_on_Magnetic_Field_Sensing.pdf, as of January 2015.
- [Cull]** Cullity B. D.; Introduction to magnetic materials.Addison-Wesley. 1972.
- [Dear]** Dearing J.A.; Environmental magnetic susceptibility. 1994.URL:http://gmw.com/magnetic_properties/pdf/Om0409%20J_Dearing_Handbook_iss7.pdf, as of January 2015.
- [Diam]** Diamagnetism;
URL: <http://en.wikipedia.org/wiki/Diamagnetism>, as of December 2014.
- [Evan]** Evans, Ken; Fluxgate Magnetometer Explained – Mar. 2006.
URL:<http://www.invasens.co.uk/FluxgateExplained.PDF>, as of January 2015.
- [Geim]** Geim A.K., Simon M.D.; Diamagnetic levitation: Flying frogs and floating magnets. Journal of Applied Physics. Volume 87, Number 9. 2000.

- [Gian]** Giancoli D.; Electric Currents and Resistance. In Jocelyn Phillips. Physics for Scientists and Engineers with Modern Physics (4th ed.). Upper Saddle River, New Jersey: Prentice Hall. p. 658. 1984.
- [Hayt]** Hayt W. H., Engineering electromagnetics, McGraw-Hill. 1989.
- [Hend]** Hendrych A., Kubinek R. and Zhukov A.V.; The magnetic force microscopy and its capability for nanomagnetic studies- The short compendium.
URL: <http://www.formatex.org/microscopy3/pdf/pp805-811.pdf>, as of January 2015.
- [Hone]** Hall effect sensing and application;
URL: <http://sensing.honeywell.com/honeywell-sensing-sensors-magnetoresistive-hall-effect-applications-005715-2-en.pdf>, as of December 2014.
- [Izfp]** Fraunhofer institute of non-destructive testing, Saarbrücken, internal document.
- [Jile]** Jiles D.; Introduction to magnetism and magnetic materials. Chapman and Hall. 1991.
- [Klaa]** Klaase J.C.P.; The Faraday balance, Van der Waals- Zeeman Institute, November 1999.
URL: <http://www.science.uva.nl/research/cmp/klaasse/fdb.html>, as of December 2014.
- [Lenz]** Lenz, J.E.; A review of magnetic sensors. Proceeding of the IEEE Volume: 78, Issue: 6. DOI: 10.1109/5.56910. Page(s): 973-989. June 1990.
- [Mart]** Martin Y. and Wickramasinghe K.; Magnetic Imaging by Force Microscopy with 1000Å Resolution. Appl. Phys. Lett. 50 (20): 1455–1457. 1987.
- [Micr]** Micro-Epsilon;
URL: <http://www.micro-epsilon.com/download/products/cat--capaNCDT--en.pdf>, as of December 2014.
- [Morr]** Morris B.L., Wold A.; Faraday Balance for Measuring Magnetic Susceptibility. Review of Scientific Instruments 39, 1937 (1968); doi: 10.1063/1.1683276. AIP. 1968.
- [Nave]** Nave Rod; Magnetic field.
URL: <http://hyperphysics.phy-astr.gsu.edu/hbase/magnetic/magfile.html>, as of December 2014.

- [Osta]** Ostanina K. and Marcon P.; Overview of methods for magnetic susceptibility measurement. PIERS Proceedings, Kuala Lumpur, Malaysia, March 27-30, 2012.
- [Pete]** Schull P. J.; Non-destructive evaluation: theory, techniques and applications. New York. Marcel Dekker, Inc. 2002.
- [Peym]** Peyman S.A., Kwan Y., Margaron O., Tarn M., Iles A. and Pamme N.; Diamagnetic repulsion- A versatile means for the manipulation of objects in microfluidic devices. Thirteenth International Conference on Miniaturized Systems for Chemistry and Life Sciences November 1 - 5, 2009, Jeju, Korea.
- [Ripk]** Ripka P.; Review of fluxgate sensors. Sensors and Actuators A: Physical. Volume 33, Issue 3, June 1992, Pages 129–141. 1992.
- [Schn]** Jander Albrecht, Smith Carl H., Schneider Robert; Magnetoresistive sensors for non-destructive evaluation. 2005. URL: http://www.nve.com/Downloads/SPIE10_Magnetoresistive_Sensors_for_Nondestructive_Evaluation.pdf, as of January 2015.
- [Serw]** Serway, Raymond A.; Principles of Physics (2nd ed.). Fort Worth, Texas; London. 1998.
- [Spal]** Spaldin N.A.; Magnetic materials: fundamentals and applications. Cambridge: Cambridge University Press. 2010.
- [Spen]** Spencer, B.; Zare, R. N. Magnetic Susceptibility Measurements Using a Laser Pendulum Apparatus. J. Chem. Educ., 1988, 65, 277-279.
- [Szie]** Dr. Klaus Szielasko, team leader, electromagnetic inspection methods, Fraunhofer IZFP, personal communication.
- [Yama]** Likhtenshtein G. I., Yamauchi J., Nakatsuji S., Smirnov A. I. and Tamura, R.; Fundamentals of Magnetism, in Nitroxides: Applications in Chemistry, Biomedicine, and Materials Science, Wiley-VCH Verlag GmbH & Co. KGaA, Weinheim, Germany. doi: 10.1002/9783527621743.ch1. 2008.

Appendix

A. Fluxgate differential set up used for examining some food samples (dried mushrooms), depict contamination with magnetic particles as shown in the image below.

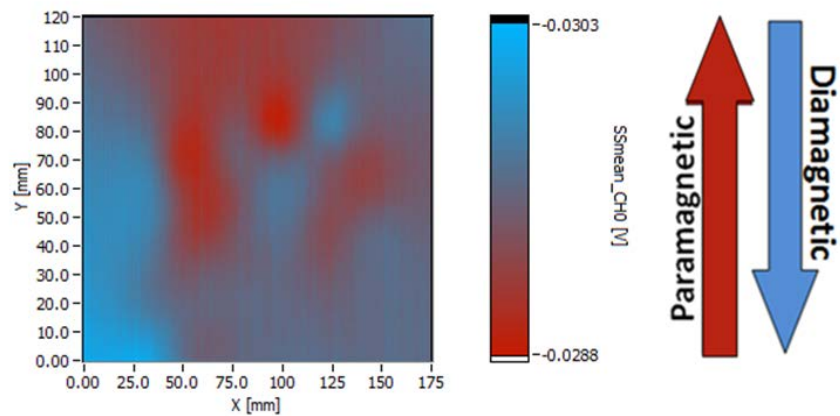


Figure 1: Food samples examined with differential fluxgate magnetometer set up

B. Following are some results with the initial set up of capacitive sensor.

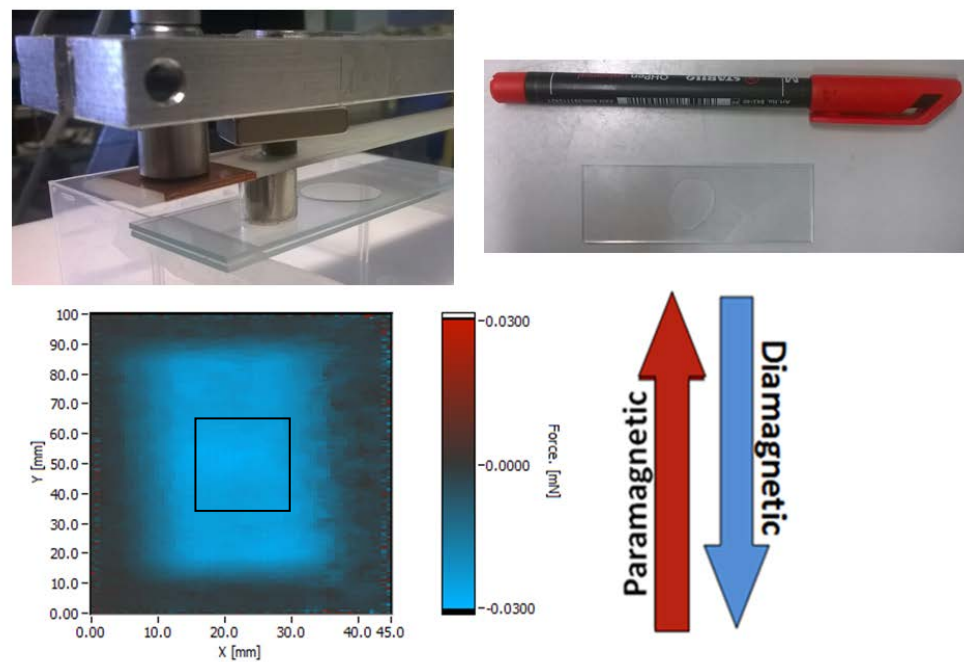


Figure 2: Glue sandwiched between two glass slides

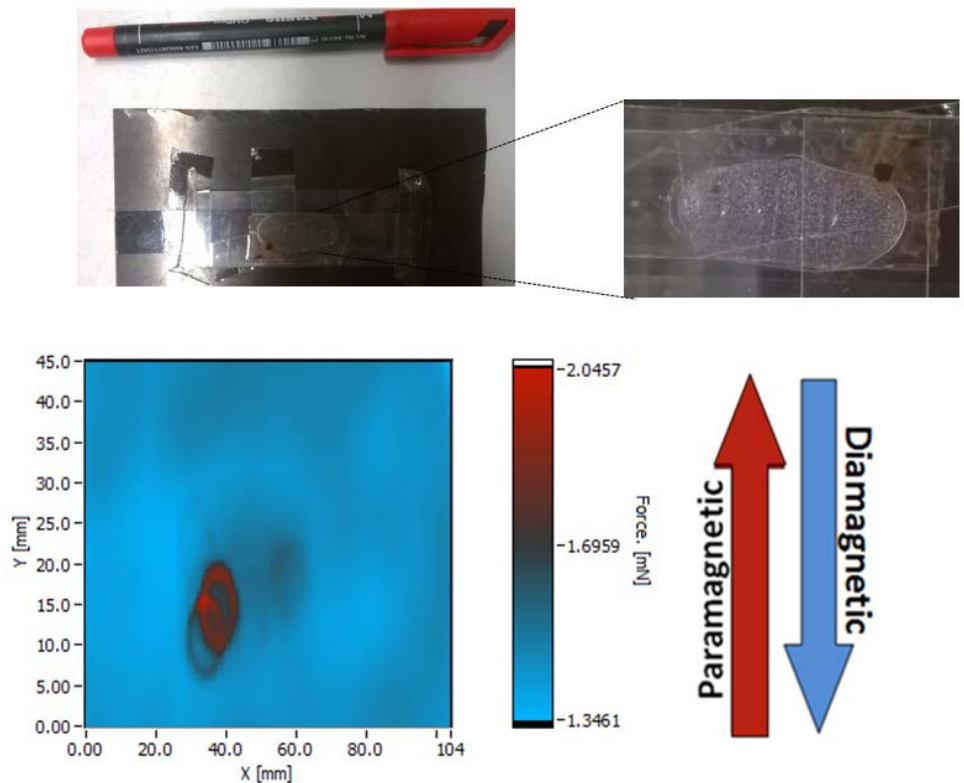


Figure 3: Super paramagnetic particles in a liquid sandwiched between two glass slides

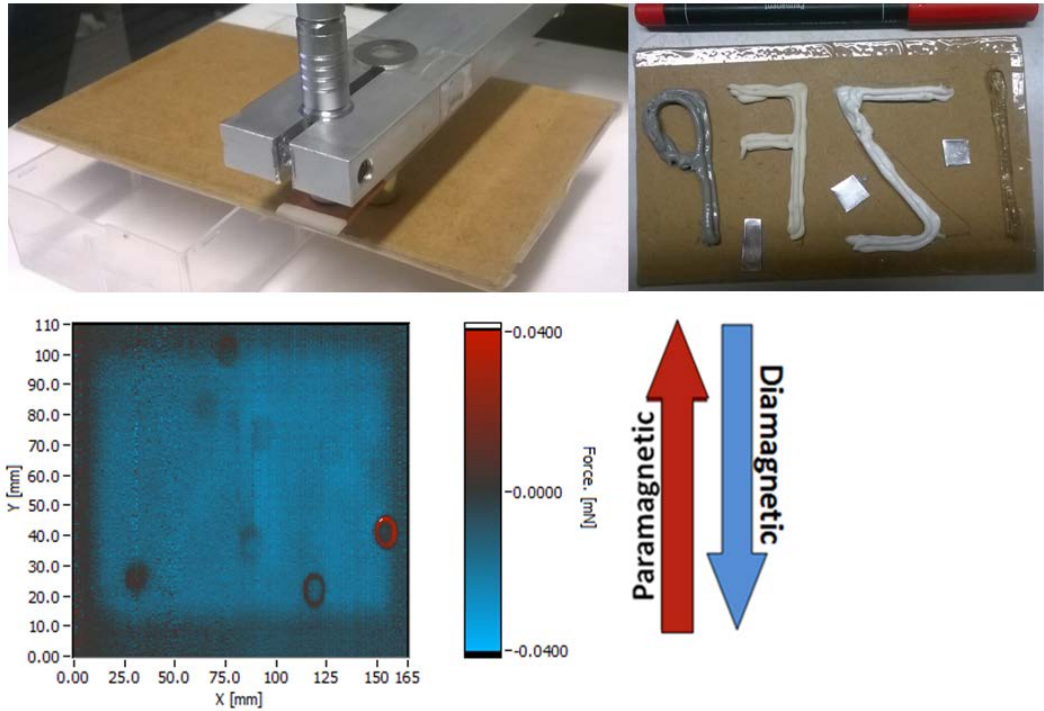


Figure 4: IZFP with glue on cardboard (4 mm thick), red round particles- ferromagnetic impurities

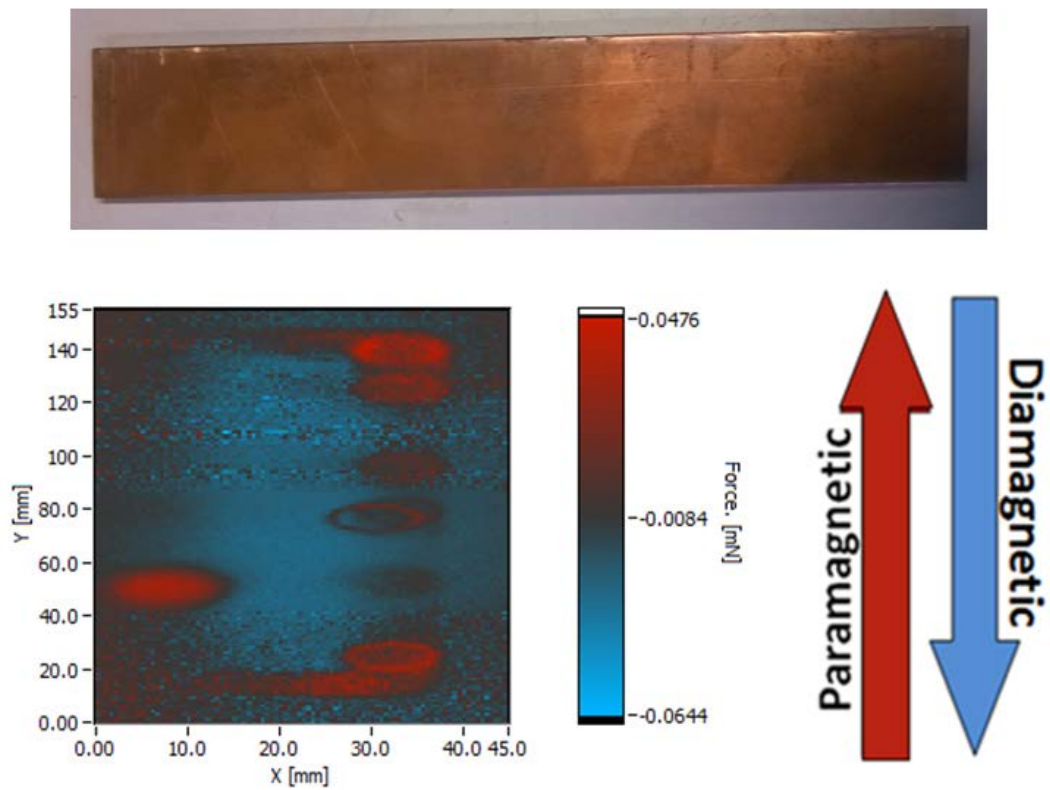


Figure 5: Copper, red circles- ferromagnetic impurities

C. Scans with final sensor

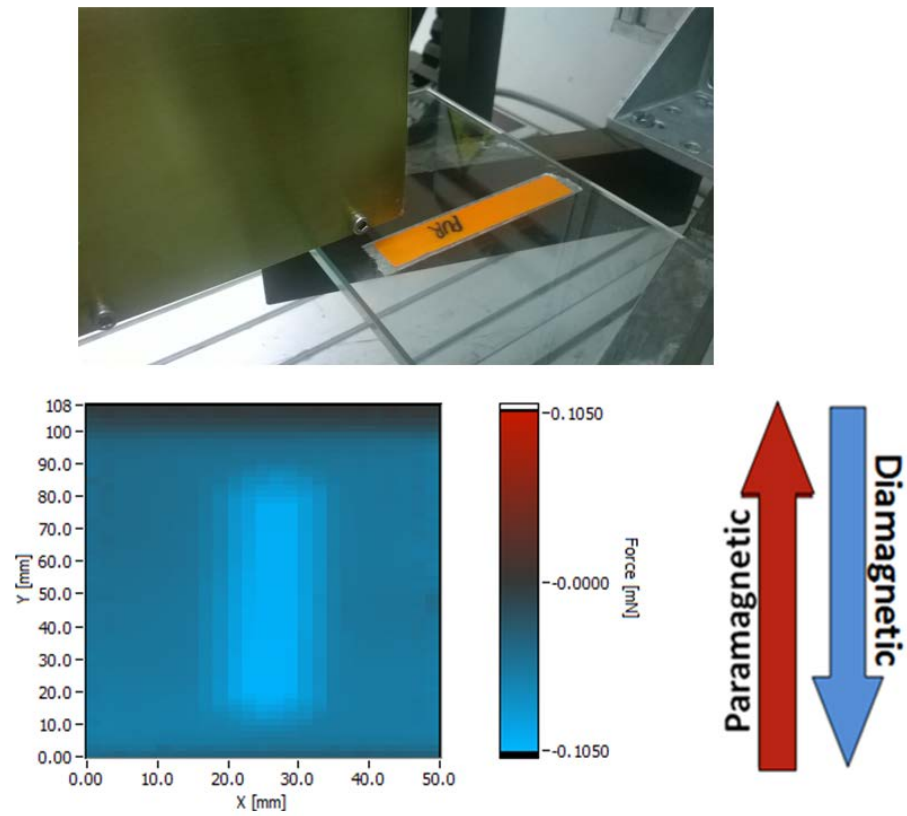


Figure 6: PUR plastic

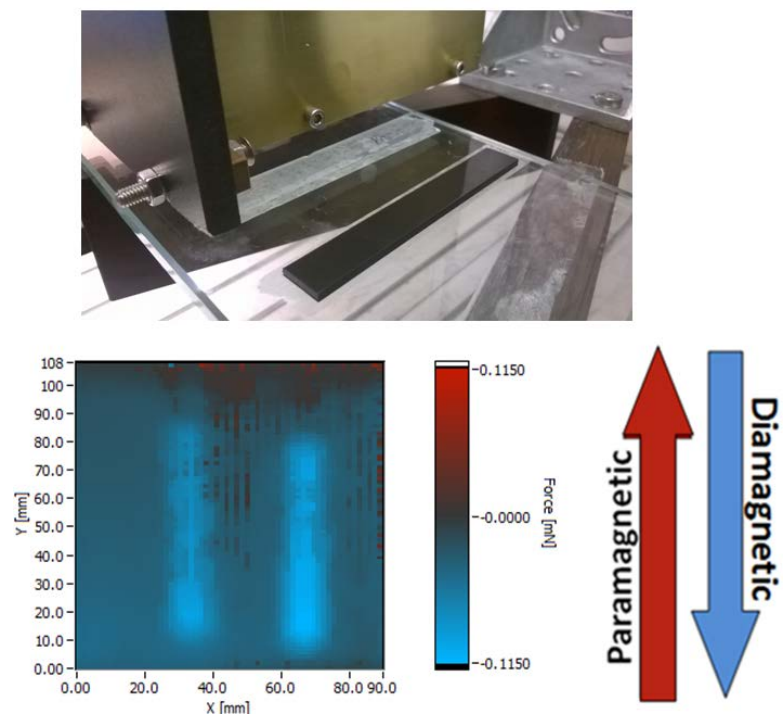


Figure 7: PE-HD, PMMA

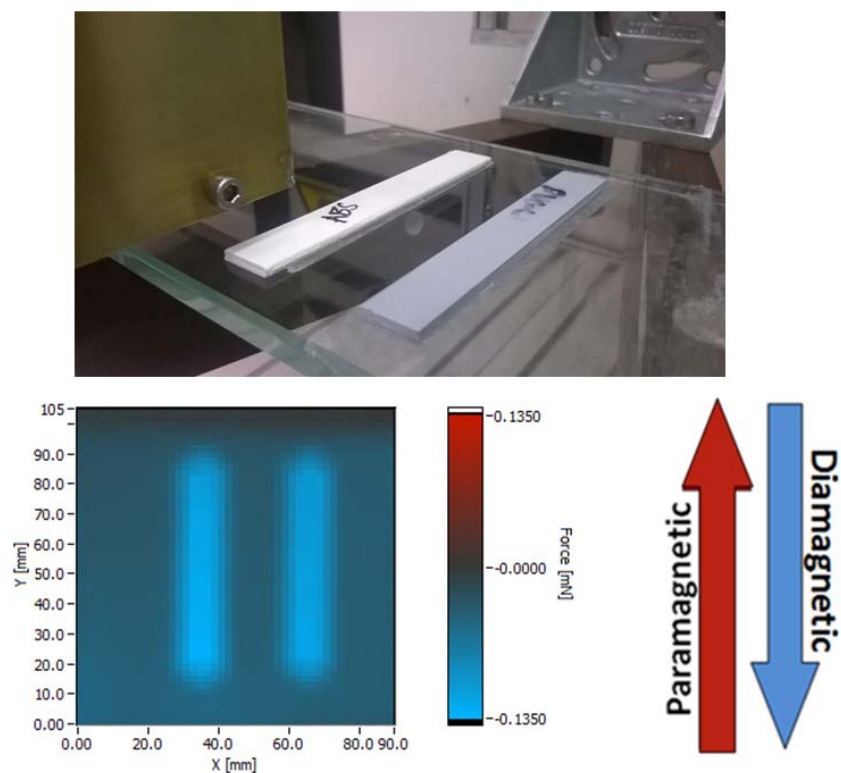


Figure 8: PVC-U, ABS

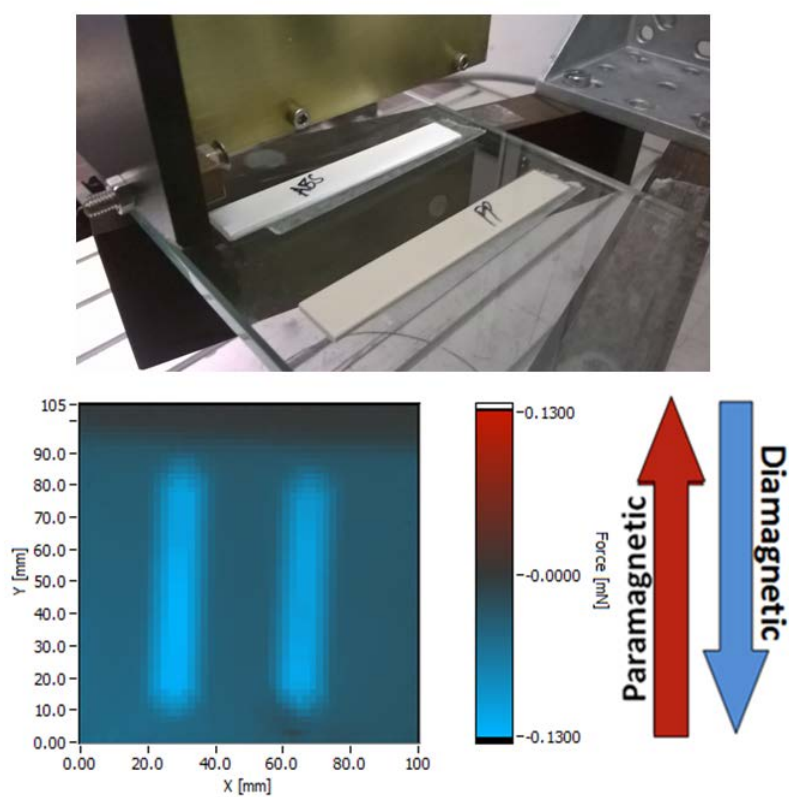


Figure 9: PP, ABS

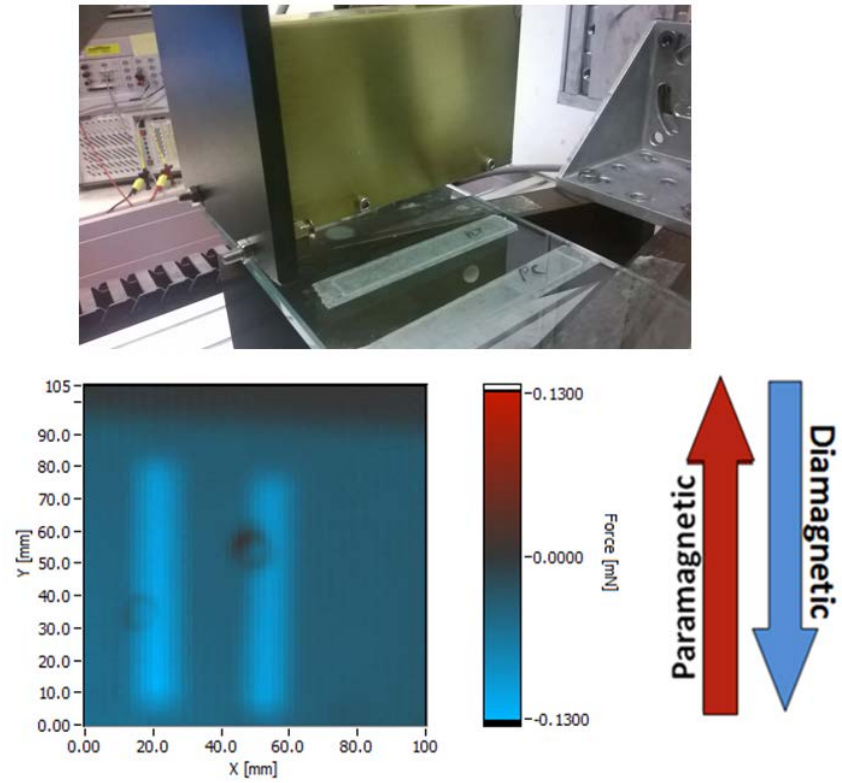


Figure 10: PC, PET

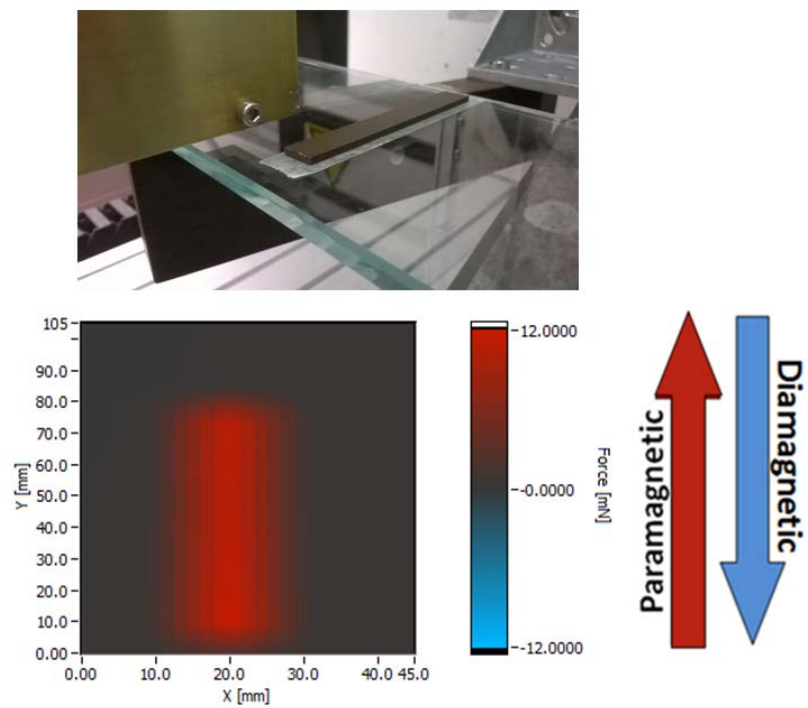


Figure 11: PF

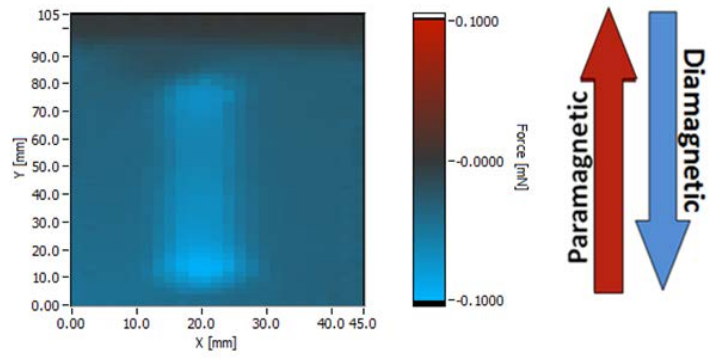


Figure 12: PE-LD